Charles University in Prague
Department of Physical Geography and Geoecology

Acoustic-gravity waves at ionospheric heights generated by meteorological activity in the troposphere

Dissertation Thesis

Tereza Šindelářová

Školitel: RNDr. Ivan Sládek, CSc.

Praha 2009

Poděkování mým nejbližším.

Acknowledgement:
RNDr. Ivan Sládek, CSc., Ing. Dalia Burešová, CSc., Ing. Jaroslav Chum, Ph.D., RNDr. Petr Pešice, Ph.D.
The thesis was made at the Institute of Atmospheric Physics, Academy of Sciences of the Czech Republic. The work was supported by the Grant Agency of the Czech Republic through grant No. 205/04/2110, grant No. 205/07/1367, and grant No. 205/08/1356.
Meteorological data were provided by the Czech Hydrometeorological Institute. The geomagnetic data from observatory Budkov were provided by the Institute of Geophysics, Academy of Sciences of the Czech Republic.

Prohlašuji, že jsem disertační práci vypracovala samostatně s použitím uvedené literatury. Tuto práci ani její část jsem nepoužila k získání jiného akademického titulu.

I hereby declare that this submission is my own work and that, to the best of my knowledge and belief, it contains no material previously published or written by another person nor material which to a substantial extent has been accepted for the award of any other degree or diploma of the university or other institute of higher learning, except where due acknowledgment has been made in the text.

_____

Tereza Šindelářová

Content

1. Introduction and theoretical background

The earth atmosphere consists of mixture of gases, water vapour, and solid particles. The existence of the atmosphere is an essential condition for life on the Earth and the atmosphere participates in formation of the environment of organisms. From this point of view, the upper atmosphere mainly acts as a filter of harmful components of solar radiation; the lower atmosphere interacts with other physical geographical spheres and is a direct component of the environment.

The composition, structure, and variability of the atmosphere are influenced by a number of chemical and physical processes that occur continuously in the atmosphere and are of various time and space scales. The main source supplying these processes with energy is the solar radiation, both direct and transformed by the atmosphere or by the earth surface. Photochemical and less frequent chemical reactions lead to changes of the chemical composition of the atmosphere. Physical processes include mainly energy and mass transfers. Both groups of course are related with each other and influence each other.

In the vertical direction, the atmosphere is organized into layers of different characteristics. The atmospheric layers are coupled in the vertical direction; the energy as well as the mass and momentum are transferred between the layers. One of the most efficient ways of the energy transfer in the vertical direction is wave motions. The energy and momentum flux from the lower atmosphere to the upper atmosphere has been known to exist and studied for a long time, while the role played by middle atmosphere in the climatic system has been recognized recently. The present study deals with effects of tropospheric convective storms on the ionosphere in the Czech Republic and discusses the results with results obtained in North America.

1.1. The ionosphere

The ratio of ionization processes and recombination processes as well as the transport of charged particles determine the distribution of ionized particles and form the stratified structure of the ionosphere. The atmospheric gases, particularly O, O_2, and N_2 are ionized by the shortwave solar radiation (EUV and X-rays). Cosmic rays contribute to the formation of the lowermost ionosphere (50-80 km). Recombination is the opposite process to the process of ionization. Its rate is determined by the

temperature and chemical composition of the atmosphere. At lower altitudes up to ~180-200 km, the rate of recombination is proportional to the square of electron density; above this height, its rate decreases and becomes proportional to the electron density. Vertical transport – ambipolar diffusion – plays an important role in the upper ionosphere, particularly in formation of the topside ionosphere.

The region of maximum concentration of ionized particles occurs at the altitudes ~250-300 km. It is termed the *F2* layer. At night, the maximum electron concentration decreases, whereas the height of maximum electron concentration increases. The electron concentration in the *E* layer rapidly decreases during the nighttime. It is determined by high rate of recombination in the lower ionosphere. The *F1* layer as a separate layer is formed particularly in summer, when the peak of ionization rate moves downward into the region, where the recombination rate is proportional to the square of electron density. In the *E* region (~90-140 km), the sporadic *E* layer might occur. It is a thin layer of a very high electron density and high variability in time and space. The lowermost part of the ionosphere (~50-90 km) is termed the *D* region. From the chemical point of view, the *D* region is the most complex part of the ionosphere (Hargreaves, 1992). It is due to the dominant role of minor species in ionization and chemistry and due to the contribution of several different types of radiation to the ionization.

The ionosphere influences the propagation of radio waves. This feature is utilised in the ionospheric sounding. Vertically propagating radio wave is reflected in the ionosphere at the height where the radio wave frequency equals the plasma frequency. Plasma frequency is proportional to the square of electron concentration; therefore radio waves of higher frequencies penetrate to higher altitudes. The ionospheric sounding by ionosondes or by continuous wave Doppler sounders is based on this principle. In the *D* region, reflecting radio waves are heavily absorbed. Therefore, a different technique is used for soundings of the *D* region. The absorption of waves is studied.

The ionospheric parameters vary in time; the time scales range from long term (secular) changes down to time scales of hours and minutes (Rishbeth and Mendillo, 2001). The state of the ionosphere is mainly controlled by the flux of ionizing radiation, which is determined by the solar zenith angle, by the phase of the 11-year solar cycle, 27-day solar rotation, and short-time perturbations like solar flares. Thus, the

ionosphere varies during the day and year, as well as during the solar cycle. Rishbeth and Mendillo (2001) studied the variability of maximum electron density of the *F2* layer (NmF2) at the midlatitude ionospheric station Slough under conditions of low or medium geomagnetic activity. They found a strong semiannual pattern with larger day-to-day fluctuations near equinoxes than during solstice periods. The variability is always largest around midday. Sudden changes in the solar wind induce irregular, often considerable changes of ionospheric characteristics due to the electromagnetic coupling between the ionosphere and magnetosphere and due to changes of circulation of the upper atmosphere. The enhanced Joule heating by auroral currents of the auroral atmosphere leads to changes in neutral wind direction and consequently to variations of electron density in the *F2* layer (Davies, 1990). Ionospheric variability increases with increasing geomagnetic activity at all latitudes, being higher at higher latitudes (Forbes et al., 2000).

Even in region with maximum concentration of ionized particles, the number density of the neutral gas exceeds the plasma density (electron density is roughly 10^{-3} of the neutral density). Thus, processes in the surrounding neutral atmosphere as well as processes in the lower atmosphere must be taken into account when considering the variability of the ionosphere. The impact of atmospheric waves on the ionosphere has recently been reviewed by Laštovička (2006).

1.2. The atmosphere – vertical structure and circulation

The traditional atmospheric stratification is based on the temperature; other stratifications emerge from the degree of ionization (neutrosphere and ionosphere) or from the chemical composition. According to the temperature profile following layers are distinguished: troposphere, stratosphere, mesosphere, and thermosphere. Each layer is characterized by a uniform change of the temperature with height; boundaries between the layers are defined at the inflexion points of the temperature profile (Fig.1).

The solar radiation coming to the Earth is the main source of energy for meteorological, chemical, and other processes in the atmosphere as well as on the earth surface. In the upper atmosphere, the most important is the absorption of short wave solar radiation. Due to the absorption, the temperature in the thermosphere and stratosphere increases with height. The temperature decrease with altitude in the

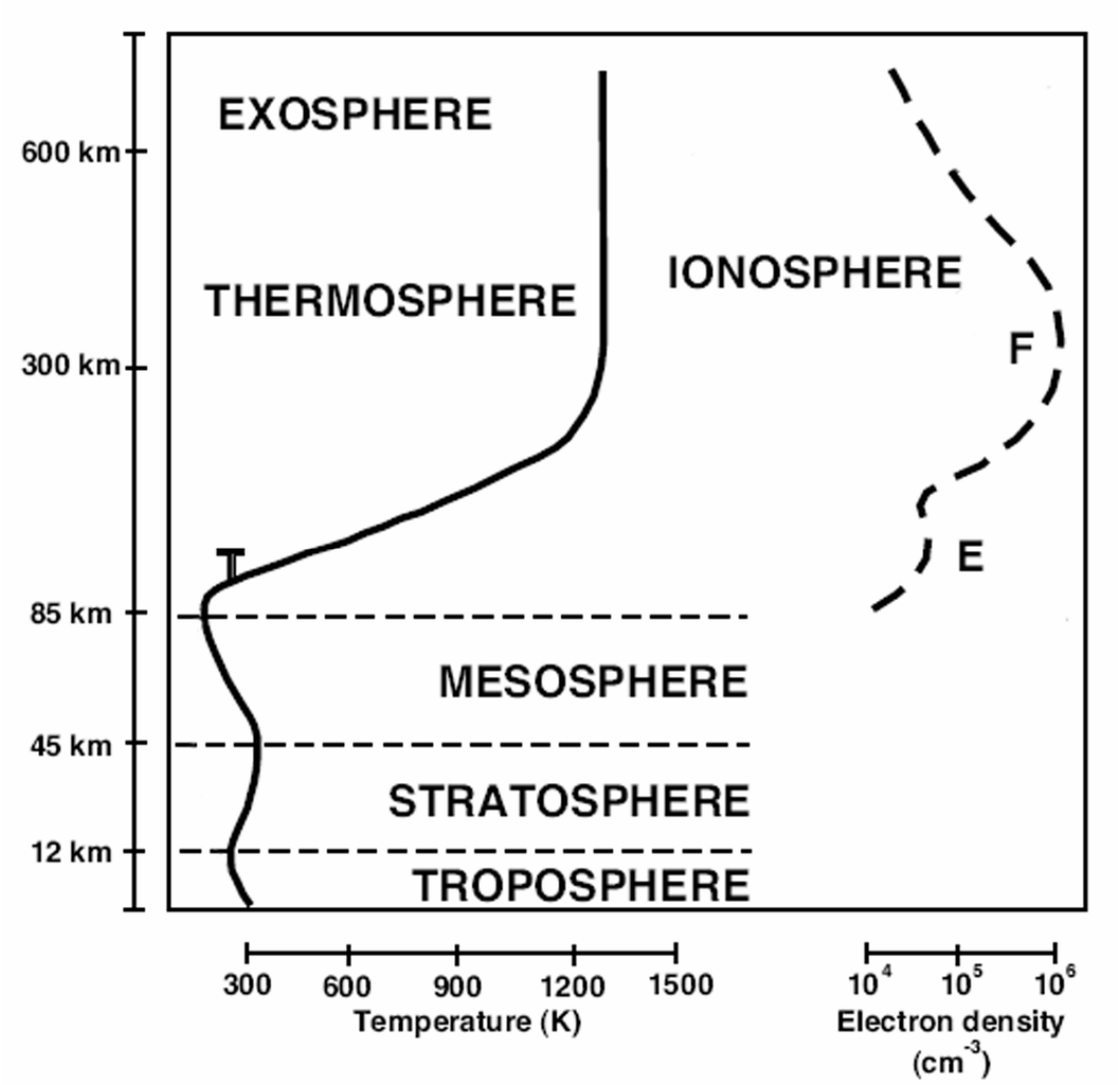

Fig.1. *Vertical profile of the atmosphere. (Source: http://upload.wikimedia.org)*

mesosphere is caused by prevailing radiation cooling. Heat exchange with surrounding atmospheric layers and adiabatic temperature changes also play an important role in the upper atmosphere. The absorption of the direct solar radiation in the lowermost troposphere is rather small and the main energy sources are the absorption of the long wave radiation emitted by the earth surface and, more important, by the heat conduction. The heat conduction occurs in the form of the molecular heat conduction in the layer immediately above the surface and in the form of turbulent heat conduction.

The circulation of the atmosphere is generally determined by the radiation balance in different latitudes and by earth rotation. Further, specific factors come in and modify the circulation in each layer. In all atmospheric layers, regular circulation patterns can

be found. Small scale and mesoscale processes dominate in the lower atmosphere, whereas large scale and long term processes prevail in the thermosphere. The mean circulation in all layers undergoes seasonal changes of the speed and direction and it is modified by wave motions of a wide period range (minutes to days). A scheme of the atmospheric circulation is shown in Fig.2.

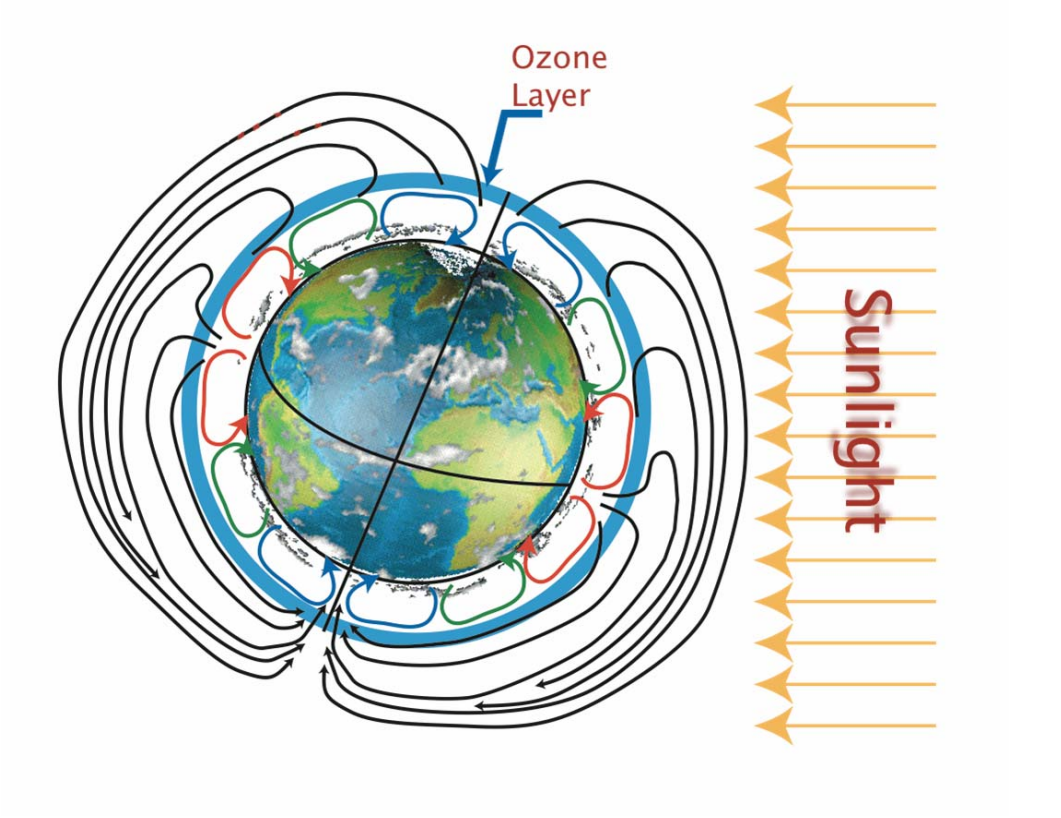

Fig.2. *Circulation of the atmosphere. Red: Hadley cell. Green: Ferrel cell. Blue: Polar cell. (Source: Friedman, 2007)*

The temperature field has a complicated structure in the troposphere. The temperature distribution is primarily determined by latitudinal variations of solar radiation input and it is significantly modified by the different influence of different types of active surface. The temperature distribution contributes to the formation of the air pressure field and consequently influences the general circulation of the troposphere. In mid latitudes, zonal westerly air flow prevails during the whole year, locally altered by the terrain and by the influence of the underlying active surface. The current state of

the troposphere is frequently modified by the development of extratropical cyclones and anticyclones.

The air flow in the lowest troposphere is predominantly turbulent. An important role in the tropospheric circulation is also played by the convection, which belongs to the processes of heat energy transfer. It includes small-scale and large-scale upward and downward movements of air parcels and contributes to the development of clouds and convective storms. The theory of convective storms was in detail described by Řezáčová et al. (2007). The term „convective storms" stands for all convective processes and phenomena which occur during the development of Cumulonimbus clouds. They include precipitation, wind, and electricity. NOAA's national weather service defines the term severe convective storms using following criteria: (1) occurrence of a tornado, (b) wind gust 25 $m \cdot s^{-1}$ or higher, (c) hail of 2 cm or higher in diameter. These criteria are based on characteristics of convective storms in the USA. In Europe and worldwide, no exact boundary between severe and non-severe convective storms has been defined. The term „thunderstorm" refers to an observation on a surface meteorological station and includes the electrical activity in convective storms.

The basic structure of a convective storm is a convective cell. It consists of an updraft and subsequent compensatory downdraft with precipitation. The single cell is the least intense type of a convective storm. As for intensity, on the opposite side is a supercell. This term describes a long lasting, renewing circulation with a rotating updraft. The supercell may produce dangerous phenomena like strong downburst, hail, and tornadoes. Another type of convective storm consists from a number of convective cells and it is termed a multicell. Several categories of multicells can be distinguished according to the spatial organization of convective cells. Multicell cluster storms are comprised by a disordered group of cells moving as a unit; cells are in a different phase of life. The group of cells may also have a linear structure. At a certain stage of organization, this formation is termed a squall line. Multicell storms can produce recurring strong precipitation and hail (Řezáčová et al., 2007; ww2010.atmos.uiuc.edu). In the Czech Republic, convective storms are usually of a multicell or single cell type. Supercells occur rather rarely.

The temperatures in the lower stratosphere are influenced by the atmospheric circulation, whereas the global temperature field in the mid and upper stratosphere is

approximately in a radiative equilibrium with substantial local variations due to vortical motions (Andrews et al, 1987). The winter hemisphere is colder than the summer hemisphere. In the lower stratosphere, westerly winds dominate; in winter stronger than in summer. The circulation in the mid and higher stratosphere and mesosphere shows distinct seasonal dependence. Easterly airflow prevails in the warm season, whereas westerly winds blow in winter. The exception is the major sudden stratospheric warming in winter, when the configuration of temperature and air pressure fields changes substantially and the wind direction changes to easterly in the middle and upper stratosphere (Labitzke and van Loon, 1999).

In the mesosphere and lower thermosphere region (MLT), the temperature distribution is determined by non-equilibrium processes. One of the techniques to measure the middle atmosphere temperature was proposed by Gusev et al. (2006). Kinetic temperatures in the 72-120 km altitude range were retrieved from Cryogenic Infrared Spectrometers and Telescopes for the Atmosphere 15 μm CO_2 limb radiances using the non-local thermodynamic equilibrium retrieval pattern. The large-scale circulation in the mesosphere and lower thermosphere region is characterized by downwelling over the winter pole with the temperature increase and upwelling over the summer pole where temperatures are low. Based on the analysis of data from the Collm observatory, eastward zonal winds prevail in Central Europe at heights near 95 km. The winds weaken short after equinoxes, in spring even temporarily change to westward. The meridional circulation is weaker, being southward during the year. Strong sudden stratospheric warming can influence the MLT dynamics. During major winter stratospheric warming events, winds in the MLT weaken or reverse from westerly to easterly and the meridional circulation strengthens. However, the prevailing or mean state of the MLT region is often masked by increased wave activity. Turbulence in the upper atmosphere occurs only up to the turbopause (105-110 km); it is not developed at higher altitudes due to the molecular viscosity rising with height (Kazimirovsky et al., 2006).

The circulation at heights above ~120 km is of global scale and changes rather slowly. It is substantially influenced by the interaction between neutral and ionized particles. The model analysis by Kazimirovsky et al. (2006) has revealed two rather stable types of the general circulation in the *E* region (100-140 km) independent of the

solar activity. The prevailing zonal wind at mid latitudes is eastward in spring and summer and westward in autumn and winter. Very variable wind directions were found for the *F* region. At solstices, the wind direction is more stable and it is possible to distinguish the prevailing southwestward direction at geographic latitudes over 35°. The prevailing meridional wind is poleward in summer for high and mid latitudes and equatorward in winter. In heights above ~200 km, the solar heating and cooling generate intense diurnal variations in wind directions. In the upper thermosphere, the wind is oriented from the warm afternoon sector to the cold early morning sector across the polar regions and zonally at lower and mid latitudes. Near noon the wind is poleward and near the midnight it is equatorward (Blum and Harris, 1975). The diurnal variations of the winds are controlled by the season and geomagnetic latitude, and by strong atmospheric tides.

1.3. Vertical coupling in the atmosphere

The atmospheric layers are coupled to each other and the energy and mass is transferred between them. The influence on the upper atmosphere from below has been known for years, whereas discussions of a possible upper atmosphere influence on lower lying atmospheric layers has started only recently.

The dense and dynamic lower atmosphere is a source of strong internal waves of a broad period spectrum which carry the energy and momentum upward through various atmospheric regions. In the process of their generation, the waves extract some energy and momentum from the surrounding medium. The amount may be small in the environment of the lower atmosphere, but may affect significantly low-density upper atmospheric regions where the waves are then dissipated and their energy and momentum are converted into heat, kinetic energy, and momentum of the mean flow. It appears that the temperature in the thermosphere is increased by long period waves coming from below; momentum deposition by dissipating waves modifies the thermospheric circulation (Gossard and Hooke, 1975).

The maximum electron density of the *F2* layer (NmF2) varies from day to day with a standard deviation of ~15 % (Rishbeth, 2006). This variability is mainly attributed to the geomagnetic activity; the day to day variability of the flux of solar electromagnetic radiation plays only a minor role. Meteorological processes in the

lower ionosphere also contribute to the day-to-day variability of the *F2* layer (Forbes et al., 2000). Various meteorological processes in the troposphere and to a limited extent also in the stratosphere and mesosphere affect the ionosphere mainly through upward propagating waves in the neutral atmosphere (Laštovička, 2006). The processes which couple the waves with ionospheric changes include modification of turbulent mixing, influences on *E*-region conductivities, modulation of the temperature and wind field in the thermosphere, and the generation of electric fields through the dynamo mechanism (Forbes et al., 2000). The wave perturbations of the rate of production do not play an important role, except for the case, when the wave front is in alignment with the direction of ionizing radiation flux. In the lower ionospheric regions, waves may modify the rate of loss of ionized particles. Most significant is the modification of the plasma transport by waves (Yeh and Liu, 1974).

However, Rishbeth (2006) recommends a cautious approach and points out the transient effect of waves on the ionosphere, particularly of waves of shorter periods, since those waves do not affect the chemical composition of the upper atmosphere. Rishbeth (2006) also expresses some doubts about the importance of meteorological activity for the ionospheric variability in European mid latitudes. He reports a study which deals with changes of the critical frequency of the *F2* layer (foF2) during severe storms and with variability of foF2 related to the variability of standard meteorological parameters. No obvious links between individual meteorological storms and the *F2* layer were observed, whereas a notable similarity between the 10-day trends of foF2 and the ground level air pressure and correlation between foF2 and the surface temperature were found. Nevertheless, Rishbeth interprets these correlations cautiously, since both ionospheric and tropospheric parameters are influenced by external sources, e.g. by the flux of solar radiation and its seasonal changes.

1.4. Atmospheric waves

Atmospheric wave motions are the result of action of inertial forces on one hand and restoring forces on the other hand. The periods of waves which can influence the ionosphere range between several minutes and several days. Waves propagate directly or indirectly to the upper atmosphere and may be altered by nonlinear interactions,

particularly in the mesosphere-lower thermosphere region. Some types of waves originate also at ionospheric heights (Laštovička, 2006).

Planetary waves extend in the period range of about 2-30 days. In summer when the easterly mean zonal circulation dominates in the middle atmosphere, planetary waves are essentially restricted in the lower atmosphere. In winter westerly mean zonal winds, the waves penetrate up to heights slightly above 100 km. The propagation to the *F* region heights is indirect via modulating the carrying agent. Planetary waves influence all ionospheric layers, critical frequencies of the layers (foEs, foF2), heights of the layers (h'E, h'F), and height of maximum electron concentration respectively (hmF2). Planetary waves typically occur in bursts of a couple of waves. Typical wave periods are about 2, 5, 10, and 16 days, but the wave spectrum is very variable on individual days. Amplitudes of the waves are unstable as well (Kazimirovky, 2006; Laštovička, 2006).

Periodic solar heating of the atmosphere is considered as a source of atmospheric tides. Dominant periods of the tides are 24 and 12 h, at higher latitudes also 8 h. The tidal amplitude in winds in the upper mesopause region at mid latitudes is larger than the speed of the prevailing wind. Tides coming from below play an important role in processes of formation of the *Es* layers and contribute significantly to the variability of foE and foF2 (Laštovička, 2006).

Waves of periods between several minutes and a few hours are called gravity waves. The spectrum is at high frequencies restricted by the Brunt-Väisälä frequency, ω_b,

$$\omega_b = \frac{g}{H}\frac{\gamma - 1}{\gamma}, \tag{1}$$

where g is the gravitational acceleration, γ is the ratio of the specific heats and H is the scale height (Davies, 1990). Fig. 3 shows the vertical profile of the acoustic cut off period and Brunt-Väisälä period computed for U.S. Standard Atmosphere, 1976 (USSA1976). Parameters of the USSA1976 were computed using the routine by S.Pietrobon (www.sworld.com.au/steven/space/atmosphere/). Yeh and Liu (1974) point out that a direct interpretation from observations of frequency cut off at Brunt- Väisälä frequency would give an unrealistic thermospheric temperature. It is hypothesized that the cut off has been Doppler shifted by neutral winds (Davies et al., 1973; Gupta et al.

1973). Hunsucker (1982) distinguishes two groups of gravity waves according to their wave velocity and period: large scale and medium scale gravity waves. Large scale gravity waves of horizontal wavelength more than 1000 km and periods between 30 min and 3 h propagate in the thermosphere with horizontal velocities 400-1000 $m \cdot s^{-1}$. Medium scale gravity waves, which are assumed to come to the thermosphere from below, have horizontal velocities between 100 and 250 $m \cdot s^{-1}$, wavelength of several hundred kilometres and periods 15-60 min. Gravity waves play an essential role in the thermal regime and composition of the middle and upper atmosphere (of the neutral atmosphere as well as of the ionosphere) and contribute significantly to its general circulation, structure and variability (Kazimirovsky et al., 2006). Vadas and Fritts (2004) emphasize the potential of gravity waves to influence very high atmospheric altitudes because of their relatively large vertical wavelength and their propagation, at least initial, in all direction from the source. When assessing the influence of gravity waves in the lower and middle atmosphere (at altitudes up to ~110 km), there is an important property of gravity waves to be reminded. Dominant energy and momentum fluxes occur at opposite ends of the frequency spectrum. It means gravity waves which have the largest amplitudes, energy densities, and horizontal scales do not have the largest energy and momentum fluxes and atmospheric effects (Fritts et al., 2006). Climatological studies of gravity waves in the middle and upper atmosphere over Japan revealed almost continuous presence of gravity waves in the *F* region (Oliver et al., 1997). In the *E* region, gravity waves contribute to the formation of the *Es* layer (e.g. Matthews, 1998; Fukao et al., 1998; Kazimirovsky et al., 2003); probably due to the enhancement of irregular neutral winds associated with gravity waves (Parkinson and Dyson, 1998). Large scale gravity waves are excited by enhanced activity in auroral zones and propagate horizontally to lower latitudes. In the ionosphere, they appear in the form of travelling ionospheric disturbances. Gravity waves may also emerge in situ during the solar eclipse or passage of the solar terminator. Boška et al. (2003) observed systematic occurrence of gravity waves of 60-90 min period at sunrise. The increased wave activity continued for several hours. The source of waves was related to the passage of the solar terminator and was located at heights of about 180-220 km. On the other hand, gravity waves associated with the evening passage of the terminator occur less regularly and are weaker (e.g. Altadill et al., 2004). Local body forces which arise

as a consequence of gravity wave breaking belong to the important sources of gravity waves at higher altitudes (Fritts et al., 2006). A significant amount of gravity waves comes to ionospheric heights from below. Meteorological activity in the lower atmosphere is a quasi-permanent source of gravity waves. Earthquakes, volcanic eruptions, big explosions belong to the sporadic sources of gravity waves (Laštovička, 2006).

Acoustic cut off frequency, ω_a is the low frequency limit of the acoustic wave band,

$$\omega_a = \frac{C}{2H} , \qquad (2)$$

where C is the speed of sound and H is the scale height (Davies, 1990).

Waves of high frequencies are strongly absorbed by the atmosphere. Georges (1967) quotes Lord Rayleigh (1894) that the rate of absorption is proportional to the wave frequency squared. Thus, only waves in the low frequency band of acoustic spectrum (infrasound) may propagate to ionospheric heights. Blanc (1985) states that only waves of frequencies lower than 1 Hz are observed in the upper atmosphere. The refractive index, n is indirectly proportional to the square root of the absolute temperature. Due to the shape of the temperature profile in the lower and middle atmosphere, infrasound excited near the surface is focused upwards in the troposphere and mesosphere and the main part of energy propagates up to the base of the ionosphere. Thus, infrasound is more efficient in energy transfer to ionospheric heights than other types of waves (Laštovička, 2006). On the other hand, infrasonic waves affect due to the focusing only spatially constricted region in the upper atmosphere. Infrasonic waves are emitted by artificial as well as natural processes. Most of the sources can be described as occasional or sporadic. They include volcanic eruptions, earthquakes, solar eclipses, passage of the solar terminator in lower latitudes, auroral activity, bolides and meteorites, nuclear and chemical explosions, supersonic jets, and spacecraft launches. Meteorological activity and ocean waves are considered as continuous sources of infrasound (Laštovička, 2006; Rind, 1978).

1.4.1. Propagation of acoustic and gravity waves in the atmosphere

When dealing with the propagation of acoustic-gravity waves in the atmosphere, several factors must be taken into account: the decreasing density of the atmosphere in

the vertical direction, the temperature variations with height, background wind field, radiative damping, and loss mechanisms which convert wave energy into heat. Those mechanisms include ion drag, thermal conductivity and viscosity (Yeh and Liu, 1974). The atmosphere is for propagating gravity waves a dispersive and anisotropic environment. A propagating wave is influenced by the effects of the gravity force, when the wave period approaches or exceeds the local Brunt-Väisälä (buoyancy) period. Since the gravity force acts only in one direction, the process is anisotropic. The dispersion of sound waves is negligible, but increases with increasing wave period (Yeh and Liu, 1974; Davies, 1990).

If the wave were propagating upwards in a non-dissipative atmosphere, its amplitude, ζ would be growing exponentially with height, h,

$$\zeta = \zeta_0 \exp\left(\frac{h - h_0}{2H}\right), \tag{3}$$

where ζ_0 is the amplitude at height h_0 (Davies, 1990).

It is not in contradiction to the energy conservation principle, since the air density decreases exponentially with height. At a certain altitude, the wave may be saturated or even break. Above the level of breaking, the turbulence sets in and leads to diffusion of heat and momentum of the wave. The smaller the initial amplitude of the wave, the higher it must penetrate to increase its amplitude enough and break (Andrews et al., 1987). However, in the real atmosphere, counteracting processes of the wave damping remove some amount of energy from the wave at each altitude. At heights where the damping processes become dominant over the air density decrease effects, the wave amplitude reaches its maximum (Georges, 1967). Thus, the waves often do not reach the amplitude of breaking at all or the height of wave breaking is possibly moved upwards. It is believed that breaking gravity waves contribute to the rapid increase of temperature in the lower thermosphere.

Molecular kinematic viscosity increases with height and counteracts the wave amplitude growth due to the decreasing atmospheric density. The amplitude of the wave reaches a maximum at a certain level that depends on the wave frequency and on the direction of propagation. The wave then vanishes. Molecular kinematic viscosity determines temporal as well as space scales of acoustic and gravity waves. Viscosity removes small scale components from the wave, thus the scale of the wave tends to

increase with height (Hines, 1960). When the waves propagate to a turbulent environment, high eddy viscosity and thermal conductivity cause a rather sudden damping of the waves. At the earth surface, eddy viscosity is 10^6 times higher than the molecular viscosity (Gossard and Hooke, 1975); the exact value varies in time determined by meteorological conditions. It is generally accepted that the eddy viscosity and thermal conductivity play a dominant role up to the turbopause; above turbopause the molecular viscosity and thermal conductivity is crucial. Thermal conductivity seems to act in a way similar to viscosity and it is significant particularly in the upper atmosphere (Pitteway and Hines, 1963). Thermal conductivity affects gravity waves slightly more than viscosity. Contrary, acoustic waves are slightly more influenced by viscosity than by thermal conductivity. Waves that are strongly affected by viscosity are also strongly influenced by thermal conductivity. Waves unaffected by viscosity are only negligibly influenced by thermal conductivity (Gossard and Hooke, 1975).

In the ionosphere, ohmic losses due to the ion drag become important. The geomagnetic field constrains motion of electrons above the height ~90 km and the motion of positive ions above ~140 km. During the daytime, collisions between neutral and ionized particles influence the propagation of waves of periods larger than about one hour. At night, this period still increases.

Variations in temperature with height alter the acoustic cut off frequency and the Brunt-Väisälä frequency (Fig.3), limits of the forbidden frequency range, where waves cannot propagate vertically. Brunt-Väisälä frequency is also influenced by changes with height in gas composition and by the decrease of the gravitational acceleration with height (Gossard and Hooke, 1975).

Further, prevailing winds act as a directional filter that disables waves propagating in a certain direction to reach the ionosphere (Rind, 1978; Cowling et al., 1971). Medium scale gravity waves propagate in a direction essentially opposite to the direction of the neutral wind (Bertin et al. 1975). Šauli (2000) describes the behavior of gravity waves in critical layers. In a critical layer, the wave frequency is shifted to zero due to winds and the wave energy is deposited here. The dissipation of gravity waves might be concentrated in a very thin layer near the critical layer. If the region of wind variations with height is wide enough, a number of wave modes reach its critical layer and then are not present in the wave spectrum in higher altitudes. In heights up to

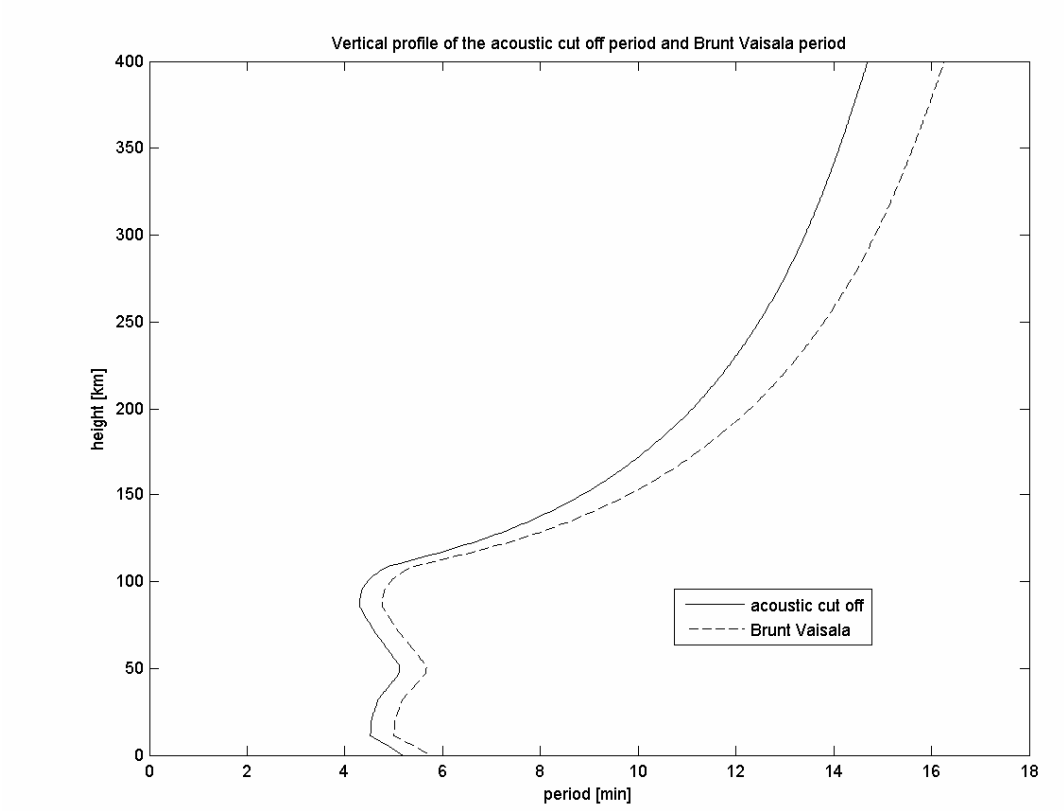

Fig.3. *Vertical profile of the acoustic cut off period and Brunt-Väisälä period in the USSA1976 (computed using the routine by S.Pietrobon, www.sworld.com.au/steven/space/atmosphere/).*

110 km, a wide range of wave frequencies deposits the energy in this way (Hines, 1968). Korsunova (1991) found in both foEs and hEs that gravity waves penetrate from below more often in winter than in summer. It is probably due to seasonal changes of the circulation in the middle atmosphere.

The properties of acoustic-gravity waves are described by the dispersion relation. The classical dispersion relation formulates the relations between the angular wave frequency and the wave vector (e.g. Gossard and Hooke, 1975; Georges, 1967).

Vadas (2007) derived a dispersion relation for gravity waves which includes the damping effects of molecular kinematic viscosity and thermal diffusivity in the thermosphere and is valid before and during dissipation. It was assumed that acoustic waves can be neglected. Incorporating this dispersion relation in a ray trace model, Vadas (2007) calculated a number of properties of a wide range of gravity waves which

originate at different altitudes, including the lower atmosphere, and propagate upwards. Dissipation altitudes, horizontal distances traveled, times taken, and maximum vertical wavelength prior to dissipation in the thermosphere were obtained for a wide range of thermospheric temperatures.

Gravity waves generated by a tropospheric source belong to medium scale gravity waves according to the classification of Hunsucker (1982). The model results of Vadas (2007) for atmosphere with no background winds show that waves with horizontal wavelength, $\lambda_h < 500$ km, intrinsic horizontal phase speed, $c_{IH} \geq 100$ m·s^{-1}, and period, $\tau <$ 60 min dissipate at altitudes ~150-250 km (i.e. the waves have a maximum momentum flux at ~150-250 km) and are observable up to heights ~165-300 km. The waves travel the horizontal distance less than ~2000 km prior to dissipating. Gravity waves with periods smaller than 7 min do not dissipate above the altitude ~150 km. In general, gravity waves dissipate at higher altitudes during active solar conditions than during extreme solar minimum, since the molecular kinematic viscosity is much smaller in the hot than in the cold thermosphere at the same height. Further, the dissipation altitude is influenced by background winds. Gravity wave propagating down the wind is Doppler shifted to a smaller intrinsic frequency and the vertical wavelength λ_z decreases while the wave propagating up the wind is shifted to a larger frequency and the vertical wavelength λ_z increases. As a result, gravity waves moving against the wind can penetrate to higher altitudes than gravity waves moving into the wind (Vadas, 2007).

Gravity waves generated by convection dissipate at the approximate altitude ~180 km. Body forces produced at the dissipation altitudes are supposed to generate medium scale gravity waves. The dissipation altitude of gravity waves launched at thermospheric heights depends closely on the thermospheric temperature; the dissipation height during extreme solar minimum is ~250 km, during very active solar conditions, the waves penetrate to heights ~450 km prior to dissipation. Upward propagating gravity waves generated in the thermosphere may appear quasi periodic with significantly decreasing amplitudes over a wave cycle or two (Vadas, 2007). The model results of Vadas were compared with a number of observational results (Vadas, 2007 and references therein) and mostly corresponded to the observations.

Sun et al. (2007) studied the propagation of gravity waves in the atmosphere with background winds using a three-dimensional transfer function model, which was based on the complex dispersion relation of gravity waves in a stratified dissipative atmosphere with background winds. The authors emphasize that unlike the ray trace model which can only be used to study a monochromatic wave, the transfer function model is applicable also to study the propagation of wave packets. Moreover, it provides the distribution characteristics of the disturbance in the time-space domain. Sun et al. (2007) found that gravity waves propagating up the wind penetrate to higher altitudes than those propagating down the wind, which corresponds with the results of Vadas (2007). The transfer function model showed that the atmosphere acts like a band pass filter for propagating gravity waves generated near the earth surface. It supports propagation of waves with periods ~15-30 min and horizontal wavelengths ~200-400 km to ionospheric heights of ~300 km. Other periods are filtered by the viscosity and thermal conductivity and by background winds; the filtering effect increases towards long and short periods. Sun et al. (2007) intend to make the comparison of model results with observations in a further study.

1.4.2. Observations of infrasonic and gravity waves generated by tropospheric weather systems

Gravity waves

Dominant mechanisms of excitation of gravity waves in the lower atmosphere are convection, orographic forcing of the air flow, and wind shear (Fritts et al., 2006). Other sources which may be significant at preferred sites or in association with specific larger scale dynamics include adjustment of unbalanced flow in the vicinity of jet streams and frontal systems. The unbalanced flow may also arise as a response to local body forces due to gravity wave dissipation and momentum flux divergence (Fritts and Alexander, 2003). Spatial and temporal scales of adjustment processes vary widely. Spontaneous adjustment of the large-scale flow occurs on a time scale of hundreds or thousands of kilometres and several hours. Shear instability and gravity wave breaking result in small-scale flows of tens of kilometres or less and of time scales of an hour or less (Fritts et al., 2006).

Convection generates gravity waves throughout the full range of phase speeds wave frequencies, and vertical and horizontal wavelengths. Convectively generated gravity waves are of horizontal wavelength ~10-1000 km and of periods of minutes to tens of hours; largest amplitudes, frequencies, and momentum fluxes accompany deep fast and spatially localized convection. Gravity waves are generated by forcing by individual convective cells and radiate in circular patterns outward from their sources (Vadas and Fritts, 2004). Three mechanisms are thought to explain the generation of gravity waves by convection. These are (1) the obstacle effect where the wind shear at cloud tops imposes relative motion over convective cells, (2) thermal forcing through latent heat release, and (3) an effect of a mechanical oscillator in which oscillatory convective plumes project those periods onto the gravity waves field (Fritts and Alexander, 2003). The mechanical forcing of the atmosphere is associated with the expansion of the air in a cell. If the forcing is impulsive, it generates a broad frequency spectrum of waves. Quasi-sinusoidal oscillations of the air column which occur in convective storms give rise to a periodic forcing and generate quasi-sinusoidal waves. The heat release in a storm tends to generate waves of a given vertical wavelength λ_z rather than waves of a given period. The heated air column generates waves whose half-wavelength $\lambda_z/2$ is equal to the overall length of the column. The three mechanisms operate in reality simultaneously (Sentman et al., 2003). Recent study of Lane and Clark (2002) has shown that oscillatory motions are the primary source of gravity waves; gravity wave structures are determined mainly by filtering effects. Zones of the deep tropical convection are the dominant sources of convectively generated gravity waves and possibly the most important sources of high frequency gravity waves on the Earth. Deep intense convection supports the generation of gravity waves of large vertical wavelengths (and phase speeds) which propagate in all directions from the source. Therefore, at least a portion of waves is able to influence high atmospheric altitudes (Vadas and Fritts, 2004 and references therein).

Mountain waves play a role particularly in the lower atmosphere, but may also penetrate to the upper atmosphere and influence local and zonal mean structures of the stratosphere, mesosphere, and lower thermosphere. Since the phase speeds are near zero, mountain waves penetrate to high altitudes only under specific conditions when sufficiently nonzero winds exist in the whole vertical column of the atmosphere. This

process therefore occurs only at a few preferred sites (Fritts et al., 2006 and references therein). The wavelengths and frequencies may vary over a wide range of scales, however a single phase speed and frequency predominates (Fritts and Alexander, 2003; Fritts et al., 2006).

Wind shear as a source of gravity waves plays a significant role near the tropopause and at higher altitudes. Particularly the shear of the jet stream is likely a source that contributes significantly to the momentum budget of the middle atmosphere (Fritts et al., 2006 and references therein). Gravity waves are generated due to the instability of the shear layer. The instability can be excited by nonlinear collapse of Kelvin-Helmholtz billows in the shear layer. There are also observations suggesting that certain linear modes of shear instability can be excited. However, compared to convection and orography, wind shear as a source of gravity waves is relatively poorly understood (Fritts and Alexander, 2003; Fritts et al.,2006).

The mechanism of gravity waves excitation during the frontogenesis is similar to that of the jet stream adjustment. Moreover, associated convection and instability dynamics may excite gravity waves at higher ends of frequency and wave number spectra (Fritts et al., 2006).

The deep tropical convection is surely the most effective tropospheric source of gravity waves. Nevertheless, the observations of gravity waves generated by tropospheric weather systems in extratropical regions were reported by a number of authors.

Bertin et al. (1975) reported observations of gravity waves with periods 20-98 min in the *F* region in winter (January 1972). The reverse ray tracing method showed that the horizontal distance of sources at meteorological altitudes is in the range less than 1000 km to more than 3000 km. The most probable sources were in the vicinity of depressions - near warm, cold, and occluded fronts, close to a depression, and close to the path of the jet stream. It is believed that gravity waves are in such cases generated by geostrophic adjustment of an unbalanced flow. The experiment was based on ionospheric observations of Faraday rotation between a geostationary satellite and the ground based receivers located in the United Kingdom and in France, together with incoherent scatter observations in France.

Šauli and Boška (2001) described increased wave activity in the period range 50-100 min during the passage of weather fronts over the Czech Republic. Šauli (2000) analysed diurnal variability of electron concentration in heights 150-255 km. The study was based on ionosonde measurements with time step 15 min, therefore waves of periods longer than 45 min were analysed. During a cold front passage in February 1990 (geomagnetically quiet period, high solar activity), statistically significant occurrence of waves with periods 50-100 min was found in the *F* region as well as in the lower ionosphere. During the campaign in October – November 1997 (geomagnetically quiet period, low solar activity), increased wave activity in the period range 80-110 min was found, particularly in the *F* region. Amplitude of gravity waves in most cases grew up to heights 200-240 km, then it decreased. The region of maximum activity of gravity waves was by ~30 km lower than the *F* layer maximum of electron concentration (Boška and Šauli, 2001). Cold fronts are considered as the most efficient meteorological sources of gravity waves in mid latitudes (Laštovicka, 2006).

Sentman et al. (2003) observed gravity waves in the OH nightglow layer (altitude ~85 km) during a very intense thunderstorm over Nebraska, USA. During the two-hour interval, the horizontal wavelength and period of the gravity waves altered. At the early stages of the thunderstorm development, the horizontal and vertical wavelengths were 50 km and 30 km, respectively. The period was 9.8 min and the corresponding phase speed 85 $m \cdot s^{-1}$. One hour later, the parameters changed, the horizontal and vertical wavelengths decreased to 40 km and 20 km. The period extended to 11 min and the corresponding phase speed was 60 $m \cdot s^{-1}$.

Kelley (1997) observed gravity waves with the main spectral peak at period of 50 min and a secondary one at about 25 min in the *F* region. The waves were associated with a storm front with thunderstorm cells of a broad spectrum of space scales, which developed at the eastern coast of Virginia, USA in summer (July 1988).

Hung et al. (1979) described observation of gravity waves during an extreme tornado outbreak in April 1974. The Doppler sounders operating at frequencies 4.0125 MHz, 4.759 MHz, and 5.734 MHz were located in the central part of the USA (Alabama, Tennessee). Waves with periods 13-15 min and 27-30 min occurred in the ionospheric *F* region more than one hour before the tornado touchdowns.

Ionospheric response to a typhoon was observed in records of the HF Doppler shift records in the eastern part of China. It included medium scale travelling ionospheric disturbances with periods near 20 min which were gradually growing longer and spread *F* after sunset. During intense typhoons, S shaped traces in Doppler records were observed (Zuo Xiao et al., 2007).

Infrasonic waves

Tropical cyclones, tornadoes, convective storms, cyclones, weather fronts, mesoscale convective complexes, and air flow over mountainous terrain are considered as the most efficient meteorological sources of infrasonic waves (Laštovička, 2006).

The occurrence of infrasound at ionospheric heights during convective storms was broadly studied in North America, particularly in the 1960s and 1970s. Observations of infrasonic waves with periods 1-5 min in the ionosphere during nearby tropospheric convective storms were repeatedly reported (Georges, 1967; Baker and Davies, 1969; Chimonas and Peltier, 1974; Davies and Jones, 1973; Georges, 1973; Prasad et al., 1975). Spectral analysis revealed peaks near the periods 3.5 and 4.5 min. An event persisted several hours; Baker and Davies (1969) found in their study most typical duration 2-4 h. The amplitude of the Doppler frequency shift ranged from the minimum detectable (~0.1 Hz) to over 2 Hz (Georges, 1967), but most typically was between 0.1 and 1 Hz (Georges, 1973).

The wave spectrum may vary from event to event or even during one convective storm (Georges, 1973; Prasad et al., 1975). Prasad et al. (1975) found different spectral content in different geographical locations. In Oklahoma, the spectral peak was at 4-5 min period stably, whereas it varied in Florida. It is accepted that a convective storm system generates a broad spectrum of acoustic waves. Georges (1973) suggests that waves of longer periods appear rather with more severe storms, especially with those producing hail. The relatively narrow period band observed at ionospheric heights is caused by atmospheric filtering (Georges, 1967). Acoustic cut off prevents waves at the low period range of the acoustic spectrum from reaching the ionosphere; crucial is the minimum cut off period which normally occurs at the temperature minimum at the mesopause. The acoustic cut off period computed for USSA1976 has a minimum of 4.3 min at the height 86 km. Waves in the short period band are damped by the absorption.

Chimonas and Peletier (1974) propose that the spectral peaks are produced by interference of multiple wave reflections between the earth surface or the lower troposphere and the lower thermosphere.

Georges (1973) points out that the ionospheric effects are observable almost exclusively in the early evening. During the daytime, infrasonic waves appear less frequently in the ionosphere due to decreased refractive index in the lower thermosphere after sunrise (Georges, 1968). Chimonas and Peletier (1974) observed waves with periods of 3.5 and 4.5 min and horizontal phase speed between 800 and 3000 $m \cdot s^{-1}$ in the nighttime *F* region. Daytime monitoring showed waves with periods of 7-10 min and the horizontal phase speed of ~200 $m \cdot s^{-1}$ in the lower *F*-region. Preferably nighttime occurrence of 1-5 min waves was noticed also by Prasad et al. (1975).

The dynamics (mechanical motion) of storms is thought to be the source of wave disturbances rather than acoustic effects associated with lightning (Blanc, 1985). Pierce and Coroniti (1966) suggest buoyancy oscillations in convective clouds as a source of waves; such oscillations have periods near the local Brunt-Väisälä period. Moo and Pierce (1972) explained the occurrence of 3-5 min waves in the ionosphere by nonlinear interactions which double the source frequency. Later, Georges (1973) found particular efficiency in producing 3-5 min waves of those storms, during which the cloud tops penetrate the tropopause. Azimuth determinations of the wave travel often show an abrupt change of the source direction. Georges (1967) explains this phenomenon by the death of one emitter and emergence of another one nearby. It leads to an assumption that the source should be individual convective cells of the storm system.

Ionospheric effects are usually observed when a convective storm is active within the radius of 250 km from ionospheric observation point (Prasad et al., 1975). Georges (1973) quoted the radius 300 km. The geographically localized nature of disturbances is caused by defocusing of infrasonic waves at the base of the thermosphere due to rapidly increasing temperature (Georges, 1967). Baker and Davies (1969) show ray path in the 1962 U.S. Standard Atmosphere for acoustic waves with period of 4 min emitted by a ground source. Waves with the initial propagation angle of 30° from the vertical or less reach to the height of 300 km within a horizontal distance of about 250 km from the

source. Waves with initial propagation angle greater than 30° are reflected back to the ground below 200 km.

Baker and Davies (1969) introduced a severe weather index, which evaluated the intensity of convective storms. As indicators of severe weather conditions, the authors took into account the presence of extensive areas of radar echoes, lines of echoes, thunderstorms, strong convective cells, and echo heights in excess of 12 km; equal weight was assigned to each indicator. Baker and Davies (1969) found that the ionospheric infrasound occurred almost exclusively on days when the severe weather index reached its maximum value. On the other hand, a number of convective storms which contrary to reasonable expectations produced no observable ionospheric effects were reported (e.g. Georges, 1973; Prasad et al., 1975).

Baker and Davies (1969) suggested several possible explanations. First, the wave periods emitted by the source may not have been within the bandpass of the atmospheric filter either because characteristic periods vary from event to event or because the atmospheric filter had been altered by the temperature variations. Second, the temperature at the mesopause had decreased sufficiently to completely close the atmospheric window. Third, the source of acoustic waves may have been absent in the convective storm (Georges, 1973; Gossard and Hooke, 1975). The third explanation was in agreement with Georges (1973) who reported the absence of infrasound in the earth surface microbarograph measurements and considered some additional unknown condition that must be satisfied before infrasound emission appears.

Georges and Young (1972) analysed some possible mechanisms of acoustic wave generation by the method of energy comparison between observed infrasound and some hypothetical generating mechanisms. Georges and Young found a serious discrepancy between the calculated and observed power of the acoustic wave source or between observed and theoretical wave spectra and thus excluded following generating mechanisms: thunders generated by cloud-to-ground or cloud-to-cloud electrical discharges and perturbation of the atmospheric mean flow by the penetration of convective cells through the tropopause. They did not rule out violent turbulence in a convective storm as a possible source of acoustic waves.

The dependence of the observed ionospheric effects on geographical location and relative position of the convective storm and the point of ionospheric observation were

analysed by Georges (1973) and Prasad et al. (1975). The ionospheric oscillations appeared more often when the assumed source convective storm was to the north (in the northern hemisphere) of the ionospheric observation point than when it was to the south. Georges (1973) explained this directional effect by the way the waves propagated under the influence of the geomagnetic field. The emission of infrasound by convective storms seemed to depend substantially on the particular geographical location on the North American continent. According to Georges (1973), all significant observations of ionospheric waves generated by severe weather came roughly from the central part of the USA, i.e. Boulder, Colorado, to Huntsville, Alabama; Urbana, Illinois, to Little Rock, Arkansas. Doppler effects tended to be the most significant near the mid-continent. Baker and Davies (1969) reported observations of 2-5 min waves during severe convective storms in Kansas and Nebraska. Prasad et al. (1975) mentioned high incidence of the events in Oklahoma, whereas observations near Boulder, Colorado showed only a few ionospheric effects of convective storms. HF Doppler shift observations in Florida (Prasad et al., 1975) revealed surprisingly low incidence of ionospheric infrasound during convective storms. According to the high values of severe weather index in June – August 1971, which was introduced by Baker and Davies (1969), frequent occurrence of infrasound was expected. Instead, Prasad et al. (1975) observed a large number of days for which the Doppler records were severely marred during severe weather activity. The authors hence supposed it may be a different class of ionospheric effects of severe convective storms and noticed that the occurrence of the sporadic *E* layer had been associated with severe tropospheric convective storms by Rastogi (1962). Further, they explained the low incidence of ionospheric infrasound during convective storms by the fact that the tropopause over Florida was higher than in the central part of the USA by about 4 km and also point out local differences in the meteorology of the thundercloud formation. Microbarograph measurements showed similar results, severe weather infrasound observed at both Boulder, Colorado, and Washington, D.C. appeared to come almost exclusively from the part of the USA. In particular, none was ever observed from the direction of Florida. Baker and Davies (1969) and Georges (1973) also mentioned the seasonal occurrence of ionospheric effects of convective storms which maximised in mid summer on the Kansas-Nebraska border, was shifted to early summer in Oklahoma and to late spring in Arkansas.

In following years, ionospheric infrasound was nearly forgotten (Laštovička, 2006). Recently, the interest has been revived, mainly in context with the development of the International Monitoring System for the Verification of the Comprehensive Nuclear-Test-Ban Treaty. The aim is to find characteristics of signal from different sources and to be able to distinguish signal of an artificial explosive source from other types of infrasound (Krasnov et al., 2006 and references therein).

Drobzheva and Krasnov dealt in detail with modelling of infrasonic fields in the ionosphere from a surface point chemical explosion (Drobzheva and Krasnov, 2003) and from an underground nuclear explosion (Krasnov and Drobzheva, 2005). Krasnov et al. (2007) also studied propagation of infrasound from a sinusoidal source. Microbaroms, weather fronts, earthquakes, tornadoes, and severe storms belong to the sources of quasi-sinusoidal infrasonic waves. Model calculation shows that the acoustic wave energy is dissipated at different altitudes depending on the wave period. The height increases with increasing period, e.g. a 2-min sinusoidal wave deposits most of its energy at heights 283-385 km, whereas a 3-min wave dissipates between 323 and 431 km and a 5-min wave between 370 and 490 km.

2. Objectives

Waves emitted by various meteorological processes in the troposphere and propagating into the upper atmosphere have been observed in different regions worldwide. Depending on the type of the source, the waves showed periods covering the range from minutes to days. In the Czech Republic, a study of the wave activity in the ionosphere during passages of cold fronts has been made (Šauli, 2000). It was focused on wave periods longer than 45 min.

In 2004, continuous Doppler shift measurements at ionospheric heights were started in the Czech Republic. The installation of the Doppler sounding system has enabled the observation of high frequency waves down to periods of ~10 s. Doppler type of sounding equipment was used in experiments which were conducted in North America particularly during 1960s and 1970s. In these experiments, the occurrence of infrasonic waves in the ionosphere during convective storms was observed for the first time and was described in a couple of publications.

The present study deals with observation of waves in the period range 1-30 min at ionospheric heights in the Czech Republic. Observations on days with convective storms are compared with observations which were made on quiet days (definition of a quiet day in Chapters 3.2.1. and 3.3.6.); the aim is to recognize ionospheric effects of convective storms. Convective storms of different intensity were included in the study and the relationship between the type of ionospheric effects and convective storm intensity were searched for. Convective storms in Central Europe and in North America develop in different climatic conditions and thus may act differently as far as their influence on the upper atmosphere is concerned. Observations in both regions are compared and reasons for possible differences are discussed.

Acoustic-gravity waves generated by severe tropospheric weather do not carry any label which would help to identify them. Of course, if the direction and speed of propagation of waves is known, then it can help to identify the source of waves. However, one point measurements were available from the Doppler measuring system in the Czech Republic in analysed years 2005 and 2006. During the severe weather event in January 2007, records from three measuring paths were available for further analysis, but the Doppler trace was disturbed by spread and the strength of signal was fluctuating. Here, an attempt was made to find a method that can help to distinguish

waves generated by fluctuations of the geomagnetic field, which is one of the most common sources of ionospheric waves.

During geomagnetic storms, large scale waves propagate from auroral regions to lower latitudes. Therefore, days with low or only slightly increased geomagnetic activity were studied and the time behaviour of the local geomagnetic field at geomagnetic observatory Budkov was checked to reveal a possible direct influence of geomagnetic activity on the ionosphere.

3. Data and methods

Data used in the study were collected on observatories in the Czech Republic during the period 2005-2007 and include ionospheric, meteorological, and geomagnetic measurements. The position of the observatories is shown in Fig.4 (the situation in 2008 when the Doppler system network was completed).

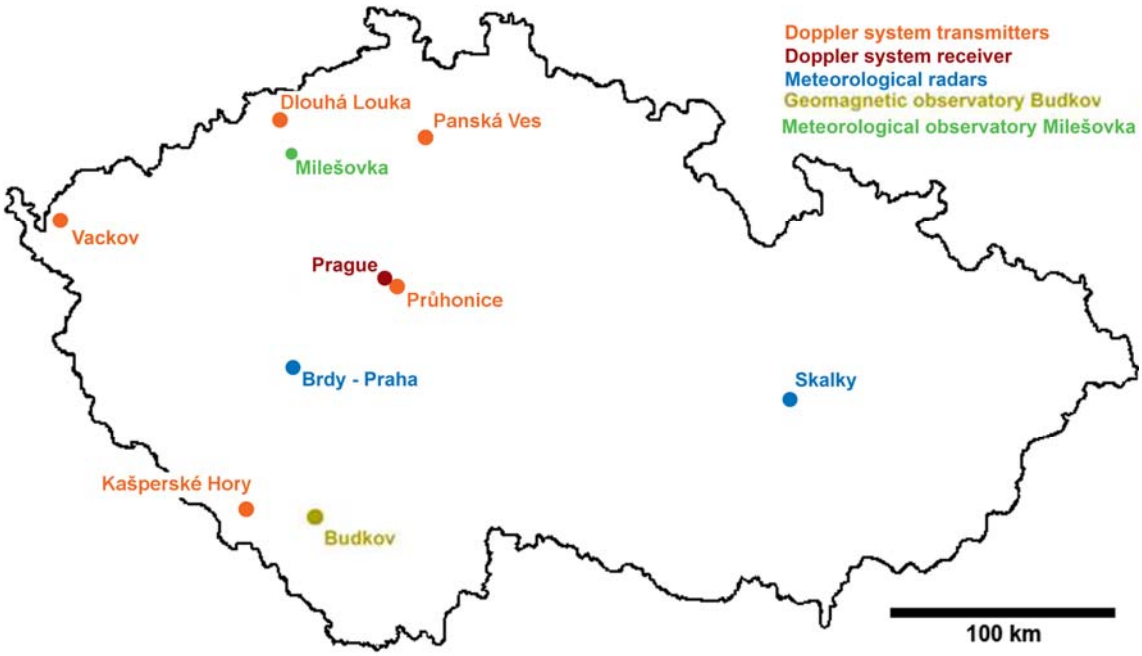

***Fig.4**. Scheme of the Doppler system network. Five point measurements were started in 2008. Location of meteorological radars in the Czech Republic, location of geomagnetic observatory Budkov, and location of meteorological observatory Milešovka are shown.*

3.1. Ionospheric data

The ionospheric sounding generally includes ground based measurements carried out by ionosondes, Doppler shift sounders, and backscatter radars. The topside ionosphere is sounded from satellites. Rocket campaigns were run in the past to determine vertical profiles of ionospheric parameters.

Here, high frequency (HF) continuous wave (CW) Doppler shift measurements and ionosonde data were used. HF CW Doppler shift measurements enable to monitor

the wave activity at ionospheric heights, including waves of short periods. From ionosonde data, information about the current state of the ionosphere and the height of reflection of the Doppler system sounding wave were obtained.

3.1.1. Ionosonde data

Ionosondes are one of the oldest and still one of the most important instruments of ionospheric sounding (Hargreaves, 1992). The ionosondes work on the same principle like radars. A radio pulse is transmitted vertically and from the time delay of the returned signal, the height of reflection is determined.

The refractive index, n is given by

$$n^2 = 1 - \frac{\omega_N^2}{\omega^2}, \tag{4}$$

ω_N is the plasma frequency and is proportional to the electron density; ω is the wave frequency. As the wave penetrates upwards, the electron density in the ionosphere increases, thus the refractive index gets smaller. At the height, where $n = 0$, the wave is reflected. It is the height where the wave frequency equals the plasma frequency. If the wave exceeds the maximum plasma frequency (the critical frequency) of the ionospheric layer, it penetrates the layer. When calculating the height of reflection, the wave is assumed to travel with the speed of light. In fact, it travels with lower speed due to the decreasing refractive index, therefore the real height of reflection is always smaller then the calculated virtual height. Due to the existence of the geomagnetic field, the radio wave is split into two modes with opposite polarization, called the ordinary and extraordinary wave. The sounding is visualised using ionograms, where the frequency vs. virtual height of reflection is plotted (Fig.5).

In the Czech Republic, the Digisonde DPS-4 has been used since 2004, when it replaced the older ionosonde. The Digisonde is located at the observatory Průhonice (49°59'N, 14°33'E). The sounding is conducted in regular 15 min intervals. In addition to the standard vertical ionospheric sounding, ionospheric drifts in the *E* layer (*Es* layer in summer) and *F* layer are measured.

Information about the current state of the ionosphere, particularly the existence and height of ionospheric layers were obtained from Digisonde data. Further, the virtual height of reflection of the 3.59 MHz wave was determined, which is the frequency of

the Doppler system sounding wave (details about Doppler type measurements in chapter 3.1.2.).

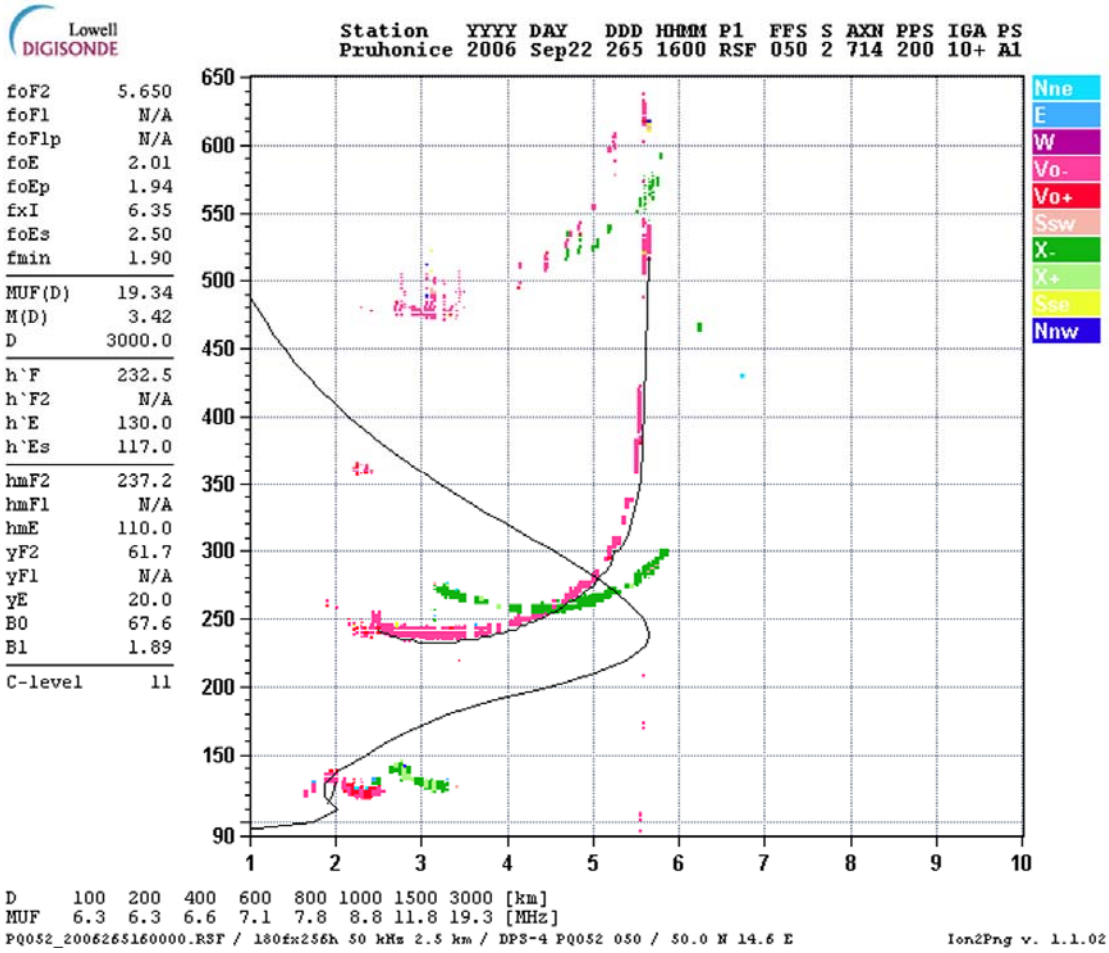

Fig.5. *Ionogram at Průhonice observatory on 22 September 2006, 16:00 UT. Reddish colors: ordinary wave. Greenish colors: extraordinary wave. Calculated verical profile of electron concentration is shown by the black line. Selected ionospheric parameters are listed in the left column.*

3.1.2. High frequency continuous wave Doppler shift measurements

Detection of high frequency changes in the ionosphere requires data sampling at relatively high frequencies. Most instruments for ionospheric sounding, including ionosondes, sample at much slower rate. The high frequency continuous wave Doppler shift sounding has been used since 1950s – 1960s and has proved as a sensitive detector of atmospheric oscillations of a wide range of periods (e.g. Bauer, 1958; Davies, 1962; Georges, 1967; Georges, 1968). A modern Doppler sounder developed in the Institute of Atmospheric Physics (IAP), Prague is able to monitor wave motions down to periods of ~10 s and is suitable for monitoring of large scale waves at the same time (Chum et al., 2005; Chum et al., 2008).

The HF CW Doppler shift sounders transmit a radio wave of a stable known frequency to the upper atmosphere. The wave is reflected by the ionosphere back to the ground. The Doppler sounders measure the frequency shift between the transmitted and received signal. From the Doppler frequency shift, the speed of the vertical movement of the reflection layer can be subsequently determined. In the ionosphere, movements of ionized particles are coupled with the dynamics of the surrounding neutral atmosphere. The exact parameters of the coupling processes depend on several factors. In general, the coupling of the ionospheric plasma with the neutral gas decreases with increasing height due to the decreasing density of the atmosphere and due to the influence of the earth magnetic field on the ionospheric plasma. Thanks to the coupling, HF CW Doppler sounding technique that is used for observations of movements of ionospheric plasma enables also monitoring of acoustic-gravity waves which propagate in the neutral upper atmosphere.

A HF CW Doppler sounder including special software was developed in the Institute of Atmospheric Physics (IAP), Prague. The transmitted frequency of 3.5945 MHz is derived from the 10 MHz Oven Controlled Crystal Oscillator (OCXO) by means of the direct digital synthesis (DDS). The OCXO of the same spectral characteristics is used at the receiving site. The desired frequency is tuned by means of DDS, but it is shifted 80 Hz away from the transmitted one in order to get the signal to noise ratio as high as possible. The best obtainable frequency resolution is ~0.018 Hz. The precise time synchronisation of the transmitters and receivers is ensured by the GPS (Chum et al., 2008).

In 2004, the first transmitter was placed at the Průhonice observatory (49°59'N, 14°33'E), which is at about 8 km distance from the receiver, located at IAP (50°02'N, 14°28'E). A great advantage of this topological arrangement is the common volume measurement with the Digisonde DPS-4 located at Průhonice. Thus, the virtual height of reflection of the 3.59 MHz wave can be determined directly from ionograms. The drawback of this arrangement is the strong ground wave that is often observed and that makes the detection of small Doppler shift (less than ~0.04 Hz) impossible. The ground wave is cleaned away in the frequency domain if necessary. However, the reflected wave is removed as well, when its Doppler shift is close to zero. On the other hand, the ground wave provides a direct verification of the stability of the oscillators and zero drift line. At the beginning of April 2005, another transmitter was installed at the Panská Ves observatory (50°32'N, 14°34'E). Two more transmitters located at Dlouhá Louka (50°39'N, 13°39'E) and at Kašperské Hory (49°08'N, 13°35'E) observatories, were set in operation at the beginning of 2007. The network was completed at the end of 2007, when the fifth transmitter at Vackov (50°14'N, 12°22'E) was added. Quite recently, second temporary receiver has been installed at Květná (50°12'N, 12°31'E). The frequencies of transmitters are mutually shifted by 4 Hz; the shift of sounding frequency enables to use only one receiver at the receiving site. The Doppler system network thus evenly covers the western part of the Czech Republic. Measurements can be conducted simultaneously on ten measuring path. Five point measurements with the receiving site at IAP, Prague are routinely used. In addition, three microbarographs were installed in 2008 near Doppler system transmitters at Panská Ves (50°31'N 14°34'E), Průhonice (49°59'N 14°32'E), and at the location Nový Kostel (50°13'N 12°26'E), which is near the Doppler transmitter at Vackov. Thus, surface pressure oscillations can be observed simultaneously with continuous HF Doppler shift measurements at ionospheric heights. The HF CW Doppler sounder was in detail described by Chum et al. (2008).

3.1.3. Analysis of HF CW Doppler shift measurements

The received signal was converted to low frequencies (from the order of MHz to the order of tens of Hz) and digitised by the precise sigma delta analogue to digital converter. A spectral analysis was subsequently performed resulting in Doppler shift

spectrograms. The overview spectrograms were in the time resolution of 1 min and display 8 hours of the record (Fig. 6). They provided basic information about the wave activity and the Doppler shift behaviour. To achieve high frequency-time resolution of the observed Doppler shift, the successive spectra were obtained by shifting Gaussian window of the width ~10 s by a time step less than the width of the window in the time domain. This technique enabled the analysis of higher frequency waves, down to periods ~10 s (Fig.7). Of course the frequency resolution was reduced in that case (Chum et al., 2008). In further analysis, a value of the Doppler shift which fits best the observation in each time step was found, thus an unambiguous function of Doppler shift on time was obtained. The function could not be determined in time intervals, when the signal containing a relatively broad band spectrum of the Doppler shift due to the reflection from a spread layer or any kind of multiray reflection was received. In such intervals, the function was replaced by a function with constant Doppler shifts or by a monotone increasing or decreasing function. The aim was to eliminate incorrect "wave motions" from the Doppler record which usually occur when the Doppler record contains a broad band spectrum of the Doppler shift and simultaneously to avoid the creation of sharp Doppler shifts at the beginning and at the end of the interval which would distort the results of the spectral analysis. The results of wavelet transform in such time intervals were not taken into account.

Analysing the spectral content of the function of Doppler shift on time, information about typical periods of the observed waves was found. To obtain simultaneously a maximum frequency and time resolution for different periods, a continuous wavelet transform based on the complex Morlet wavelet was applied. Using a complex wavelet and computing the modulus and angle, it was possible to get amplitude and phase of waves. To evaluate the intensity of wave activity in the ionosphere, information about wave amplitudes was required.

The Fourier transform was used in addition to the wavelet transform. Gravity waves originating from different sources are nearly always present in the upper atmosphere and gravity waves generated by severe weather do not carry any label which would enable their identification. Therefore, gravity wave spectra on quiet days were analysed in the first step. Thus, it was possible to identify periods of waves emitted by regular sources (e.g. solar terminator). A quiet day meant a day with quiet or unsettled

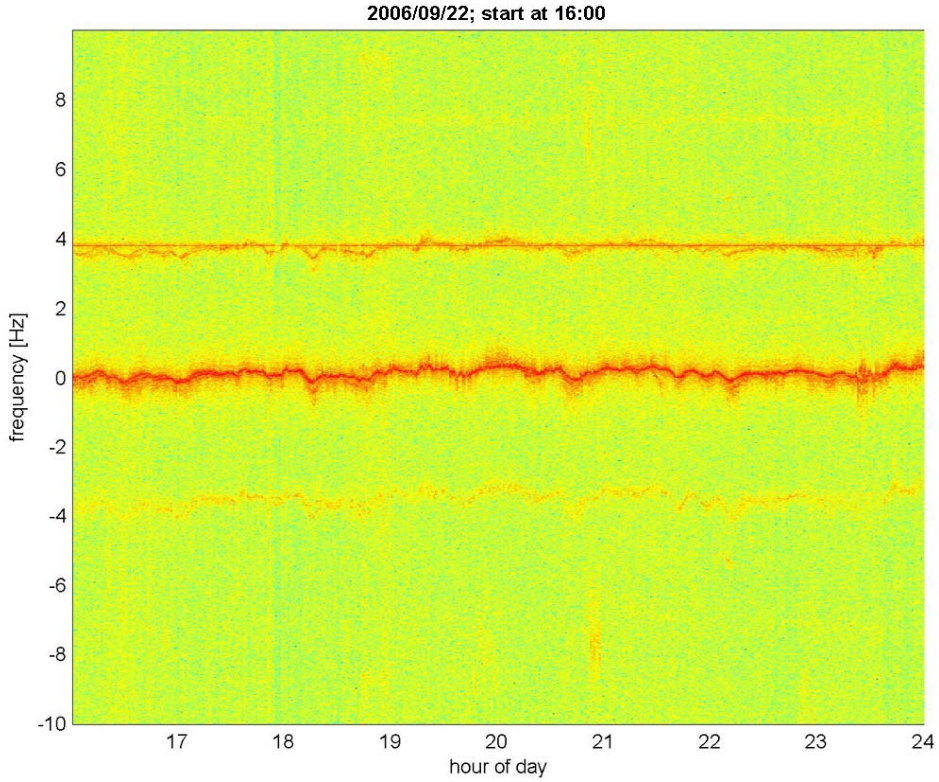

Fig.6. *Overview Doppler shift spectrogram; 22 September 2006, time=0 is at 16:00 UT. Top trace near 4 Hz: Measuring path Průhonice-Prague. A strong ground wave makes reliable detection of small Doppler shifts impossible. Middle trace near 0 Hz: Measuring path Panská Ves-Prague. Doppler shift measurements from Panská Ves-Prague path were analysed in the present study. Bottom trace near -4 Hz: weak signal of test measurements at Dlouhá Louka-Prague path.*

geomagnetic field (Kp $\leq$ 3, Dst $\geq$ -20 nT) and low meteorological activity in the troposphere; i.e. weather in Central Europe was governed by a high air pressure system or a flat low. Due to known different effects of the morning and evening passage of the solar terminator on the ionosphere (Boška et al., 2003; Altadill et al., 2004), the late night/morning part of the day (~00:00-06:00 UT) and the afternoon/evening part of the day (~16:00-24:00 UT) were analysed separately. During the daytime (~06:00-16:00 (or to 18:00) UT), the HF signal was usually reflected in the *E* region and experienced low Doppler shift close to zero. Median, upper and lower quartiles were calculated from wave spectra obtained for individual quiet days and served as a reference Fourier spectrum. Due to a relatively low number of cases in the data set, the application of

median and quartiles was supposed to be more representative than the mean value and related standard deviation, particularly due to the influence of extreme values. The computed statistics was compared with the spectral content of the Doppler shift measurements during individual cases of nearby convective storms. Periods, whose amplitudes in the frequency domain exceeded significantly mean values for quiet days, it means exceed the upper quartile, were found.

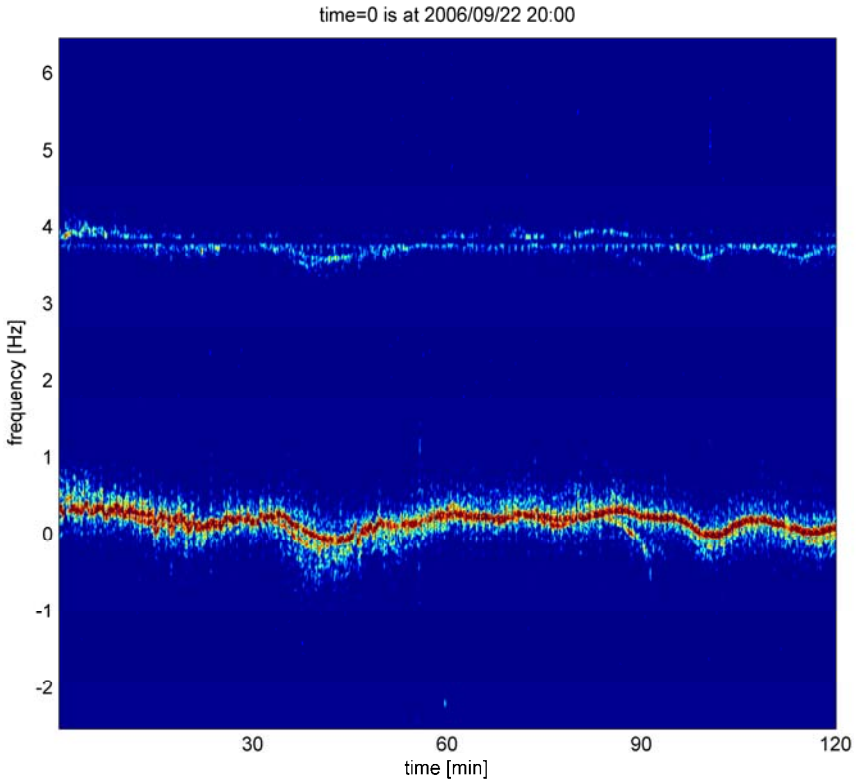

Fig.7. *Detailed Doppler shift spectrogram; 22 September 2006, time=0 is at 18:00 UT. Top trace near 4 Hz: Průhonice-Prague measuring path. The ground wave was removed. A weak signal does not permit to perform a reliable spectral analysis of the signal. Bottom trace near 0 Hz: Panská Ves-Prague measuring path.*

A cautious approach was required to the interpretation of Doppler shift measurements. Large scale disturbances of geomagnetic origin, as well as micropulsations of the geomagnetic field, which influence the ionospheric plasma through electromagnetic forces, can be detected in HF Doppler shift measurements and have similar pattern to that induced by waves in the neutral atmosphere. A possible

geomagnetic origin of waves was investigated using the data from geomagnetic observatory Budkov.

3.2. Geomagnetic data

Two types of geomagnetic data were used. The state of global geomagnetic field was evaluated using planetary indices of geomagnetic activity. Records at the geomagnetic observatory Budkov (Southern Bohemia) were used to observe fluctuations of the local geomagnetic field.

3.2.1. Geomagnetic indices

The Dst index (disturbed storm time index) is used to monitor the occurrence and severity of geomagnetic storms and allows to determine the phase of the geomagnetic storm with a sufficient precision. The Dst index is expressed in nanotesla [nT]. The estimation of the Dst index is based on averaged values of the horizontal component of the earth magnetic field which is hourly measured at low latitude geomagnetic observatories. The strength of horizontal components of the geomagnetic field at low latitudes is strongly influenced by the state of the ring current. During storm time when the strength of the ring current increases due to the coupling of the earth magnetosphere with the interplanetary geomagnetic field, the strength of horizontal component of geomagnetic field decreases. Other currents contribute to the Dst as well, particularly the magnetopause current. The Dst index is corrected as the contribution of the magnetopause current as well as that of the quiet-time ring current are suppressed. The storm onset often appears as a sudden increase of the Dst index. This phase is termed as the sudden storm commencement (SSC). The Dst remains increased during the so called initial phase of storm; it usually lasts for several hours. When the Dst index starts to decrease, the main phase of storm develops. The recovery of the geomagnetic field is slow and may continue up to several days, the Dst index returns gradually to average values. Dst lower than -20 nT is usually interpreted as a minor storm. When Dst drops under -50 nT a moderate storm is in progress. Dst values lower than -100 nT indicate a strong to severe storm (http://pluto.space.swri.edu; http://swdcwww.kugi.kyoto-u.ac.jp).
A general state of the geomagnetic field is described by the Kp index (planetarische Kennzeichen, = planetary index) (www.ukssdc.ac.uk). The Kp index is derived from

measurements of the K index at subauroral geomagnetic stations. Local geomagnetic disturbances are determined by measuring the range between the highest and lowest values of the most disturbed horizontal field component during a 3-hour interval. Before that, the source magnetograms are modified by removing the quiet day variation pattern (www.gwdg.de). The resulting Kp index takes values from 0 to 9 on a quasi-logarithmic scale. Eight values in 3-hour intervals are determined on each day. According to the Kp index values, geomagnetic conditions are interpreted as follows: Kp=0-1 quiet, Kp= 2-3 unsettled, Kp= 4 active, Kp=5 minor storm, Kp=6 major storm, Kp=7-9 severe storm (www.astrosurf.com).

Planetary geomagnetic indices were used, besides the meteorological data, as the main criterion for selection of quiet days. On quiet days, the geomagnetic field was quiet or unsettled ($Kp \leq 3$, $Dst \geq -20$ nT) and there was not a geomagnetic storm on the day before and after the selected quiet day. On days with convective storms which were included in the study the geomagnetic indices were $Kp \leq 4$ and $Dst \geq -30$ nT.

3.2.2. Time behaviour of the local geomagnetic field

Data from the geomagnetic observatory Budkov were analysed to obtain information about fluctuations of the local geomagnetic field. The observatory is situated near Budkov in Southern Bohemia (geographical coordinates 49°04'N, 14°01'E) and is operated by the Institute of Geophysics, Prague (IG).

A continuous wavelet transform was applied on the records of horizontal and vertical components and the amplitude of the local geomagnetic field. Data with time resolution of 1 s were used. The wavelet transform was based on the complex Morlet wavelet; amplitudes of fluctuations were obtained as the modulus of the resulting wavelet coefficients. The wavelet spectra of individual field components were compared with the wavelet spectra of the HF Doppler shift measurements.

Further, cross-correlations between the Doppler signal and geomagnetic field components were computed. Cross-correlation analysis is able to reveal a possible direct relationship between ionospheric and geomagnetic oscillations; it has previously been described between short period ionospheric waves and geomagnetic micropulsations (e.g. Marshall and Menk, 1999). On the basis of wavelet analysis, the time interval of occurrence of waves was found. Using a band pass filter, wave periods

shown by the wavelet analysis of the Doppler signal were filtered. Thus processed signals were used for the computation of the cross-correlation. In the case that ionospheric waves occurred simultaneously with geomagnetic oscillations of corresponding periods (according to the wavelet transform) and/or the cross-correlation values were $|c| \geq 0.5$, a possible geomagnetic origin of the waves was taken into account.

When searching for the link between observed ionospheric oscillations and the pulsations of the geomagnetic field, the height of reflection of the Doppler sounding wave has to be considered, since the Doppler shift is sensitive to the electron density profile (Chum et. al, 2009). When the Doppler sounding wave reflects near the critical frequency of the *F2* or *F1* layer, Doppler record shows a highly correlated ionospheric response to geomagnetic fluctuations (e.g. Marshall and Menk, 1999). On the contrary, the *Es* layer might even prevent the observation of geomagnetically induced ionospheric oscillations.

3.3. Meteorological data

Meteorological data include meteorological radar observations, satellite observations, aerological observations, surface weather observations, and monitoring of the lightning activity. Using combination of the mentioned data, the events were selected and the influence of the tropospheric weather on the ionosphere was studied.

3.3.1. Meteorological radar data

Meteorological radar data enable to follow the dynamics and actual position of weather systems. The Czech radar network (CZRAD) operated by the Czech Hydrometeorological Institute (CHMI) consists of two radars located at Brdy-Praha (49°39'N, 13°49'E) and at Skalky (49°30'N, 16°47'E). The radars are able to monitor the dynamics of active weather systems up to the horizontal distance 256 km. The radar volume data are updated every 10 min (Novák and Kráčmar, 2000). Quasi-three-dimensional projections of maximum radar reflectivity and echo top heights in 30 min intervals were used. Echo top composites represent the height of the upper boundary of clouds, whose radar reflectivity is higher than a given threshold value (4 dBZ in CZRAD) (Řezáčová et al., 2007). Quasi-three-dimensional projections of maximum

radar reflectivity show projection of column maximum reflectivity on the horizontal plane and on two vertical planes up to the height 14 km in the north-south direction and in the west-east direction (Fig. 8).

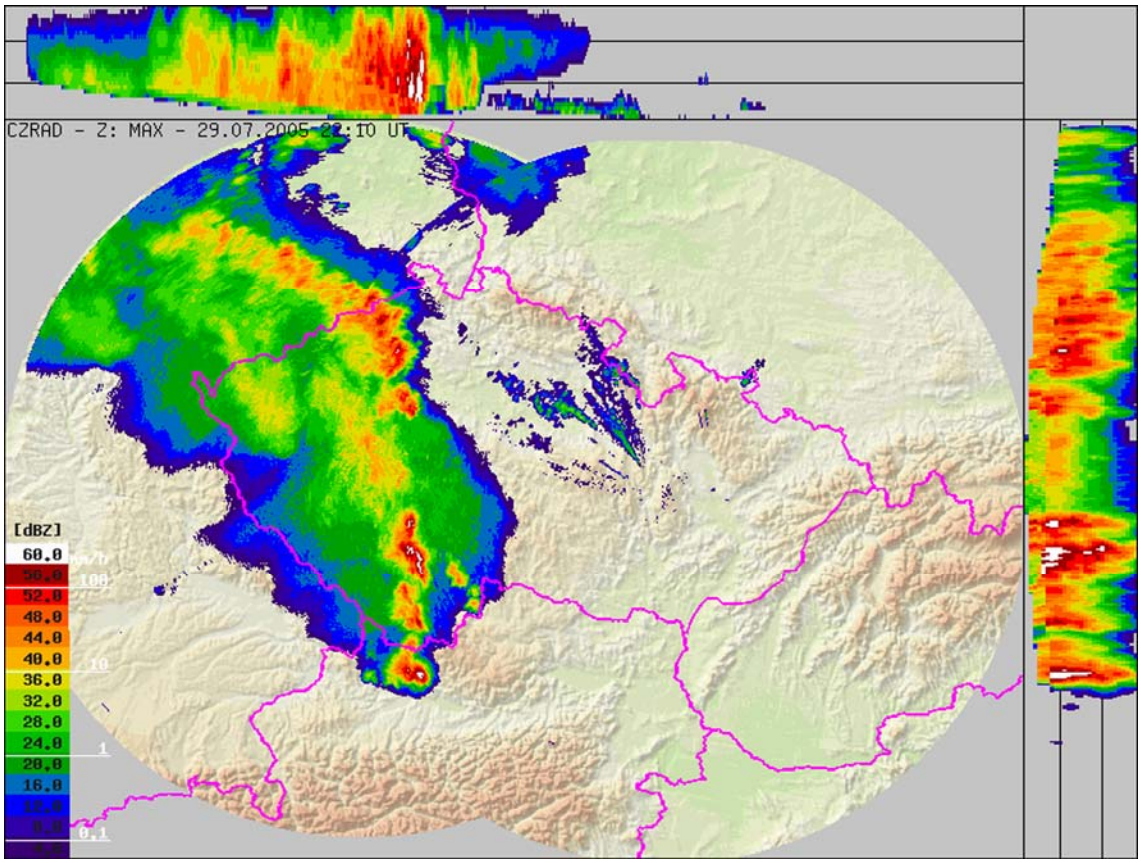

Fig.8. *Quasi-three-dimensional projection of maximum radar reflectivity on 29 July 2005, 22:10 UT. Intense convective storms with clouds reaching over 14 km were passing over the Czech Republic. Top frame: projection of the maximum radar reflectivity on the vertical plane in the west-east direction. Heights 5 and 10 km are indicated by black lines. Right frame: the same, but on the vertical plane in the north-south direction. Middle frame: projection of maximum radar reflectivity on the horizontal plane. (Source: Czech Hydrometeorological Institute)*

The functioning of meteorological radar is based on the capability of particles in precipitation to backscatter microwaves. The position of the target is determined from the elevation angle and azimuth of the antenna and from the time delay between the transmission and reception of the signal. The reflectivity Z of meteorological targets is

proportional to the sum of the sixth power of particle diameters in the unit volume. The unit of reflectivity is $1mm^6 \cdot m^{-3}$. For practical purposes, the logarithmic unit dBZ is used, where $Z[dBZ] = 10 \cdot \log (Z [mm^6 \cdot m^{-3}])$ (Novák, 2000).

From radar reflectivity, the precipitation intensity can be estimated and subsequently the strength of convective phenomena can be deduced. There are two threshold values of maximum radar reflectivity routinely used in the Czech Hydrometeorological Institute to evaluate the intensity of convective phenomena: 40 dBZ for convective phenomena (showers, rain, thunderstorms) and 52 dBZ for severe convective events (heavy rain, hail) (Pešice et al., 2003). The type of clouds (convective clouds or stratiform clouds) can be recognized from quasi-three-dimensional radar composites as well.

3.3.2. Aerological data

The aerological data are available from two upper air stations for the Czech Republic. The measurements at the upper air station Prague-Libuš (50°01'N, 14°27'E, 304 m a.s.l.) are scheduled daily at 00:00, 06:00, 12:00, 18:00 UT; the upper air station Prostějov (49°27´N, 17°08´E, 216 m a.s.l.) conducts the sounding at 00:00 and 12:00 UT. Both stations are operated by the CHMI and belong to the network of regular World Meteorological Organization (WMO) aerological stations. Here, measurements from the observatory Prague-Libuš were used.

Vertical profiles of air pressure, temperature, relative humidity, and wind speed and direction at Prague-Libuš were available up to the pressure level 100 hPa; it corresponded to heights ~16-16.5 km on the analysed days. The actual height of the tropopause was obtained from aerological data as well.

3.3.3. Satellite data

Meteosat Second Generation (MSG) images in the IR10.8 channel were used in combination with vertical temperature profiles to obtain additional information about the height of clouds during convective storms (Fig.9).

The geostationary MSG satellite screens the Earth every 15 min, starting from the Southern Pole. The area of the Czech Republic is screened in the 11^{th} minute of each term. Molecular absorption of heat radiation practically does not occur in the IR10.8

channel. The channel covers the spectral band 9.8-11.8 μm. It means it lays within the atmospheric window at wavelength ~10-13 μm. Radiation temperature calculated from radiance values in the IR10.8 channel approximates the real temperature of the upper boundary of the cloud. The temperature of cloud tops is assumed to be in equilibrium with surrounding environment and is assumed to decrease with height. Thus the height of clouds can be estimated by comparison of temperatures of the upper boundary of clouds with vertical temperature profiles from aerological measurements.

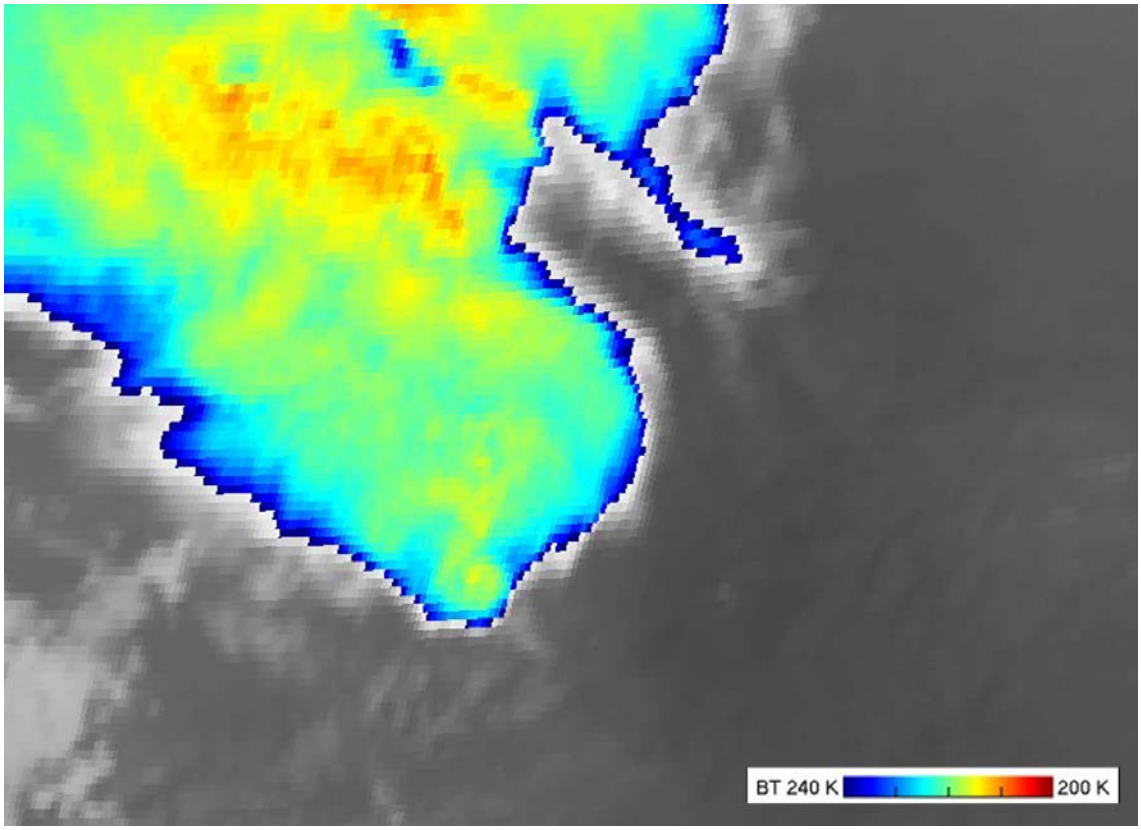

Fig.9. *MSG satellite image in the channel IR10.8 covering the same area as Czech meteorological radars; 29 July 2005, 22:00 UT. Bottom right: colour bar indicating the temperature [K]. (Source: Czech Hydrometeorological Institute)*

However, there exist at least three important exceptions.

(1) The temperature of growing overshooting tops in convective storms is lower than the surrounding temperature, as the overshooting tops cool in accordance with the saturated adiabat. The lowest observed temperatures of overshooting tops in mid

latitudes were by 10-20 K lower than the actual temperature of the tropopause. When overshooting tops loose energy and start sinking, the increase of temperature might be higher than the previous temperature decrease as a consequence of mixing with the warmer air of lower stratosphere.

(2) When the dome in the central part of the convective storm penetrates the tropopause, it is in thermal equilibrium with surrounding warm air of the lower stratosphere and seems to be lower than the margins of the storm.

(3) The height of clouds is estimated incorrect when there are semitransparent clouds above convective storms (Řezáčová et al., 2007).

It is essential to note that the resulting height, estimated on the basis of screening in one thermal channel, was an approximation of the real cloud height. Nevertheless, it was sufficient for the purpose of this study, because the satellite images were used as a complement to radar composites and the exact determination of the height of clouds was not demanded. The aim was to compare the height of clouds with the height of the tropopause.

3.3.4. Surface meteorological observations

The large-scale weather situation in Central Europe was evaluated using the surface charts. The charts are drawn on the basis of observations in the network of surface meteorological stations at synoptic hours. They provide information about the location of pressure systems, weather fronts, and instability lines. Station circles for meteorological stations are plotted on in charts as well. Charts issued by Deutscher Wetterdienst are available in the Internet (www2.wetter3.de) daily at primary synoptic hours 00:00, 06:00, 12:00, and 18:00 UT (Fig.10).

The surface meteorological observatory of IAP is situated at Milešovka (50°33'N, 13°56'E, 837 m a.s.l.) in the western part of the Czech Republic. It is close to the measuring path of the HF CW Doppler system Panská Ves – Prague. Milešovka is an isolated peak which is higher than its surroundings by ~400 m. The position of the observatory is convenient particularly for the measuring of the wind speed and direction. The measurements are not influenced by obstacles in the vicinity of the observatory and the values therefore approach the values in the free atmosphere. The wind speed at the observatory is 85 % of the geostrophical wind speed and the wind

direction deflects from the direction of the geostrophical wind by ~25° (Brázdil et al., 1999). The complete meteorological and climatological observations are conducted at the observatory. Since 1998, the automatic meteorological station has measured air-temperature and humidity, air pressure, visibility, wind velocity and wind direction, soil-temperature in the depths of 5, 10, 20, 50, and 100 cm, precipitation amount, sunshine duration, and cloud height. In addition, the observers determine cloud amount, cloud type, weather situation, depth of snow cover and other meteorological phenomena.

Hourly averages of the wind speed at Milešovka observatory were included in calculation of an index which compares the meteorological activity in the troposphere during analysed convective storm events (see Chapter 3.3.6).

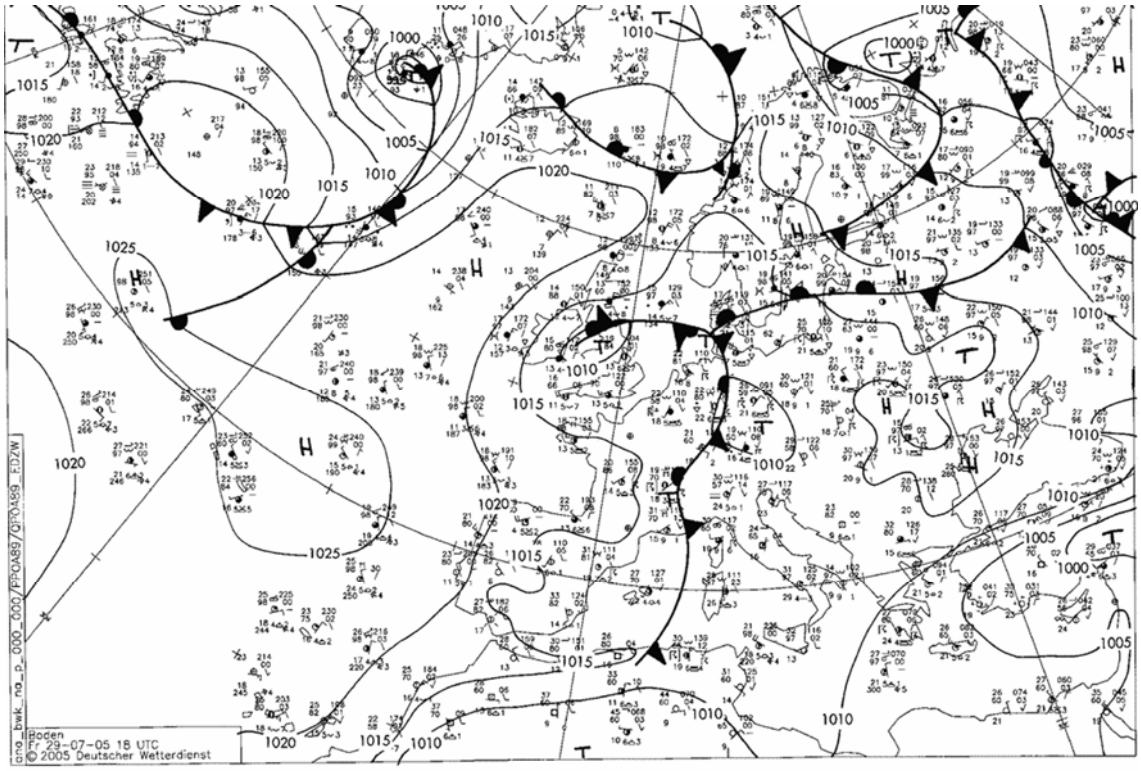

Fig.10. *Synoptic chart on 29 July 2005, 18:00 UT. A cold front was approaching from the west; pressure gradient over Central Europe was rather low. Station circles at selected meteorological stations are shown. (Source: www2.wetter3.de)*

3.3.5. Monitoring the lightning activity

General composites of observations of the lightning activity in Europe for years 2005-2007 are at disposal in Internet (www.wetterzentrale.de). The location of discharges is detected in a ground based positioning system. At 7 stations across Europe, the time of arrival of an electromagnetic impulse emitted by the lightning is recorded and then, the position of the lightning is determined with the precision of 0.5°. The time of observation is available in one hour resolution. Thus, the composites enable to follow the approximate motion and development of convective storms (Fig.11). Also available are composites of lightning intensity, from which the intensity of a thunderstorm may be evaluated.

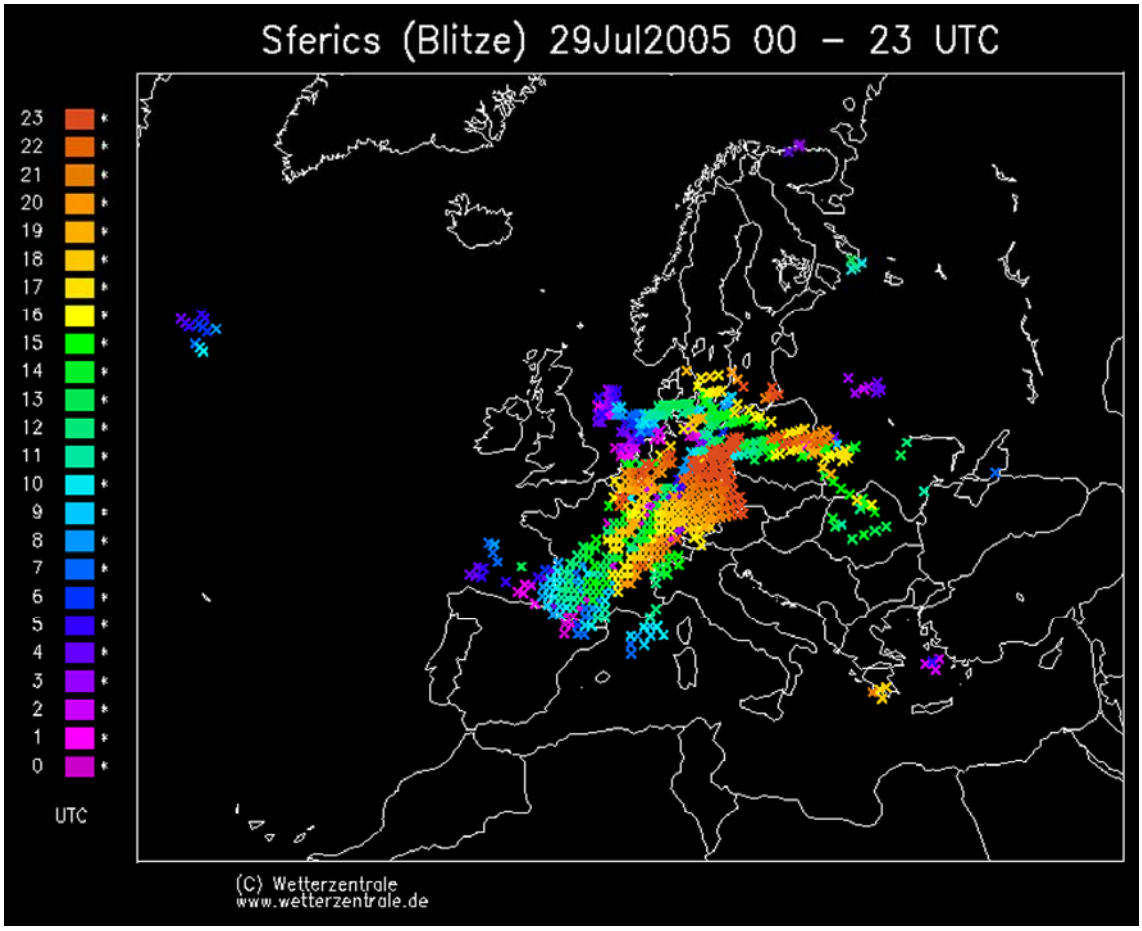

Fig.11. *Lightning activity over Europe on 29 July 2005. (Source: www.wetterzentrale.de)*

3.3.6. The analysis of meteorological data – criteria for selection of quiet days and the evaluation of intensity of convective storms

First, the large-scale weather situation in Central Europe was evaluated using surface synoptic charts. Particularly, passages of weather fronts and instability lines were checked. Thunderstorms were located in general composites of lightning activity. From radar composites, the type and vertical extent of clouds was determined. Using vertical temperature profiles and satellite images in the IR10.8 channel, the additional information about the height of cloud tops was obtained. The height of cloud tops was compared with the height of the tropopause. The hourly averages of wind speed at Milešovka observatory were considered.

A day with low meteorological activity in the troposphere was defined as follows:

(1) There was no weather front or instability line passing over the Czech Republic and there was not a distinct horizontal pressure gradient which would cause strong winds.

(2) There were no convective storms within the radius 250 km from the HF CW Doppler system measuring path Panská Ves – Průhonice, which approximately corresponds to the area covered by the radar Brdy-Praha.

(3) The clouds did not penetrate the tropopause.

(4) The hourly average wind speed was lower than 10 $m \cdot s^{-1}$.

The occurrence of convective storms in the monitored region was examined using the radar composites and lightning activity composites. In radar composites, cells with reflectivity higher than 40 dBZ were located. Their position was subsequently compared with the location of lightning activity. The height and vertical extent of clouds was estimated using vertical projections of maximum radar reflectivity and echo top heights. When there were very high convective storms, in which the clouds exceed the operational range of radars (14 km), satellite images in the IR10.8 channel and vertical temperature profiles from aerological measurements were used to complete the information about the vertical extent of clouds.

An index, I was calculated to compare convective storm activity in studied cases. The extent of the area of maximum radar reflectivity 52+ dBZ in the horizontal plane projection for each event in 30 min time step was determined and expressed as a

number of pixels, **h**. The maximum of all the events, h_{max} was found and ratio **H** was calculated,

$$\mathbf{H} = \mathbf{h} / h_{\max} . \tag{5}$$

The extents of areas of maximum radar reflectivity 52+ dBZ in the north-south direction and in the east-west direction, **v1** and **v2** at heights above 10 km were determined in the same way and maxima, $v1_{max}$ and $v2_{max}$ were found. Ratios **V1** and **V2** and were computed,

$$\mathbf{V1} = \mathbf{v1} / v1_{\max} , \tag{6}$$

$$\mathbf{V2} = \mathbf{v2} / v2_{\max} . \tag{7}$$

Parameter **R** was obtained as

$$\mathbf{R} = \mathbf{H} + \mathbf{V1} + \mathbf{V2} . \tag{8}$$

The maximum and minimum **R**, R_{max} and R_{min} were found for each event. The maximum hourly average wind speed at the observatory Milešovka, W was found for each event. The parameter, C which describes the height of clouds was determined as follows: Clouds penetrating the tropopause, C=1. Clouds reaching to the tropopause region, C=0.5. The height of cloud tops lower than the tropopause, C=0. The index, I was then computed as

$$I = R_{\min} + R_{\max} + W + C . \tag{9}$$

4. Results

Ionospheric effects of convective storms in July 2005 – January 2007 were analysed. Wave activity in the period range 1-30 min on days with convective storms and on quiet days was compared to find differences in observed wave spectra. Waves with amplitudes lower than 0.1 Hz were considered as a noise and were not further analysed. Other (non-wave) effects in Doppler records which occurred during convective storms were studied as well.

4.1. Observations on quiet days

Eleven quiet days were selected in May to September 2006. The weather in Central Europe was governed by a high air pressure system or there was the air pressure field with a low horizontal gradient. In one case, a low pressure trough was present. The height of clouds estimated from radar composites was lower than 10 km; the height of the first tropopause was in the range 10 742 - 13 090 m. The wind speed at Milešovka observatory was lower than 10 $m \cdot s^{-1}$ in hourly average and 17.5 $m \cdot s^{-1}$ in a gust. Convective storms did not develop within the distance ~250 km from the site of the Doppler sounding system. Planetary geomagnetic indices indicated quiet to slightly disturbed geomagnetic conditions. The maximum Kp index was lower than or equal to 2, respectively 3 on one day. The minimum Dst index was higher than -20 nT on all days.

Wave activity in the period range 1-30 min and non-wavelike irregularities were observed in the ionosphere. The increased wave activity appeared mainly in time intervals, when simultaneous fluctuations of the local geomagnetic field were recorded. On six days, waves were observed around the time of sunset. It leads to an assumption that those might have been gravity waves generated by the passage of the solar terminator. However, the Doppler record was correlated with geomagnetic measurements. Having one point and one frequency measurements, it was difficult to decide with confidence about the origin of observed waves. In a few cases, observed waves were not correlated with geomagnetism or the correlation was rather vague (for details see Appendix I).

The observations were significantly influenced by the presence of the *Es* layer. In intervals when the Doppler sounding wave was reflected from the *F* layer, the Doppler

trace was usually clear and waves always occurred. Very low or no wave activity was observed particularly on days in July when the non-transparent *Es* layer was often present. Moreover, the Doppler record was disturbed by spread and ripples which made the detection of waves difficult. Georges (1967) is convinced that as ionospheric irregularities get smaller and eventually approach the size of Fresnel zone in the ionosphere, the Doppler trace becomes spread or blurred in the frequency dimension. In the *Es* region, spread might be associated with the passage of small patches of *Es* ionization. Rippled structure of the Doppler trace is caused by focusing and defocusing of the signal when a small scale travelling disturbance is passing.

The discrete trace with a shift to lower or higher frequencies often occurred. At that time, the non-transparent *Es* layer appeared/disappeared or a transparent *Es* layer was present. The effect might have been caused by a sudden change of the reflection height of the Doppler system sounding wave from the *F* layer to the *Es* layer and vice versa. On the other hand, the discrete Doppler trace did not occur always at the time when the non-transparent *Es* layer appeared or disappeared.

In a few cases, S-shaped trace in the Doppler record was observed. The S-shape results from the reflection of the sounding wave from a concave surface (Georges, 1967). Observations of transient phenomena like S-shapes in the infrasonic range were more detailed described by Chum et al. (2008).

4.2 Ionospheric effects of convective storms

The most favourable atmospheric conditions for the development of convective storms occur in Central Europe in summer. In the Czech Republic, the convective storm season continues from May to September (Sehnalová, 2007). The strongest convective storms which presumably generate intense waves in a wide range of periods usually occur in the afternoon and early evening. On the other hand, convective storm season might not be the season of the most distinct ionospheric effects, particularly in the acoustic wave domain. High temperatures in the summer atmosphere, especially at the bottom of the thermosphere, cause defocusing of the infrasound during the propagation upwards.

Ionospheric effects of convective storms in July 2005 and in May to August 2006 were studied and compared with the effects of a severe weather event that occurred in January 2007.

4.2.1. Observations in July 2005

In May 2005 – September 2005, the ionosphere was often disturbed by geomagnetic storms of various intensity; the Dst index dropped lower than -100 nT. On 29 July 2005, the minimum Dst index was – 26 nT at 18:00 UT; the maximum Kp index was 4+ at 15:00-18:00 UT. On 30 July 2005, the minimum Dst index was -33 nT at 05:00-06:00 UT; the maximum Kp index was 4- at 00:00-03:00 UT. During the analysed days, the ionosphere was recovering after minor geomagnetic disturbance which culminated on 28 July 2005 at 06:00 UT with the Dst index decreased to -50 nT. In spite of it, the events were included in the study since convective storms of such intensity develop very rarely in the Czech Republic.

During the day of 29 July 2005, suitable conditions for strong convection developed in wet warm air flowing to Central Europe in front of the cold front. The actual passage of the cold front in the evening hours (~18:00-01:00 UT on 29/30 July 2005) was accompanied by intense convective storms with cloud tops reaching to heights ~15-16 km and wind gusts 20-40 $m \cdot s^{-1}$. Convective storms passed the Doppler system measuring path between ~22:40 and 23:30 UT. Along the north western boarder of the Czech Republic, a supercell storm and four tornadoes were observed at ~18:00-20:30 UT (analysis of the weather situation by the Czech Hydrometeorological Institute, www.chmi.cz). On 30 July 2005, the intense convective storm activity continued. In the afternoon, convective storms started developing in Southern Bohemia and moved towards north-east. They reached the highest intensity around 20:00 UT. The height of convective clouds exceeded 16 km as follows from MSG satellite images and vertical temperature profiles. Probably a supercell storm was observed between ~17:00 and 19:00 UT in Southern Bohemia (http://bourky.astronomie.cz).

Waves with periods ~2.5-5 min superimposed on gravity waves were observed in the *F* region already at 18:00 UT (Fig.12). The wave activity in the infrasonic range was ceasing after midnight as convective storms were passing further to the east and were abating. The Fourier spectrum of the Doppler record shown in Fig.13 (red line)

indicated much higher wave activity on 29 July 2005 compared to quiet days (reference Fourier spectrum is represented by black lines).

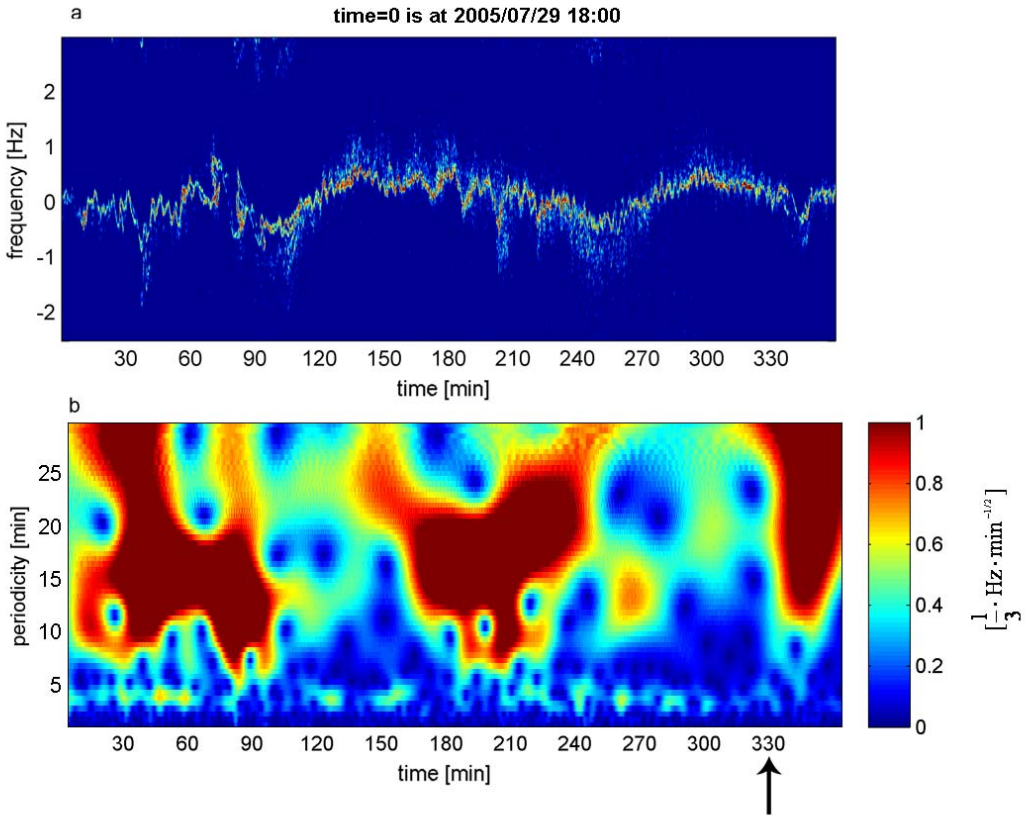

Fig.12. ***a*** *Doppler shift spectrogram on 29 July 2005, start time at 18:00 UT; measurements at Panská Ves – Prague path are shown.* ***b*** *Wavelet analysis of the signal. The arrow denotes the approximate time of passage of convective storms under the measuring path.*

Wave effects in the Doppler shift record may have been caused not only by acoustic-gravity waves propagating in the neutral atmosphere, but also by magneto-hydrodynamic waves. Therefore, oscillations of components of the geomagnetic field at the observatory Budkov were analysed (Fig.14). The wavelet analysis of Doppler records, wavelet analysis of components of the local geomagnetic field and the cross-correlations between the signals suggest that ~2.5-5 min waves observed at ~18:00-19:00 UT are not of geomagnetic origin. They were presumably emitted by convective storms in the troposphere.

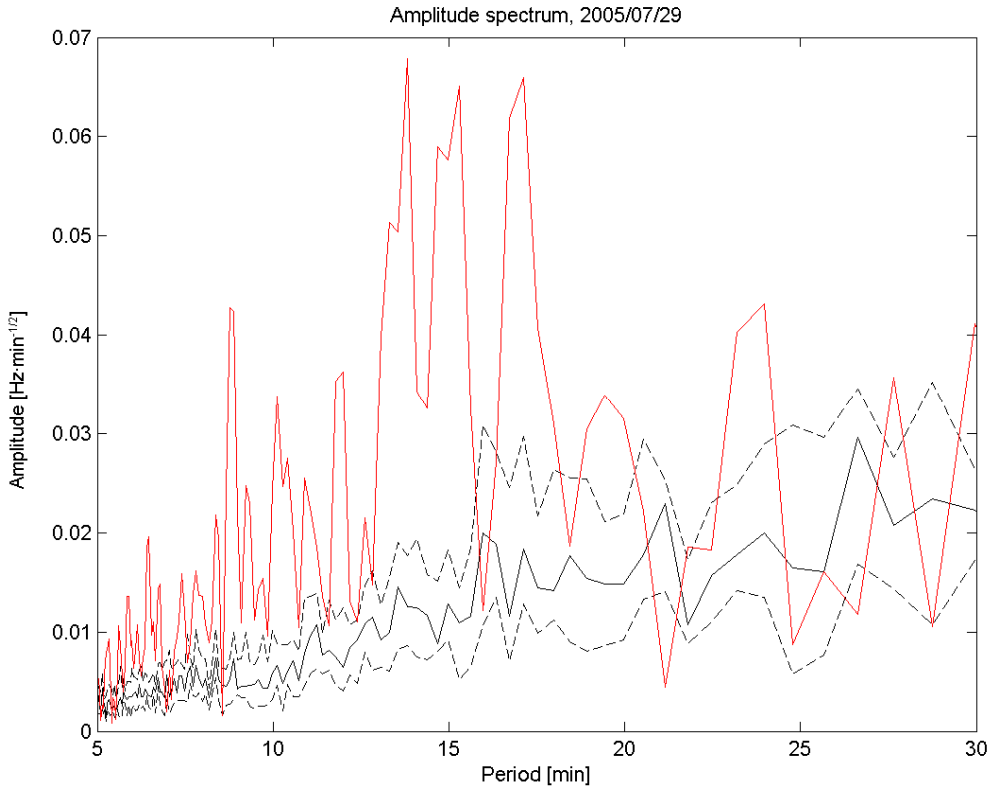

Fig.13. *Fourier transform shows much higher wave activity on 29 July 2005 than on quiet days. Red line: amplitude spectrum on 29 July 2005. Black solid line: median of Fourier spectra on quiet days. Black dashed lines: lower quartile and upper quartile of Fourier spectra on quiet days.*

Waves with periods ~3-5.5 min occurred in the ionosphere at ~20:15-20:40 UT and at ~23:10-23:30 UT. Wavelet analysis does not show geomagnetic oscillations in corresponding time and period range, but the Doppler signal is correlated with the west-east component and with the amplitude of the local geomagnetic field respectively. The waves were observed in the *F* region at heights ~240-250 km and ~260-270 km (true height from the profile) respectively. Waves with periods shorter than 4.3 min can propagate from the troposphere to the ionospheric *F* region; waves of longer periods are restricted by the acoustic cutoff, whose minimum is 4.3 min at 86 km in the USSA1976. To decide whether the observed waves are gravity waves or magneto-hydrodynamic waves from Doppler measurements themselves, it is necessary to have measurements from 3 or more sounding paths. Then, it would be possible to compute the speed of propagation of waves and to conclude about the origin of waves.

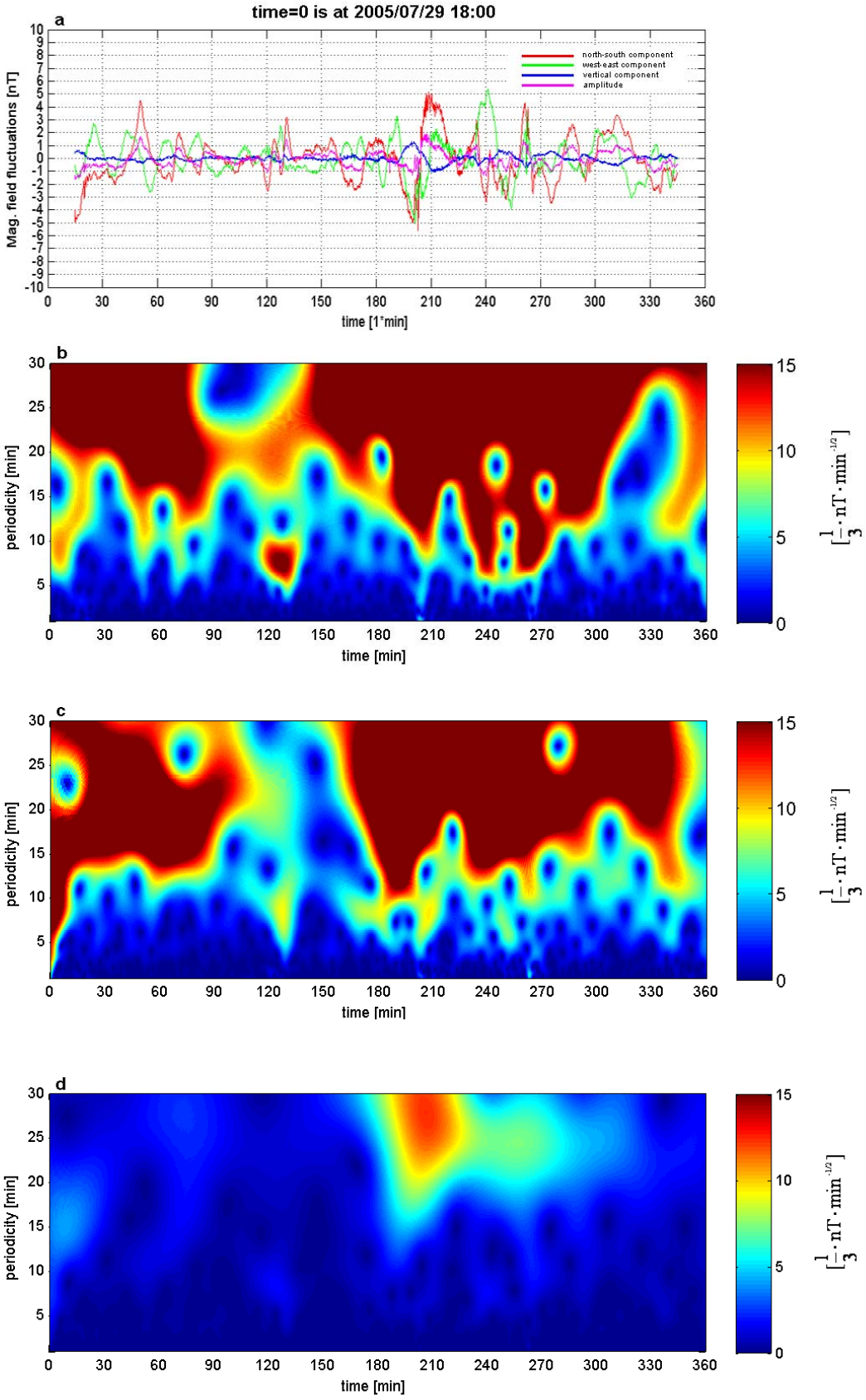
time=0 is at 2005/07/29 18:00
a
north-south component
west-east component
vertical component
amplitude
Mag. field fluctuations [nT]
time [1*min]
b
periodicity [min]
time [min]
c
periodicity [min]
time [min]
d
periodicity [min]
time [min]
$[\frac{1}{3} \cdot nT \cdot min^{-1/2}]$

Fig.14. a *Fluctuations of the local geomagnetic field at the observatory Budkov on 29 July 2005, start time at 18:00 UT. Red: north-south component. Green: west-east component. Blue: vertical component. Magenta: amplitude. Periods over 30 min have been filtered.* ***b*** *Wavelet transform of fluctuations of the north-south component of the geomagnetic field at observatory Budkov;* ***c*** *same as b but for the west-east component;* ***d*** *same as b and c but for the vertical component.*

Waves with periods in the range ~2-6 min observed in the Doppler records at ~19:50-20:10 UT and ~21:10-22:55 UT occurred simultaneously with geomagnetic fluctuations according to the wavelet analysis and the cross-correlation. The oscillations with periods over 6 min are correlated with fluctuations of the geomagnetic field in the whole analysed time interval. The results for 29 July 2005 are summarized in Tab.1.

On 30 July 2005, a relatively weak wave activity was recorded in the late afternoon and evening hours (Fig.15). Unlike the day before, the *Es* layer occurred during the whole studied interval with critical frequency higher than 3.59 MHz. It should be noted here that a negligible Doppler shift and/or a spread trace are usually observed when the reflection occurs from the *Es* layer. Waves with periods ~6-17 min occurred at ~20:25-20:50 UT, spectral peaks of the Fourier amplitude spectrum at ~6-8 min, ~9.5 min, and ~12 min exceeded significantly mean values for quiet days (Fig.16). The wavelet analysis of components of the local geomagnetic field showed the occurrence of fluctuations of the north-south and east-west components in the same time and period range like the ionospheric waves. The Doppler signal was correlated with the north-south component of the local geomagnetic field (Tab.2).

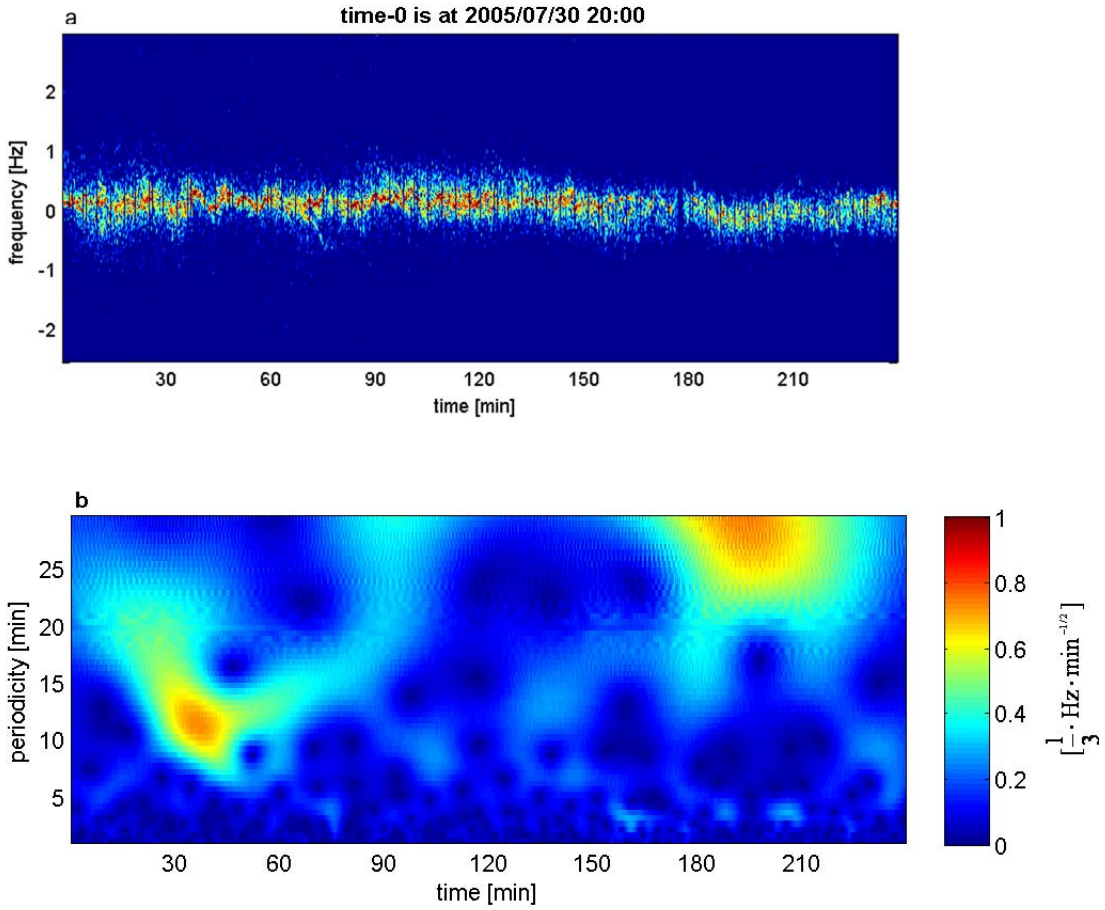

Fig.15. a *Doppler shift spectrogram at the Panská Ves sounding path during convective storm activity on 30 July 2005, start time at 20:00 UT;* ***b*** *Wavelet transform of the signal. Relatively low wave activity was observed. Infrasonic waves of significant amplitudes did not occur.*

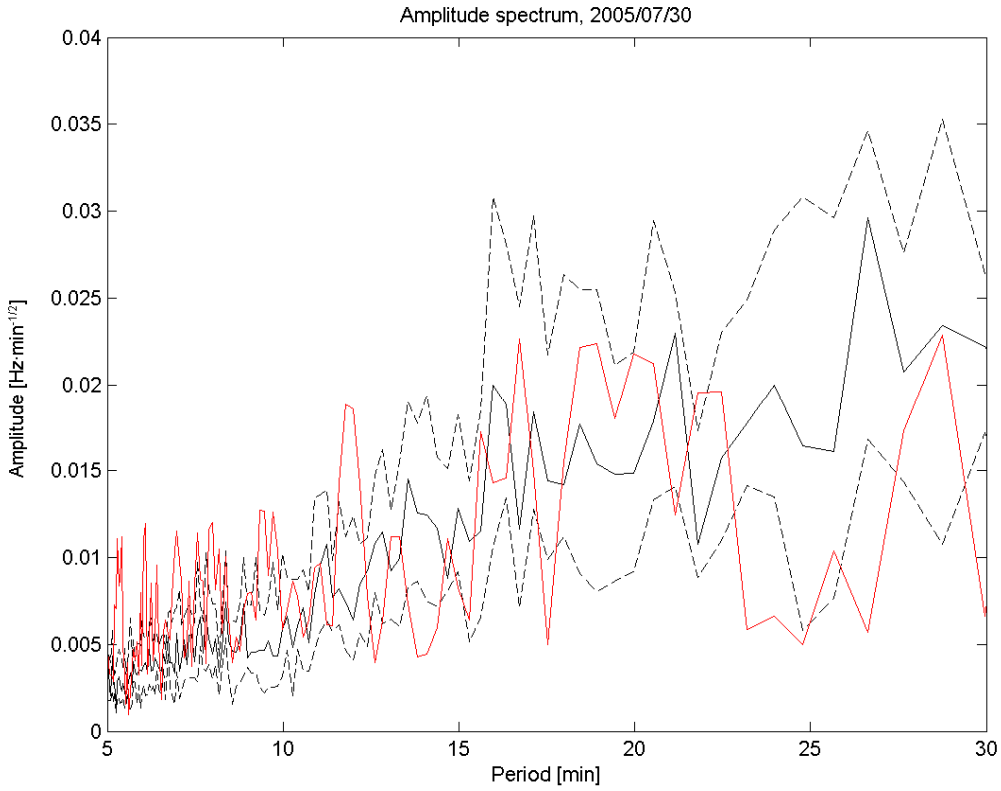

Fig.16*. Fourier transform of the Doppler signal on 30 July 2005 at 20:00-24:00 UT. Red line: amplitude spectrum on 30 July 2005. Black solid line: median of Fourier spectra on quiet days. Black dashed lines: lower quartile and upper quartile of Fourier spectra on quiet days. The wave activity was not significantly increased compared to quiet days, particularly at periods longer than ~12 min.*

4.2.2. Observations in May – August 2006

Twenty-three convective storm events which occurred in periods of quiet to active geomagnetic conditions (2006: Dst $\geq$ -30, Kp $\leq$ 4) were analysed. In most cases, convective storms developed at a cold front which was passing over the Czech Republic. The height of convective clouds varied between ~10 and 16 km. In nine cases, convective clouds penetrated the tropopause whose height was in the range ~10-13 km. The intensity of summer convective storms was compared using the index, *I* (Eq.9). Convective storms in July 2005 were shown for comparison as well (Fig.17).

Increased wave activity compared to quiet days was observed during convective storms in the studied period range 1-30 min. In nearly all cases, ionospheric oscillations

occurred simultaneously with fluctuations components of the local geomagnetic field. Therefore, geomagnetic origin of observed waves cannot be excluded. It should be reminded here that less strict selection criteria, as far as geomagnetic conditions are concerned, were used for days with convective storms ($Kp \leq 4$; $Dst \geq -30$) than for quiet days ($Kp \leq 2$; $Dst \geq -20$ nT).

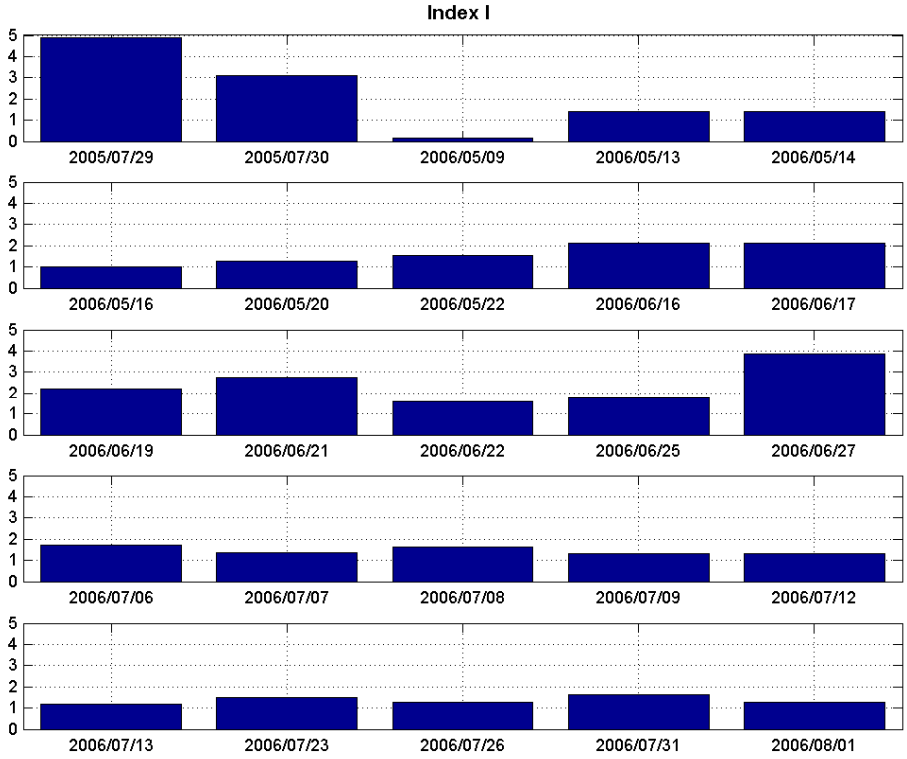

Fig.17. *Index to compare meteorological activity in the troposphere during summer convective storm events. The intensity of convective storms on 29 July 2005 stands out.*

On 19 June 2006, waves with periods ~6-25 min were observed at ~22:05-22:45 UT after the passage of intense convective storms (for details see Appendix II). The Doppler signal was correlated with the vertical component of the local geomagnetic field, although the correlation coefficient was only -0.57. The coefficients of correlation between the Doppler signal and both horizontal components were lower than 0.5, thus it suggested rather independence. It would be possible to exclude or confirm the geomagnetic origin of observed waves from the speed of propagation of waves. The speed of propagation of magneto-hydrodynamic waves approaches the speed of light,

acoustic-gravity waves propagate at much lower rate. In 2006, multipoint Doppler shift measurements essential for calculation of the speed were not available. The same is true for all other analysed events; geomagnetic origin of waves could be excluded or confirmed, if the propagation speed could have been computed.

Severe convective storms occurred between 19 and 27 June 2006, although they did not reach the intensity of convective storms on 29 July 2005. However, *Es* layer with critical frequency higher than 3.59 MHz was present most of the time in most studied cases. The *Es* layer may hinder the observation of possible wave activity in the *F* region. It should be reminded here, that the amplitude of acoustic-gravity waves increases with height, and thus the waves are better observable, as they are propagating up in the rarefied upper atmosphere. Moreover, the Doppler record was often disturbed by spread or smeared trace; discrete trace with Doppler shift occurred as well and it was not possible to perform reliable spectral analysis of the measurements. All these effects were observed also in Doppler record on quiet days in time intervals when the *Es* layer was present.

Non-wave effects observed in the HF Doppler shift records included multiple trace, spread trace, ripples, and S-shaped trace. All of these effects occurred also on quiet days. Their origin might be

(1) Multiple trace – the sounding wave was split in the ordinary and extraordinary mode; the discrete multiple trace might be caused by simultaneous reflection of the sounding wave from the *F* layer and transparent *Es* layer.

(2) Spread trace occurred in time intervals when there was a spread ionospheric layer recorded in ionograms. This effect was most often observed, when there was a spread *Es* layer.

(3) S-shaped trace is formed, when there is concave-shaped disturbance in the reflecting layer (e.g. Georges, 1967).

One must keep these effects on mind when interpreting the results of wavelet analysis, since all of them complicate the estimation of unambiguous function of the Doppler shift on time and thus lead to less reliable results of spectral analyses.

The observations in year 2006 are in detail listed in Appendix II.

4.2.3. Observations in January 2007

On 18 January 2007, a deep cyclone was passing over Europe. The large pressure gradient between Scandinavia and Mediterranean (~50 hPa) triggered an exceptionally strong air flow. The average wind speed measured in the Czech Republic was 15-20 $m \cdot s^{-1}$, and in wind gusts it was over 40 $m \cdot s^{-1}$. Wind speed at Milešovka reached over 30 $m \cdot s^{-1}$; (to compare, the average wind speed in January for years 1961-1990 was 9.6 $m \cdot s^{-1}$). The cold front was passing over the Doppler system network between ~20:15 and 23:45 UT. Its passage was accompanied by thunderstorms with exceptionally high lightning activity compared to usual winter thunderstorms. Due to a different stratification and energetic potential of the lower atmosphere in winter, the vertical extent of clouds during the January event was significantly less compared to summertime events and clouds did not reach to the tropopause. 18 January 2007 is

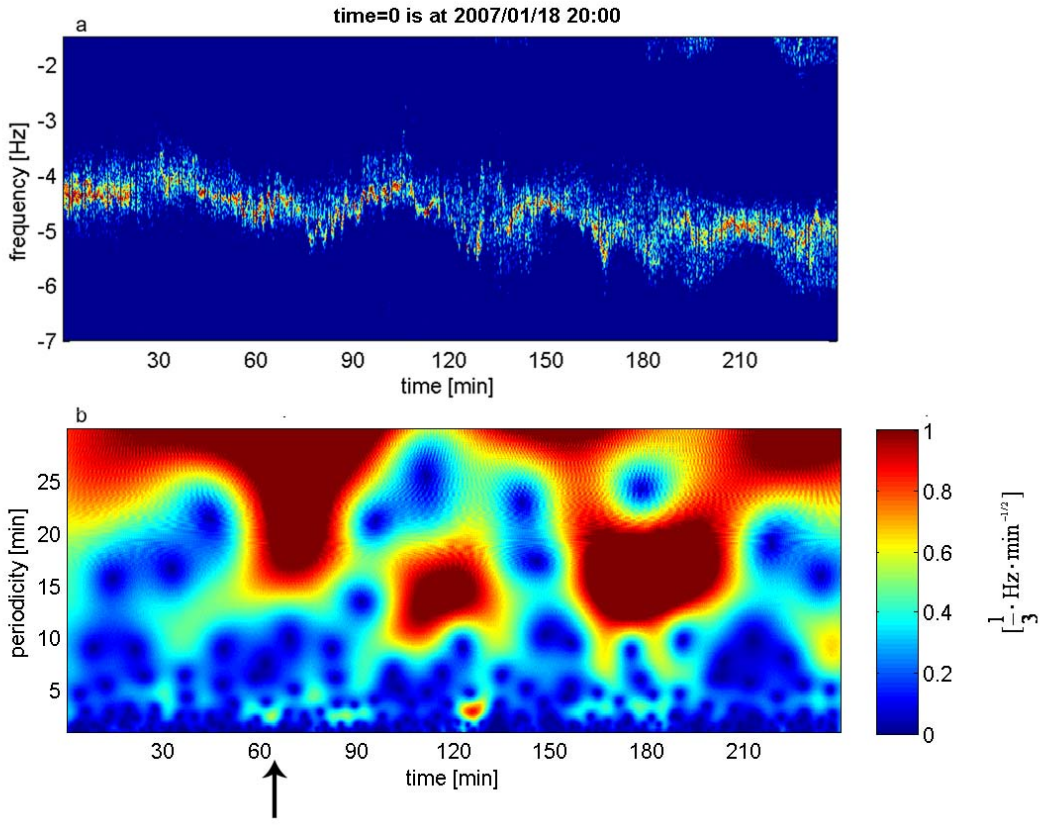

Fig.18. a *Doppler shift spectrogram at the Dlouhá Louka sounding path during the windstorm and passage of the distinct cold front on 18 January 2007, start time at 20:00 UT;* ***b*** *Wavelet transform of the signal. Arrow denotes the approximate time of passage of the cold front under the measuring path.*

a case of very strong winter convection in connection with a strong turbulence (weather situation analysis by the Czech Hydrometeorological Institute, www.chmi.cz).

The Dst index dropped down to -29 nT on 17 January 2007 at 10:00 UT, but there was not significant geomagnetic disturbance in progress on the days before 18 January 2007 as well as on the days after. On 18 January 2007, minimum Dst index was -26 nT at 09:00 UT; the maximum Kp index was 4 at 21:00-24:00 UT.

The Doppler record from the Průhonice measuring path was disturbed by a strong ground wave. Therefore, the measurements were not further analysed. Increased wave activity in the ionosphere was observed on all the other measuring paths. Oscillations with periods ~2-4 min observed at Dlouhá Louka path at ~20:50-21:35 UT are most probably infrasonic waves which may have been generated in the troposphere (Fig.18). Waves of infrasound periods, not correlated with geomagnetic fluctuations, were also observed at Panská Ves path (~22:40-22:45 UT) and at Kašperské Hory path (~21:55-22:00 UT). However, the waves persisted only for about one wave cycle. Moreover, the amplitudes of oscillations at Kašperské Hory path were ~0.05 Hz, it means they did not exceed the threshold of noise. Short period waves observed in other time intervals as well as waves with periods longer than ~5 min occurred simultaneously with geomagnetic oscillations. The analysis of fluctuations of the local geomagnetic field at observatory Budkov is shown in Fig.19. The results of observations are summarized in Tab.3-6.

The analysis of measurements was limited by the quality of the Doppler records. The Doppler traces were disturbed by spread which made the detection particularly of short period waves difficult. For the same reason, the speed of propagation of waves was not calculated from the multipoint measurements. The height of reflection of the Doppler sounding wave was not determined due to technical problems of the ionosonde.

Fig.19 a *Fluctuations of the local geomagnetic field at the observatory Budkov on 18 January 2007, start time at 20:00 UT. Red: north-south component. Green: west-east component. Blue: vertical component. Magenta: amplitude. Periods over 30 min have been filtered.* ***b*** *Wavelet transform of fluctuations of the north-south component of the geomagnetic field at observatory Budkov;* ***c*** *same as b but for the west-east component;* ***d*** *same as b and c but for the vertical component.*

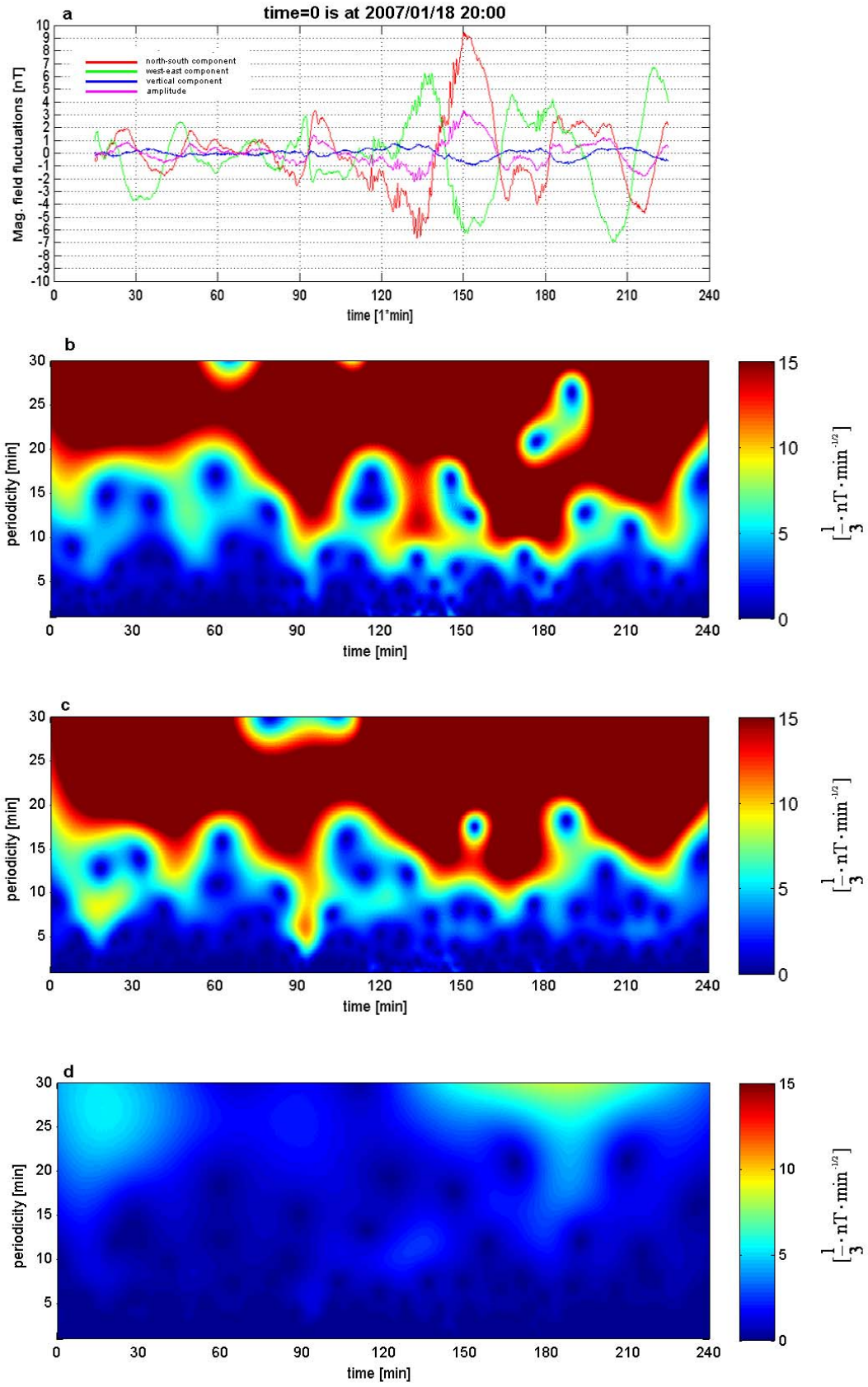
a
time=0 is at 2007/01/18 20:00
north-south component
west-east component
vertical component
amplitude
Mag. field fluctuations [nT]
time [1'min]
b
periodicity [min]
time [min]
c
periodicity [min]
time [min]
d
periodicity [min]
time [min]

5. Discussion

The results in the Czech Republic differ significantly from those obtained in North America in the 1960s and 1970s. In the Czech Republic, infrasound was rarely observed in the ionosphere during convective storms in the troposphere (Šindelářová et. al., 2009a; Šindelářová et al., 2009b). In the central part of the USA, observations of infrasonic waves during nearby convective storms were frequently reported.

In both regions, similar measuring technique, the continuous HF Doppler sounders, were used. Baker and Davies (1969) performed the sounding on frequencies between 9 and 13 MHz in their experiment which was carried out in the central part of the USA in 1966-1968. The authors published the observational results on individual days between May and September 1967. During this period, the blanketing frequency of the sporadic *E* layer (fbEs) at Boulder observatory was always lower than the frequencies of the Doppler sounder. Thus, it can be supposed that the Doppler sounding wave could reflect from the *F* layer. Baker and Davies (1969) state the height of reflection between 200 and 300 km. Georges (1967) used frequencies between 3.3 MHz and 5.1 MHz in the Arkansas experiment. He noted that during the day time, ionospheric disturbances were not observed and points out that the sounding frequencies reflected in the *E* region.

In the Czech Republic, the 3.59 MHz sounding frequency was used. The critical frequency of the *Es* layer (foEs) often exceeds 3.59 MHz in summer. The Doppler sounding wave was thus often reflected from the *Es* layer. It clearly came out on quiet days that wave activity in the gravity wave domain was observed in the Doppler shift records only in time intervals, when the sounding wave was reflected from the *F* layer. During convective storms on 30 July 2005, wave activity observed by the Doppler measuring system was weak despite intense convective storms in the troposphere. It was in contrast to the observations made on the day before. On 29 July 2005, the Doppler sounding wave was reflected from the *F* layer whereas on 30 July 2005, the *Es* layer persisted throughout the day; in some intervals, it was non-transparent. It can be assumed, that the observations during other convective storms were influenced in a similar way.

On the other hand, on several days, the *Es* layer did not occur during the whole period of observation and the sounding wave was reflected in some intervals from the

Es layer and in some intervals from the *F* layer. Waves of periods in the gravity wave domain were observed in the *F* region, but the Doppler signal was correlated with geomagnetic records. Therefore geomagnetic origin of waves must be considered. Waves of periods of infrasound did not occur. It leads to an assumption, that convective storms in the Czech Republic are not as efficient in emitting infrasonic waves as convective storms in the central part of the USA. The reason might be different environments in which convective storms develop in Central Europe and in the central part of the USA.

The main mountain ranges of North America extend in the north-south direction along the western coast. The circulation in the southern part of North America is in summer governed by anticyclones above Hawaii and Azores. Westerly winds are restricted by the Cordillera at the western coast of North America. In the region to the east from Cordillera, the tropical air mass from the Atlantic Ocean advances up to Canada. A thermal low develops above the continent and supports the flow of warm wet air from the Gulf of Mexico in the central part of the USA. The air mass from the Gulf of Mexico can advance relatively far to the north, since meridional air flow is not restricted by any significant orographic barrier in the region.

In Central Europe, western air flow prevails throughout the year, governed by the permanent centres of action in the troposphere, Azores anticyclone in the south and Island depression in the north. The sources of moist air mass are the Atlantic Ocean and to some extent also the Mediterranean Sea. The air flowing from the Atlantic is not as warm and moist as the air flowing to the central USA from the Gulf of Mexico. Mediterranean is not as large and in the most part of the year not as warm compared to the Gulf of Mexico. Therefore, the air mass is not transformed in such a degree above the Mediterranean as above the Gulf of Mexico (Brooks et al., 2003). Moreover, the range of the Alps extending roughly in the west-east direction forms a barrier for the air flow from Mediterranean to Central Europe.

Brooks et al. (2003) conducted an extensive study of the spatial distribution of severe thunderstorm and tornado environments and Brooks et al. (2007) analysed the annual cycles of convectively important atmospheric parameters in different regions. Following text dealing with the convective storm environments is based on the two mentioned papers of Brooks.

The combination of CAPE (convective available potential energy) and wind shear (magnitude of the vector wind difference between the surface and 6 km [$m \cdot s^{-1}$]) over a deep level of the atmosphere is a good parameter to recognize severe thunderstorms from less severe events. CAPE is important for thunderstorms to have strong updrafts; wind shear organizes the storms and increases the probability that they will be severe.

One of the biggest differences between the environments in Europe and in the central part of the USA is that CAPE tends to be lower in Europe. CAPE ~1000 $J \cdot kg^{-1}$ is not common in the USA (~7 % of all soundings), but it occurs much less often in Europe (~1 %). CAPE ~2000 $J \cdot kg^{-1}$ practically does not occur in Europe. In the most part of the USA east of the Rocky Mountains, with the exception of the Appalachian, CAPE reaches values of 2000 $J \cdot kg^{-1}$ five or more days per year. No location in Europe averages as much as 1 day per year.

CAPE can be thought of as a combination of steep lapse rates in the mid-troposphere and abundant boundary-layer moisture. The high terrain of the Rocky Mountains plays an important role in generating steep lapse rates of air temperature in the Central Plains. In Europe, a source of high lapse rate air comparable with the Rocky Mountains does not exist. The lapse rate of at least 7 $K \cdot kg^{-1}$ between pressure levels 700 and 500 hPa occurs on 50-250 days per year in the central part of the USA, with maximum over the Rocky Mountains decreasing towards the Mississippi River. The maximum frequency over the continental Europe is about 50 days. The low level moisture differences are even larger since a source of moisture comparable to the Gulf of Mexico is absent in Europe. Defining the threshold for abundant low level moisture as 10 $g \cdot kg^{-1}$ of mean mixing ratio in the lowest 100 hPa above the ground, most of the central and south-eastern part of the USA has at least 90 days of abundant moisture per year with maximum of more than 300 days over southern Florida. Over continental Europe, abundant moisture occurs on less than 60 days per year.

Winds from the Gulf of Mexico blowing at the ground and winds from the Rocky Mountains in the mid-troposphere result in a strong wind shear. At the same time, they bring high abundant moisture and high lapse rate air together. Therefore, the central part of the USA is an ideal location for development of severe convective storms. In Europe, favourable environments for severe thunderstorms occur most frequently in the southern

part of the continent, particularly over the Spanish plateau and at the Adriatic Sea, although the rates are half of the peaks in the USA.

The identification of suitable environments only means that severe convection is favoured, not that it will certainly occur. The efficiency of the atmosphere in producing severe thunderstorms in favourable environments has not been known yet. The global distribution of environments supportive for the development of intense thunderstorms presented by Brooks et al. (2003) corresponds with the global distribution of intense thunderstorms detected and diagnosed using the observations of the Tropical Rainfall Measuring Mission satellite (TRMM) in 1998-2004 (Zipser et al., 2006).

Conditions which support the development of severe thunderstorms occur in North America a large period of time during the year. Particularly the spring is a season of existence of favourable severe thunderstorm environments. In Europe contrary, a seasonal peak was not found. The results of Brooks et al. (2007) suggest that synoptic and mesoscale conditions are necessary to get environments which support severe convection.

The study of ionospheric effects of convective storms was to a large extent limited by the quality of the Doppler shift measurements and by the fact that in analysed years 2005 and 2006, the Czech Doppler system network was still built and consisted of only two measuring path. Therefore, it was not possible to calculate the speed and direction of propagating waves which would probably lead to better understanding of the origin of the waves. Moreover, owing to technical problems of the measuring path Průhonice only one point measurements were available for the analysis. The most intense convective storms most often occurred in the late afternoon and early evening of the local time. However, during the daytime (~06:00-16:00 (or to 18:00) UT), the HF signal always experienced low Doppler shift close to zero and was strongly attenuated. The signal might have been attenuated by the *D* layer which forms during the daytime and is known to absorb radio waves. Thus, the Doppler shift data suitable for further analysis were often not at disposal during the peak of convective storm activity over the Czech Republic. In summer, the critical frequency of the *Es* layer is often higher than 3.59 MHz. Thus it can be expected that the sounding signal reflected from the *Es* layer. A negligible Doppler shift and/or a spread trace are usually observed when the reflection occurs from the *Es* layer. A discrete trace with a shift to higher or lower

frequencies which occurred in the Doppler records is obviously connected with a sudden change of the reflection height between *Es* layer and *F* layer. Further, the 3.59 MHz wave often approached critical frequencies of the *E* layer, *Es* layer or *F1* layer, particularly during the daytime. These factors probably led to disturbed trace in Doppler records in significant part of observational intervals and prevented to study the wave activity.

6. Conclusions

The aim of the present work was to study ionospheric effects of rather short time duration that were possibly generated by convective storm activity in the troposphere. The continuous Doppler shift measurements, started in 2004, have enabled the ionospheric observations with high resolution in time. Here, the wave activity in the period range 1-30 min and other non-wave effects were studied. Using measurements of fluctuations of the local geomagnetic field at the observatory Budkov in Southern Bohemia, a possible geomagnetic origin of observed waves was examined. The results obtained in two different climatic regions (the Czech Republic and the central part of the USA) were compared.

Infrasound generated by convective storms was rarely observed in the Czech Republic. The results significantly differ from those obtained in the central part of the USA. Possible reasons seem to be:

(1) The continuous HF Doppler shift observations are obviously influenced by the height of reflection of the sounding wave. In the time intervals, when the sounding wave was reflected from the non transparent *Es* layer, very low or no wave activity was observed. During the experiments in North America, the Doppler sounding was conducted on frequencies which predominantly reflected from the ionospheric *F* layer whereas the 3.59 MHz sounding wave used in the Czech Republic reflected frequently from the *Es* layer.

(2) Spatial distribution of environments supportive for development of the most intense convective storms, which are supposed to generate infrasound, suggests much lower frequency of occurrence of such storms in Central Europe when compared to the central USA.

Waves of periods in the gravity wave domain were observed always when the Doppler sounding wave reflected from the *F* layer. The amplitudes of waves were slightly higher on days with convective storms – the median was 0.2 Hz, whereas on quiet days, the median was 0.16 Hz. However, the Doppler signal was nearly in all cases correlated with fluctuations of components of the local geomagnetic field. Therefore, geomagnetic origin of observed waves must be considered. It is possible to distinguish acoustic-gravity waves and magneto-hydrodynamic waves from the Doppler shift measurements solely using the speed of propagation of waves. It is known, that the

speed of propagation of magneto-hydrodynamic waves approaches the speed of light, whereas acoustic-gravity waves propagate at much lower rate. This method can be used for the analysis of data from year 2007, when multipath measurements were started.

The Doppler sounding technique is useful for observations of infrasonic waves and short period gravity waves. Studying long period waves is limited by the duration of a clear Doppler trace which is necessary when an unambiguous function of the Doppler shift on time is determined as an input for the spectral analysis. In the studied events, the Doppler record was often disturbed by spread, multiple trace, discrete trace etc. Another factor to consider is that the reflection height of the Doppler sounding wave is not constant. Particularly in summer, when the *Es* layer is often present, the reflection height may change in order of several tens of km during a short time interval. It is known that the wave characteristics change with height due to changes of physical and chemical parameters of the atmosphere; further, the influence of geomagnetic field must be considered, particularly in the *F* region.

In this study, it was intended to lay groundwork for future work that should include:

(1) Analysis of simultaneous HF Doppler shift measurements in the ionosphere and surface microbarograph measurements (started in 2008) that could help to better understand the vertical propagation of waves generated by weather systems in the troposphere.

(2) The Czech Doppler sounding system enables measurements on two sounding frequencies 3.59 MHz and 7 MHz. Measurements on the frequency 7 MHz will be started during the present Solar Cycle 24 as the electron concentration in the ionosphere (hence, also critical frequencies of ionospheric layers) will increase towards the maximum of the Solar Cycle. Using multifrequency measurements, it will be possible to observe the vertical propagation of waves. It could contribute to distinguishing waves coming from below.

(3) Multipath HF Doppler shift measurements will enable to study horizontal propagation of waves in the upper atmosphere and thus e.g. to distinguish unambiguously acoustic-gravity waves and magneto-hydrodynamic waves.

7. Summary

Continuous Doppler shift observations of ionospheric effects of convective storms were conducted for the first time in the Czech Republic and also in Central Europe. The measuring technique enabled to study the effects of short time duration (here, waves in the period range 1-30 min). Effects of summer convective storms of different intensity were analysed; a winter severe weather event was included in the study as well. The intensity of summer convective storms was compared by an index (*I*) based on the extent of area of high radar reflectivity, the intensity of convection, the vertical extent of convective clouds, and the wind speed at Milešovka observatory. The period and time of occurrence of waves were determined using the continuous wavelet transform based on complex Morlet wavelet. The wave activity on days with convective storms was compared with observations on quiet days. In two cases out of 26 studied, increased wave activity in the infrasonic period range was found. On 29 July 2005, waves with periods ~2.5-5 min were observed in the *F* region. On 18 January 2007, ~2-4 min waves occurred. A possible geomagnetic origin of the waves was examined by computing the wavelet analysis of fluctuations of the local geomagnetic field at the observatory Budkov and by computing the cross-correlation between the Doppler signal and geomagnetic data. The comparison of Doppler measurements and geomagnetic data showed that the observed oscillations cannot be entirely assigned to pulsations of the local geomagnetic field. Exceptionally strong meteorological activity in the troposphere is considered as a source of the waves. Oscillations with periods ~5-30 min observed on these two days were most probably of geomagnetic origin. During the other analysed events, wave activity which could be unambiguously attributed to tropospheric meteorological processes was not found in the analysed period range. The oscillations either were possibly connected with fluctuations of the local geomagnetic field or the pattern did not differ significantly from the pattern on days with low meteorological and geomagnetic activity. The results of observation in the Czech Republic significantly differ from the results obtained in the central part of the USA, where infrasonic waves appeared to occur relatively often. Different sounding frequencies were used in the Czech Republic and in the USA, thus wave activity was observed at different heights in the ionosphere. It is known that wave characteristics change with the altitude. Another reason might be lower intensity of convective storms in the Czech Republic, which is supported by the circulation of the troposphere in both regions, the orography of both continents and the position of the continents and seas.

8. Tables

The table for each day contains

Col.1: period of observed waves

Col.2: time of observation

Col.3: periods of observed waves, whose amplitudes exceed upper quartile of the reference Fourier spectrum. (The comparison with the reference spectrum was not done for the data on 18 January 2007).

Col.4: quality of the Doppler trace, other effects observed in the Doppler record

Col.5: Virtual height of reflection of the 3.59 MHz wave

Col.6: Amplitude of waves in observed period range (band pass filter was used). Waves of amplitudes lower than 0.1 Hz were considered as noise.

Col.7: Wavelet analysis of components of the local geomagnetic field, occurrence of geomagnetic fluctuations in the corresponding time and period range (NS: north=south component; WE: west-east component; V: vertical component; B: amplitude of the local geomagnetic field)

Col.8: cross-correlation between the Doppler signal and components of the local geomagnetic field. The maximum (of the absolute value) and time shift of maximum are shown, in case the absolute value is higher than 0.5. Negative time shift means that geomagnetic fluctuations precede the Doppler signal. However, the sign must be interpreted very cautiously, since in most cases it was not possible to determine the exact start of the event in both Doppler shift and geomagnetic records. The symbols are the same like for Col.7.

Tab.1: Observations on 29 July 2005

Period [min]	**Time (UT)**	**Fourier [min]**	**Doppler record**	**Reflection height, layer [km]**	**Amplitude [Hz]**	**Wavelets geomag. field**	**Cross-correlation**
2.5-5	18.00-19.00	2.5-5	OK(double trace,signal strength)	F(230-260)	0.35	No	No
2.5-4	19.10-19.20	2.5-4	S-shape,signal strength	F(250)			
2.5-3.5	19.30-19.40	2.5-3.5	double trace, S-shape, signal strength	F(275-295)			
2.5-6	19.50-20.10	2.5-6	OK(till 20.00 double trace)	F(295-290-275)	0.2	NS;EW	No
3-5.5	20.15-20.40	3-5.5	OK	F(275-270-255)	0.15	No	EW=0.52 at t=73s
2-3	20.43-20.48	2-3	OK(spread)	F(255)	0.06	not evaluated - noise	
2.5-5.5	21.20-21.55	2.5-5.5	OK(spread)	F(245-245-255-275)	0.34	NS;EW	No
2.5-5	22.00-22.05	2.5-5	spread	F(275)			
2.5-4.5	22.15-22.55	2.5-4.5	OK	F(300-315)	0.26	NS;EW	No
3-5.5	23.10-23.30	3-5.5	OK	F(280)	0.11	No	B=0.51 at t=27s
6-18	18.00-18.20	6-18	OK(signal strength)	F(230)	not calc.	NS;EW	not calc.

Tab.1: Observations on 29 July 2005 (cont.)

6-23	18.20-19.00	6-20	OK(double trace, signal strength)	F(230-240-265-265)	0.63	NS;EW	EW=0.52 at t=1078s V=-0.67 at t=-1284s
>24	18.20-18.50	24-25;27;30	OK(double trace, signal strength)	F(230-240-265)	not calc.	NS;EW	not calc.
4.5-20	19.00-19.40	4.5-20	S-shapes,double trace, signal strength	F(265-250-275-295)			
>24	19.10-19.20	24-25;27;30	S-shape,double trace signal strength	F(250)			
9-17	19.20-20.20	9-17	OK(till 19.35 S-shape, till 20.00 double trace,smeared)	F(250-275-295-290-275)	0.4	NS;EW	NS=0.53 at t=-45s EW=-0.53 at t=-28s V=0.55 at t=-217s B=0.54 at t=-78s
>17	19.40-20.00	17-20;24-25; 27;30	OK(double trace,smeared)	F(295-290)	0.21	NS;EW	NS=0.76 at t=777s EW=0.66 at t=-390s V=-0.59 at t=328s B=0.74 at t=778s

Tab.1: Observations on 29 July 2005 (cont.)

3- 20	21.00-21.15	3-20	OK	F(245)	0.6	NS;EW;V	NS=0.55 at t=-187s EW=-0.63 at t=173 s V=0.52 at t=196s B=0.55 at t=-143s
5.5-24	20.40-22.00	5.5-20	OK	F(255-245-245-245--255-275)	0.58	NS;EW;V	No
8-18	22.10-22.40	8-18	OK	F(305-315-315)	0.2	NS;EW	NS=0.52 at t=-333s B=0.54 at t=-332s
15-24	22.50-23.15	15-20	OK	F(216-300-285)	0.08	not evaluated - noise	
>3.5	23.30-24	3.5-20; 24-25;30	OK(double trace, signal strength)	F(280-305)	not calc.	NS;EW	not calc.

Tab.2: Observations on 30 July 2005

Period [min]	**Time (UT)**	**Fourier [min]**	**Doppler record**	**Reflection height, layer [km]**	**Amplitude [Hz]**	**Wavelets geomag. field**	**Cross-correlation**
3.5-4.5	21.15	3.5-4.5	OK	Es(100)	0.015	not evaluated - noise	
7-10	21.43-21.48	7-8;9.5	spread	Es(100)			
6.5-7.5	22.23-22.28	6.5-7.5	spread	transp.Es(285;95)			
2.5-4	22.37-22.42	2.5-4	spread	transp.Es(275;100)			
3.5-4	23.10	3.5-4	spread	transp.Es(290;100)			
3-4.5	23.22-23.38	3-4.5	spread	transp.Es(290;95-290;95; 300;95)			
6-17	20.25-20.50	6-8;9.25-9.75	OK(till 20.40 spread)	Es,transp.Es,Es(105-300;105;100)	0.2	NS;EW	NS=-0.56 at t=960s
>22	23.00-23.35	-					

Tab.3: Observations on 18 January 2007, measuring path Kašperské Hory

Period [min]	Time (UT)	Doppler record	Reflection height	Amplitude [Hz]	Wavelets geomag. field	Cross-correlation
4-6.5	21.20-21.40	OK(till21.25 signal strength)	20.00-24 UT No data	0.12	NS;EW	EW=0.62 at t=21s V=-0.6 at t=196s
2.5-4	21.40-21.50	OK		0.2	No	V=0.52 at t=-166s
3-4	21.55-22.00	OK		0.05	not evaluated - noise	
2.5-8	22.10-22.20	OK(smeared)		0.26	NS	NS=0.53 at t=319s B=0.61 at t=289s
3.5-8	22.40-23.05	spread,signal strength				
2.5-4	23.10-23.15	OK(spread)		0.15	No	EW=-0.59 at t=125s V=0.51 at t=-33s
3-4.5	23.40-23.45	smeared				
10-14	23.05-23.20	till 23.15 OK,then signal strength (spread)		0.1	NS;EW	NS=0.72 at t=-507s V=-0.57 at t=-478s B=0.62 at t=-524s

Tab.3: Observations on 18 January 2007, measuring path Kašperské Hory (cont.)

>14	21.10-23.05	OK(spread;till21.25 signal strength, 22.00-22.10 signal strength, 22.50-23.05 signal strength)	0.38	NS;EW	No
>14	23.25-24	signal strength			

Tab.4: Observations on 18 January 2007, measuring path Průhonice

Period [min]	Time (UT)	Doppler record	Reflection height	Amplitude [Hz]	Wavelets geomag. field	Cross-correlation
2-3	20.35-20.40	OK(spread)	20.00-24 UT No data	0.07	not evaluated - noise	
2.5-4.5	20.45-20.55	smeared				
3.5-6	21.10-21.15	smeared,ground wave				
2-3	21.00-21.25	smeared,ground wave				
1.5-3	21.35-21.50	signal strength,ground wave				
3.5-6.5	21.25-21.45	signal strength,ground wave				
2-4	22.05	smeared,ground wave				
3-4	22.15-22.30	smeared,ground wave				
2-4	22.35-22.40	smeared				
3.5-5	23.15-23.25	spread, ground wave				
2.5-4	23.40-23.55	spread				
7-12	21.25-21.40	signal strength,ground wave				
17-23	21.10-21.25	smeared,ground wave				
11-19	21.50-22.25	ground wave				

Tab.4: Observations on 18 January 2007, measuring path Průhonice (cont.)

>12	22.00-23.30	signal strength,smeared, ground wave

Tab.5: Observations on 18 January 2007, measuring path Panská Ves

Period [min]	Time (UT)	Doppler record	Reflection height	Amplitude [Hz]	Wavelets geomag. field	Cross-correlation
3.5-6	20.25-20.35	spread	20.00-24 UT No data			
2-4	20.05-21.05	smeared,signal strength				
2.5-5	22.00-22.10	OK(spread)		0.38	No	NS=0.61 at t=55s EW=0.62at t=65s V=-0.71 at t=75s B=0.54 at t=31s
2.5-4	22.20-22.25	smeared				
6-10	22.20-22.35	smeared				
2.5-4	22.40-22.45	OK(spread)		0.12	No	No
3.5-6	22.55-23.25	smeared				
3.5-5.5	23.40-23.50	spread				
>5	20.00-20.35	smeared,signal strength				
>11	20.50-21.40	spread				
5-27	21.45-22.20	spread				

Tab.5: Observations on 18 January 2007, measuring path Panská Ves (cont.)

>20	22.25-23.20	spread			
13-19	22.40-23.00	spread			
10-21	23.05-23.35	OK(spread)	0.21	NS;EW	No

Tab.6: Observations on 18 January 2007, measuring path Dlouhá Louka

Period [min]	Time (UT)	Doppler record	Reflection height	Amplitude [Hz]	Wavelets geomag. field	Cross-correlation
2.5-6	20.25-20.35	spread	20.00-24 UT No data			
3.5-6.5	20.40-20.45	spread				
2-4	20.50-21.10	OK(spread)		0.18	No	No
2-3.5	21.15-21.35	OK		0.18	No	No
4-6	21.10-21.20	OK(spread)		0.11	No	NS=-0.63 at t=-232s B=-0.62 at t=-238s
2-4	22.00-22.10	OK(spread)		0.31	No	EW=-0.52 at t=187s
2-8	22.10-22.25	spread				
2-5	22.35-23.10	spread				
2.5-4	23.20	spread				
3-5	23.50-23.55	spread				
>15	20.00-21.45	OK(till 20.40 signal strength,spread)				
8-23	21.40-22.20	OK(after 22.00spread)				
10-25	22.30-23.25	spread				

Tab.6: Observations on 18 January 2007, measuring path Dlouhá Louka (cont.)

>24	23.20-24	spread

9. References

Altadill, D., Apostolov, E.M., Boška, J., Laštovička, J., Šauli, P., 2004. Planetary and gravity wave signatures in the F region ionosphere with impact to radio propagation predictions and variability. Annals Geophys., 47, p. 1109 – 1119.

Andrews, D.G., Holton, J.R., Leovy, C.B., 1987. Middle atmosphere dynamics. International geophysical series, 40, Academic Press, New York, USA. 489 pp.

Baker, D.M., Davies, K., 1969. F2-region acoustic waves from severe weather. J. Atmos. Sol. Terr. Phys. 31, p. 1345 – 1352.

Bauer, S. J., 1958. An apparent ionospheric response to the passage of hurricanes, J.Geophys. Res., 63, 265-269.

Bertin, F., Testud, J., Kersley, L., 1975. Medium scale gravity waves in the ionospheric F-region and their possible origin in weather disturbances. Planetary Space Science, 23, p. 493 – 507.

Blanc, E., 1985. Observations in the upper atmosphere of infrasonic waves from natural or artificial sources: A summary. Ann. Geophys., 3, p. 673 – 688.

Blum, P.W., Harris, I., 1975. Full Non-linear Treatment of the Global Thermospheric Wind System. I. Mathematical Method and Analysis of Forces. II. Results of the Comparison with Observations. J.Atmos. Terr. Phys. 37, p. 193 – 235.

Boška, J., Šauli, P., 2001. Observations of gravity waves of meteorological origin in the F-region ionosphere. Phys. Chem. Earth (C), 26, p. 425 – 428.

Boška, J., Šauli, P., Altadill, D., Solé, G., Alberca, L.F., 2003. Diurnal variation of the gravity wave activity at midlatitudes of the ionospheric F region. Stud. Geophys. Geod., 47, p. 579 – 586.

Brázdil, R., Štekl, J., et al. (1999). Klimatické poměry Milešovky (Climatic patterns of Mt. Milešovka), (in Czech). Academia, Prague, 433 pp.

Brooks, H.E., Lee, J.W. and Craven, J.P., 2003. The spatial distribution of severe thunderstorm and tornado environments from global reanalysis data. Atmos. Res., 67-68, p.73-94. doi:10.1016/S0169-8095(03)00045-0.

Brooks, H.E., Anderson, A.R., Riemann, K., Ebbers, I., Flachs, H., 2007. Climatological aspects of convective parameters from the NCAR/NCEP reanalysis. Atmos. Res., 83, p. 294 – 305. DOI: 10.1016/j.atmosres. 2005.08.005

Chimonas, G., Peletier, W.R., 1974. On severe storm acoustic signals observed at ionospheric heights. J. Atmos. Terr. Phys., 36, p. 821 – 828.

Chum, J., Hruška, F., Baše, J., Maděra, J., Burešová, D., Laštovička, J., Šindelářová, T., Krasnov, V.M., Drobzheva, Ya.V., 2005. HF frequency Doppler sounding system for ionospheric research in the Czech Republic. EGU General Assembly. Vienna, Austria.

Chum, J., Laštovička, J., Šindelářová, T., Burešová, D., Hruška,F., 2008. Peculiar transient phenomena observed in the infrasound range. J. Atmos.Sol. Terr. Phys., 70, p. 866-878, DOI:10.1016/ j.jastp.2007.06.013

Chum, J., Hruška, F., Burešová, D., Šindelářová, T., Hejda, P., Bochníček, J., 2009. Ionospheric oscillations caused by geomagnetic Pi2 pulsations and their observations by multipoint continuous Doppler sounding; first results. Adv. Space Res., Article in press, doi: 10.1016/j.asr.2009.04.030

Cowling, D.H., Webb, H.D., Yeh, K.C., 1971. Group rays of internal gravity waves in a wind stratified atmosphere. J. Geophys. Res., 76, p. 213 – 220.

Davies, K., 1962. Measurements of ionospheric drifts by means of a Doppler shift technique, J. of Geophys. Res., 67, 4909-4913.

Davies, K., 1990. Ionospheric Radio. Peter Peregrinus Ltd., London, 580 pp.

Davies, K. and Jones, T.B., 1973. Acoustic waves in the ionospheric F2-region produced by severe thunderstorms. J. Atmos. Terr. Phys., 35, p.1737 – 1744.

Davies, K., Jones, T.B., Weaver, P.F., 1973. Ionospheric winds in the F region and their effects on the limiting periods of gravity waves. Planet. Space Sci., 21, p.147 – 149.

Drobzheva, Ya. V., Krasnov, V. M., 2003. The acoustic field in the atmosphere and ionosphere caused by a point explosion on the ground. J. Atmos. Sol. Ter. Phys., 65, 369 – 377. DOI: 10.1016/S1364-6826(02)00141-4

Forbes, J.M., Palo, S.E., Xiaoli Zhang, 2000. Variability of the ionosphere. J. Atmos.Sol.Terr. Phys., 62, p.685 – 693.

Friedman, J.S., 2007. Atmospheric Circulation: Thermal structure and the mesospheric refrigerator. Published on web www.naic.edu/~jonathan/presentations/Mesofridge.ppt

Fritts, D.C., Alexander, M.J., 2003. Gravity wave dynamics and effects in the middle atmosphere. Rev. Geophys., 41(1), 1003.DOI: 10.1029/2001RG000106.

Fritts, D.C., Vadas, S.L., Kam Wan, Werne, J.A., 2006. Mean and variable forcing of the middle atmosphere by gravity waves. J. Atmos. Sol. Terr. Phys., 68, p. 247 – 265. DOI: 10.1016/j.jastp.2005.04.010

Fukao, S., Yamamoto, M., Tsunoda, R.T., Hayakawa, H., Mukai, T., 1998. The SEEK (Sporadic-E Experiment over Kyushu) campaign. Geophysical Research Letters 25, p. 1761 – 1764.

Georges, T.M., 1967. ESSA Technical Report IER 57-ITSA 54. Ionospheric Effects of Atmospheric Waves. Institute for Telecomunication Sciences and Aeronomy, Boulder, 341 pp.

Georges, T.M., 1968. HF Doppler studies of traveling ionospheric disturbances. J. Atmos. Terr. Phys., 30, p. 735 – 746.

Georges, T.M., 1973. Infrasound from convective storms: Examining the evidence. Rev. Geophys. Space Phys., 11, p. 571 – 594.

Georges, T.M. and Young, J.M., 1972. Passive sensing of natural acoustic-gravity waves at the earth's surface. In: V.E. Derr (Editor), Remote sensing of the Troposphere. U.S. Government Printing Office, Washington, D.C., Cat. No. C55.602:T75: 21-1 to 21-23.

Gossard, E.E., Hooke, W.H., 1975. Waves in the Atmosphere. Atmospheric Infrasound and Gravity Waves – their Generation and Propagation. Elsevier Scientific Publishing Company, Amsterdam, 456 pp.

Gupta, A.B., Nagpal, O.P., Setty C.S.G.K., 1973. Effects of atmospheric temperature gradients and netral winds on the lower cutoff period of gravity waves. Ann. Geophys., 29, p. 301 – 305.

Gusev, O., Kaufman, M., Grossmann, K.-U., Schmidlin, F.J., Shepherd, M.G., 2006. Atmospheric neutral temperature distribution at the mesopause altitude. J. Atmos.Sol.Terr. Phys., 68, p.1684 – 1697. DOI: 10.1016/j.jastp.2005.12.010

Hargreaves, J.K., 1992. The solar-terrestrial environment. Cambridge Atmospheric and Space Science Series, 5, Cambridge University Press, Cambridge, 420 pp.

Hines, C.O., 1960. Internal atmospheric gravity waves at ionospheric heights. Can. J. Phys., 38, p. 1441 – 1481.

Hines, C.O., 1968. Some consequences of gravity-wave critical layers in the upper atmosphere. J. Atmos. Terr. Phys., 30, p. 795 – 823.

Hung, R.J., Plan, T., Smith, R.E., 1979. Coupling of ionosphere and troposphere during the occurrence of isolated tornadoes on November 20, 1973. J. Geophys. Res., 84, p.1261-1267.

Hunsucker, R., 1982. Atmospheric gravity waves generated in the highlatitude ionosphere: a review, Rev. Geophys. Space Phys., 20, p .293 – 315.

Kazimirovsky, E.S., Herriaz, M., de la Morena, B.A., 2003. Effects on the ionosphere due to phenomena occuring below it. Surv. Geophys., 24, p.139 – 184.

Kazimirovsky, E.S., Kokourov, V.D., Vergasova, G.V., 2006. Dynamical climatology of the upper mesosphere, lower thermosphere and ionosphere. Surv. Geophys.,27, p.211 – 255. DOI 10.1007/s10712-005-3819-3.

Kelley, M.C., 1997. In situ ionospheric observations of severe weather related gravity waves and associated small-scale plasma structures. J. Geophys. Res., 102, A1, p.329 – 335.

Korsunova, L.P., 1991. Volnovyje vozmuščenija v parametrach sloja Es na srednich širotach (Wave-like disturbances in sporadic-E layer parameters at middle latitudes), (in Russian). Geomagnetizm i Aeronomia, 31, p. 192 – 194.

Krasnov, V.M., Drobzheva, Ya.V., 2005. The acoustic field in the ionosphere caused by an underground nuclear explosion. J. Atmos. Sol. Ter. Phys., 67, 913 – 920. DOI: 10.1016/j.jastp.2005.02.014

Krasnov, V.M., Drobzheva, Ya.V., Laštovička, J., 2006. Recent advances and difficulties of infrasonic wave investigation in the ionosphere. Surveys in Geophysics, 27, p. 169 – 209. DOI: 10.1007/s10712-005-6203-4.

Krasnov, V.M., Drobzheva, Ya.V., Laštovička, J., 2007. Acoustic energy transfer to the upper atmosphere from sinusoidal sources and a role of nonlinear processes. Journal Atmos. Sol. Ter. Phys., 69, 1357-1365. DOI: 10.1016/j.jastp,2007.04.011

Labitzke, K., van Loon, H., 1999. The stratosphere: phenomana, history, and relevance. Springer, Berlin, 179 pp.

Lane, T.P, Clark, T.L., 2002. Gravity waves generated by the dry convective boundary layer: two-dimensional scale selection and boundary layer feedback. Quarterly Journal of Royal Meteorological Society, 128, 1543 – 1570.

Laštovička, J., 2006. Forcing of the ionosphere by waves from below. J. Atmos. Sol. Terr. Phys., 68, p. 479 – 497. DOI: 10.1016/j.jastp.2005.01.018

Marshall, R.A., Menk, F.W., 1999. Observations of Pc 3-4 and Pi 2 geomagnetic pulsations in the low –latitude ionosphere. Ann. Geophys., 17, p.1397-1410.

Matthews, J.D., 1998. Sporadic-E: current views and recent progress. J. Atmos. Terr. Phys. 60, p. 413 – 435.

Moo, C.A., Pierce, A.D., 1972. AGARD Conference Proc. No. 115, Ref. 17.

Novák, P., 2000. Meteorological interpretation of Doppler weather radar measurements. Doctoral thesis, Faculty of Mathematics and Physics, Charles University, Prague.

Novák, P., Kráčmar, J., 2000. Using data from the Czech weather radar network for detection of convective storms, 1st European tornadoes and severe storms konference, Toulouse, 1-4 February 2000. Published on web www.chmi.cz/meteo/rad/pub/ssc2000/

Oliver, W.L., Otsuka,Y., Sato, M., Takami, T., Fukao, S., 1997. A climatology of F region gravity wave propagation over the middle and upper atmosphere radar. J. Geophys. Res. 102, p. 14,499 – 14,512.

Parkinson, K.L., Dyson, P.L., 1998. Measurements of mid-latitude E-region, sporadic-E and TID-related drifts using HF Doppler-sorted interferometry. J. Atmos. Sol. Terr. Phys. 60, p.509-522.

Pešice, P., Sulan, J. and Řezáčová, D., 2003. Convection precursors in the Czech territory. Atmos. Res., 67-68, p. 523-532. doi:10.1016/S0169-8095(03)00070-X.

Pierce, A.D., Coroniti, S.C., 1966. A mechanism for the generation of acoustic-gravity waves during thunderstorm formation. Nature, 210, p. 12099-1210.

Pitteway, M.L.V., Hines, C.O., 1963. The viscous damping of atmospheric gravity waves. Can. J. Phys., 41, p. 1935 – 1948.

Prasad, S.S., Schneck, L.J., Davies, K., 1975. Ionospheric disturbances by severe tropospheric weather storms. J. Atmos. Terr. Phys., 37, p.1357 – 1363.

Rastogi, R.G., 1962. Thunderstorms and sporadic E-layer ionization over Ottawa, Canada. J. Atmos. Terr. Phys., 24, p.533-534, IN3-IN8, 535-540

Rayleigh, Lord (J. W. Strutt), 1894. Theory of Sound. McMillan and Co. Ltd., London; Dover Publications, Inc., New York (1945).

Řezáčová, D., Novák, P., Kašpar, M., Setvák, M., 2007. Fyzika oblaků a srážek (Physics of clouds and precipitation), (in Czech). Academia, Praha, 576 pp.

Rind, D., 1978. Investigation of the lower thermosphere results of ten years of continuous observations with natural infrasound. J. Atmos. Terr. Phys., 40, p.1199 – 1209.

Rishbeth, H., 2006. F-region links with the lower atmosphere? J. Atmos. Sol. Terr. Phys., 68, p. 469 – 478. DOI: 10.1016/j.jastp.2005.03.017

Rishbeth, H., Mendillo, M., 2001. Patterns of F2-layer variability. J. Atmos. Sol. Terr. Phys., 63, p. 1661 – 1680.

Sehnalová, P., 2007. Roční chod výskytu bouřek a bouřkových jevů v ČR (Annual course of thunderstorms and convective storms in the Czech Republic), (in Czech). Bachelor thesis, Faculty of Science, Charles University, Prague.

Sentman, D.D., Wescott, E.M., Picard, R.H., Winick, J.R., Stenbaek-Nielsen, H.C., Dewan, E.M., Moudry, D.R., Sao Sabbas, F.T., Heavner, M.J., Morrill, J., 2003. Simultaneous observations of mesospheric gravity waves and sprites generated by a Midwestern thunderstorm. J. Atmos.Sol.Terr. Phys., 65, 537 -550. DOI: 10.1016/S1364-6826(02)00328-0.

Sun, L., Wan, W., Ding, F., Mao, T., 2007. Gravity wave propagation in the realistic atmosphere based on a three-dimensional transfer function model. Ann. Geophys., 25, p. 1979 – 1986.

Šauli, P., 2000. Vlnové jevy v ionosféře spojené s průchodem gravitačních vln troposférického původu (Wave-like effects in the ionosphere connected with the passage of the gravity waves of tropospheric origin), (in Czech). Doctoral thesis, Faculty of Mathematics and Physics, Charles University, Prague.

Šauli, P., Boška, J., 2001. Tropospheric events and possible related gravity wave activity effects on the ionosphere. J. Atmos. Sol. Terr. Phys., 63, p.945 – 950.

Šindelářová, T., Burešová, D., Chum, J., Hruška, F., 2009a. Doppler observations of infrasonic waves of meteorological origin at ionospheric heights. Adv. Space Res., 43, p. 1644-1651. DOI:10.1016/j.asr.2008.08.022

Šindelářová, T., Burešová, D., Chum, J., 2009b. Acoustic-gravity waves in the ionosphere generated by severe tropospheric weather. Stud. Geophys. Geod. DOI:10.1007/s11200-009-0028-4

Vadas, S.L., 2007. Horizontal and vertical propagation and dissipation of gravity waves in the thermosphere from lower atmospheric and thermospheric sources. J. Geophys. Res., 112, A06305. DOI:10.1029/2006JA011845

Vadas,S.L., Fritts, D.C., 2004. Thermospheric responses to gravity waves arising from mesoscale convective complexes. J. Atmos. Sol. Terr. Phys., 66, p.781 – 804. DOI:10.1016/j.jastp.2004.01.025

Yeh, K. C., Liu, C. H., 1974. Acoustic-gravity waves in the upper atmosphere. Rev. Geoph. and Space Phys. 12, p.193-215.

Zipser, E.J, Cecil, D.J., Chuntao Liu, Nesbitt, S.W., Yorty, D.P., 2006. Where are the most intense thunderstorms on Earth? Bull. Amer. Meteor. Soc., 87, p.1057-1071.

Zuo Xiao, Sai-guan Xiao, Yong-qiang Hao, Dong-he Zhang, 2007. Morphological features of ionospheric response to typhoon. J. of Geophys. Res., 112, A04304, doi:10.1029/2006JA011671.

Internet sources

www.astrosurf.com

www.chmi.cz

www.gwdg.de

www.sworld.com.au/steven/space/atmosphere/

www.ukssdc.ac.uk

www2.wetter3.de

www.wetterzentrale.de

http://bourky.astronomie.cz

http://pluto.space.swri.edu

http://swdcwww.kugi.kyoto-u.ac.jp

http://upload.wikimedia.org

Appendix I

The Doppler shift observations on quiet days in May – September 2006 are summarized. The table for each day contains

Col.1: period of observed waves

Col.2: time of observation

Col.3: quality of the Doppler trace, other effects observed in the Doppler record

Col.4: Virtual height of reflection of the 3.59 MHz wave

Col.5: Amplitude of waves in observed period range (band pass filter was used). Waves of amplitudes lower than 0.1 Hz were considered as noise.

Col.6: Wavelet analysis of components of the local geomagnetic field, occurrence of geomagnetic fluctuations in the corresponding time and period range (NS: north-south component; WE: west-east component; V: vertical component; B: amplitude of the local geomagnetic field)

Col.7: cross-correlation between the Doppler signal and components of the local geomagnetic field. The maximum (of the absolute value) and time shift of maximum are shown, in case the absolute value is higher than 0.5. Negative time shift means that geomagnetic fluctuations precede the Doppler signal. However, the sign must be interpreted very cautiously, since in most cases it was not possible to determine the exact start of the event in both Doppler shift and geomagnetic records. The symbols are same like in Col.6.

The CD-ROM contains following plots for each quiet day:

1. Detailed Doppler shift spectrogram recorded at the measuring path Panská Ves - Prague.
2. Height of reflection of the 3.59 MHz wave. Blue line: reflection from the Es layer. Red line: reflection from the F layer – ordinary wave. Green line: reflection from the F layer – extraordinary wave.
3. Wavelet transform of the Doppler signal at Panská Ves path; periods 1-30 min.
4. Wavelet transform of fluctuations of the north-south and the west-east component of the geomagnetic field at observatory Budkov, periods 1-30 min.
5. Wavelet transform of fluctuations of the vertical component of the geomagnetic field at observatory Budkov, periods 1-30 min.

3 May 2006

Period [min]	**Time (UT)**	**Doppler record**	**Reflection height, layer [km]**	**Amplitude [Hz]**	**Wavelets, geomag.field**	**Cross-correlation**
5-7.5	22.05-22.15	CLEAR (signal strength)	F(250-280)	0.12	NS;EW	EW=-0.8 at t=-261s
>8	18.00-19.50	till 18.40 double trace, then CLEAR	F(250-260)	0.47	NS;EW	NS=0.65 at t=71s B=0.59 at t=77s
13-16	19.50-20.15	CLEAR	F(255-250)	0.06	not evaluated - noise	
15-26	21.40-22.25	CLEAR(after 22.00 signal strength)	F(255-300)	0.11	NS;EW	NS=-0.67 at t=-98s V=-0.6 at t=657s B=-0.67 at t=-123s
13-26	23.10-24	CLEAR (till 23.20 signal strength)	transp.Es,F(335;105-340-335-325)	not calc.	NS;EW	not calc.

11 June 2006

Period [min]	**Time (UT)**	**Doppler record**	**Reflection height, layer [km]**	**Amplitude [Hz]**	**Wavelets, geomag.field**	**Cross-correlation**
3-4	19.05-19.10	discrete trace,signal strength	F(270-260)			
6.5-9	18.55-19.20	CLEAR(19.00-19.10 discrete trace,signal strength)	F(270-260)	0.09	not evaluated – noise	
12-22	18.20-18.55	CLEAR(till 18.30 double trace, signal strength)	F,transp.Es,F(270-260;110--265-270)	0.18	NS	EW=0.62Hz at t=739s
>26	19.00-19.25	CLEAR(19.00-19.10 discrete trace, signal strength)	F(270-260)	0.05	not evaluated – noise	
>14	19.30-20.35	CLEAR	F(260-270)	0.32	NS;EW	NS=0.52 at t=-304s V=-0.6 at t=-320s B=-0.53 at t=-1244s
>14	23.35-24	spread	transp.Es,F(300;100-290)	not.calc.	NS;EW	not calc.

2 July 2006

Period [min]	**Time (UT)**	**Doppler record**	**Reflection height, layer [km]**	**Amplitude [Hz]**	**Wavelets, geomag.field**	**Cross-correlation**
3.5-7.5	16.00-16.20	CLEAR(signal strength)	F,transp.Es,Es(240-260;115 -110)	0.17	NS	NS=-0.6 at t=-225s B=-0.62 at t=-222s
5.5-8.5	19.35-19.40	CLEAR(smeared)	Es,transp.Es(105-250;110)	0.07	not evaluated - noise	
4.5-8	19.50-20.00	CLEAR	transpEs,Es(250;110-110)	0.08	not evaluated - noise	
4-6	21.20-21.30	CLEAR(triple trace)	transp.Es(280;110-290;110)	0.1	No	NS=-0.5 at t=217s EW=-0.56 at t=-110s
4-9	22.50-23.00	after 22.55 discrete double trace,spread	F,transp.Es(320-320;105)			
12-16	16.50-17.10	smeared,double trace	transp.Es,F(290;110-290-290)			
>12	22.55-24	CLEAR(after 22.55 discrete double trace,spread)	F,transp.Es,F(320-320;105-290 -310-310)	not.calc.	NS	not calc.

17 July 2006

Period [min]	**Time (UT)**	**Doppler record**	**Reflection height, layer [km]**	**Amplitude [Hz]**	**Wavelets, geomag.field**	**Cross-correlation**
5-7.5	16.20-16.25	double trace	transp.Es(270;105-300;135)			
5-8	16.40-16.50	16.45 discrete double trace	transp.Es,Es(300;135-110-115)			
7-11	17.10-17.20	CLEAR	Es(115-110)	0.06	not evaluated - noise	
6.5-14	18.05-18.15	spread	Es(105)			
4-5	18.30-18.35	spread,ripples	Es,F(110-260)			
2.5-9	18.40-19.05	spread,ripples	F,transp.Es(260-260;110)			
4-6.5	22.20-22.30	CLEAR(22.25 discrete trace)	F(250-255)	0.15	No	V=-0,55 at t=-234s
6-8.5	22.50-22.55	discrete trace,spread	F(255)			
7-9	23.05-23.10	discrete trace,spread	F(250)			
11-28	18.20-19.15	till 18.25 spread	Es,F,Es(110-110-260-260;			
		18.30-19.00 spread,ripples	110-105)			
>20	21.05-21.35	spread	transp.Es,F(275;110-275;105-260)			
13-24	21.50-22.40	CLEAR(spread)	F(260-250)	0.25	EW;V	NS=-0.58 at t=-869s EW=-0.65 at t=10s V=-0.56 at t=484s B=0.6 at t=-132s
>14	23.00-24	CLEAR (spread,at 23.00 discrete trace)	F(255-265)	not calc.	EW	not calc.

18 July 2006

Period [min]	Time (UT)	Doppler record	Reflection height, layer [km]	Amplitude [Hz]	Wavelets, geomag.field	Cross-correlation
5-5.5	19.00-19.05	spread	transp.Es(225;105)			
5-7.5	19.10-19.20	spread	transp.Es,Es(225;105-100)			
7-10	19.30-19.40	spread	transp.Es(270;105)			
6-8	22.00-22.10	spread	F,transp.Es(265-270;105)			
2.5-6	22.20	spread	transp.Es,Es(270;105-105)			
8-11	22.35-22.45	spread,ripples	Es,transp.Es(105-260;105)			
3.5-8.5	23.00-23.10	spread,ripples	transp.Es,Es(270;105-100)			
>18	19.10-19.25	spread	transp.Es,Es,transp.Es(225;105-100 -270;105)			
14-26	20.40-21.10	CLEAR(till 20.45 spread)	transp.Es,F,Es(265;105-255-260-105)	0.12	NS;EW; V	NS=0.72 at t=-355s EW=0.71 at t=-562s V=-0.76 at t=383s B=-0.72 at t=-997s
15-25	21.35-22.35	spread,ripples	Es,F,transp.Es,Es,transp.Es(101-101-250 -270;105-105-260;105)			
>17	23.15-23.40	spread	Es,transp.Es,F(100-290;105-295)			

19 July 2006

Period [min]	Time (UT)	Doppler record	Reflection height, layer [km]	Amplitude [Hz]	Wavelets, geomag.field	Cross-correlation
5.5-8.5	16.00-16.10	CLEAR(double trace,signal strength)	F,transp.Es(270-275;135)	not calc.	No	not calc.
6.5-9	16.50-17. 05	CLEAR	transp.Es,Es,transp.Es(320;115-115-275;121)	0.06	not evaluated – noise	
5.5-8	17.25-17.30	discrete double trace	transp.Es(280;120)			
1.5-3	20.00	ripple,spread	transp.Es(250;100)			
13-21	16.15-16.30	signal strength,double trace	transp.Es(275;135-290;120)			
>12	17.40-18.50	till 18.15 discrete multiple trace, 18.15-18.25 smeared	Es,F,transp.Es,Es(110-110-275-255; 110-110)			
4-13	19.40-19.50	spread,ripples	transp.Es,F,transp.Es(250;110-255--250;100)			
>14	19.50-22.00	CLEAR(19.50-20.05 spread, ripples)	F,transp.Es,F(250-250;101-250-245--245-250-250-255-260-250)	0.29	NS;EW	NS=0.6 at t=1724s B=0.6 at t=1726s
12-25	22.20-22.50	CLEAR(22.35 S-shape)	F(250-255-245-250)	0.2	NS;EW	NS=-0.68 at t=907s EW=-0.77 at t=-920s V=0.71 at t=1028s B=-0.62 at t=879s
>5	23.20-24	CLEAR	F(255-245-255)	not calc.	NS;EW	not calc.

9 September 2006

Period [min]	Time (UT)	Doppler record	Reflection height, layer [km]	Amplitude [Hz]	Wavelets, geomag.field	Cross-correlation
13-18	18.00-18.15	CLEAR	F(255-250)	0.12	NS;EW	NS=-0.6 at t=-620s V=-0.6 at t=212s B=-0.51 at t=-653s
13-23	18.25-18.55	CLEAR	F(250-255)	0.16	No	EW=-0.6 at t=-224s
>24	17.00-18.50	CLEAR(till 18.05 double trace)	F(250-260)	not calc.	NS	not calc.
>15	19.15-20.25	CLEAR	F(245-255)	0.19	NS;EW	EW=-0.58 at t=-1210s V=-0.52 at t=1104s B=-0.5 at t=1150s
14-24	21.20-21.50	CLEAR	F(245-250)	0.16	NS	NS=0.67 at t=-1280s B=0.65 at t=-1292s
13-19	22.10-22.25	22.15-22.25 double trace	F(250-275)	0.11	NS	NS=0.71 at t=-397s EW=-0.74 at t=-47s V=-0.66 at t=360s B=0.79 at t=-384s
>15	22.40-24	CLEAR(after 23.35 signal strength)	F(290-340,approaching fxF2)	not calc.	NS;EW	not calc.

10 September 2006

Period [min]	Time (UT)	Doppler record	Reflection height, layer [km]	Amplitude [Hz]	Wavelets, geomag.field	Cross-correlation
7.5-13	16.15-16.30	CLEAR	F(250-240)	0.1	No	No
>17	17.30-18.10	CLEAR(17.30-17.45 double trace)	F(250-260)	0.2	NS;EW	NS=0.56 at t=1157s EW=0.75 at t= 1071s
>13	18.30-19.25	CLEAR	F(245-260)	0.26	No	NS=0.54 at t=711s EW=-0.71 at t=-340s B=-0.5 at t=-951s
>22	19.25-20.00	CLEAR(19.30-19.35 discrete trace, 19.35-19.45 micropulsations)	F(245-250)	not calc.	NS	not calc.
2.5-3	19.35-19.45	CLEAR	F(245)	0.09	not evaluated - noise	
12-16	19.50-20.00	CLEAR(19.55 discrete trace--no shift)	F(245)	0.09	not evaluated – noise	
13-22	20.35-21.05	CLEAR(20.50-21.05 double trace)	F(255-270)	0.14	EW	NS=-0.6 at t=574s V=0.57 at t=753s B=-0.63 at t=488s
14-25	21.20-21.50	CLEAR	F(275-285)	0.16	EW	EW=0.57 at t=557s V=-0.78 at t=-786s
>13	22.50-23.45	till 23.30 CLEAR(23.10-23.30 double trace),then double trace, discrete trace,spread	F(270-300)	0.28	NS	NS=-0.78 at t=-1183s EW=0.66 at t=-1024s V=0.73 at t=-1167s B=0.77 at t=-1190s

14 September 2006

Period [min]	Time (UT)	Doppler record	Reflection height, layer [km]	Amplitude [Hz]	Wavelets, geomag.field	Cross-correlation
2.5-4.5	16.50-16.55	double trace	Es,transp.Es(95-260;95)			
12-30	17.25-18.20	CLEAR(17.40-18.05 double trace)	F(270-280)	0.2	NS;EW	NS=-0.76 at t=984s EW=-0.7 at t=1569s V=0.65 at t=1023s B=-0.74 at t=976s
>25	18.20-18.55	CLEAR	F(260-270)	not calc.	NS;EW	not calc.
16-20	19.30-19.50	CLEAR	F(245-250)	0.06	not evaluated - noise	
12-22	19.55-20.45	CLEAR	F(235-245)	0.16	NS	NS=0.62 at t=-197s EW=0.57 at t=-585s B=0.6 at t=-194s
>18	21.40-22.45	after 21.55 double trace	F(245-310)			
>15	23.30-24	23.30-23.50 signal strength	F(325,approaching fxF2)			

21 September 2006

Period [min]	Time (UT)	Doppler record	Reflection height, layer [km]	Amplitude [Hz]	Wavelets, geomag.field	Cross-correlation
3-4	21.05-21.10	CLEAR	F(225)	0.02	not evaluated-noise	
3-3.5	22.40-22.45	CLEAR(signal strength)	F(303-396;foF2=3.05MHz)	0.04	not evaluated-noise	
1-4.5	22.55-23.05	CLEAR(signal strength)	F(396-319;foF2=3.05-3.1MHz)	0.33	NS;EW	NS=-0.86 at t=-26s EW=0.85 at t=-13s V=0.79 at=47s B=-0.86 at t=-28s
5-11	15.55-16.00	double trace	F(245)			
11-13	14.30-14.35	CLEAR	F(240)	0.04	not evaluated-noise	
16-24	14.20-14.45	CLEAR	F(245-240)	0.09	not evaluated -noise	
9-15	15.05-15.25	CLEAR(double trace)	F(260-250)	0.1	No	EW=0.64 at t=200s
15-30	16.25-17.20	CLEAR(double trace)	F(245-235)	0.13	NS;EW	NS=0.69 at t=-261s EW=0.6 at t=930s B=0.68 at t=-250s
17-26	17.20-17.50	CLEAR	F(235)	0.09	not evaluated-noise	
11-16	18.10-18.25	CLEAR	F(235)	0.08	not evaluated-noise	
>27	18.30-19.20	CLEAR(after 19.05 spread)	F(235-245)	not calc.	NS	not calc.
11-19	19.10-19.45	CLEAR(spread)	F(245)	0.14	NS;EW	NS=-0.56 at t=-3s EW=-0.6 at t=-550s V=-0.62 at t=622s B=-0.59 at t=-41s
11-15	20.10-20.20	CLEAR	F(240)	0.04	not evaluated - noise	

21 September 2006 (cont.)

Period [min]	Time (UT)	Doppler record	Reflection height, layer [km]	Amplitude [Hz]	Wavelets, geomag.field	Cross-correlation
11-19	20.40-21.05	CLEAR(till 20.50 spread; ~21.05 micropuls.)	F(230-225)	0.12	NS;EW	EW=-0.57 at t=-591s V=0.57 at t=-718s B=-0.5 at t=-1035s
16-19	21.15-21.30	CLEAR	F(225)	0.04	not evaluated-noise	
11-18	21.35-22.10	CLEAR(till 22.00 double trace)	F(245-275)	0.13	EW	EW=-0.67 at t=85s
19-26	22.25-22.45	CLEAR(~22.40-22.45 micropuls.)	F(275-395;foF2=3.28-3.05MHz)	0.09	not evaluated-noise	
>17	23.10-24	CLEAR(~23.00-23.05 micropuls.; spread signal strength)	F(360-320-360-365; foF2=3.1-3.05MHz)	not calc.	NS;EW	not calc.

22 September 2006

Period [min]	**Time (UT)**	**Doppler record**	**Reflection height, layer [km]**	**Amplitude [Hz]**	**Wavelets, geomag.field**	**Cross-correlation**
2-3.5	20.15-20.25	CLEAR	F(250-255)	0.06	not evaluated - noise	
1.5-3	20.45-20.50	CLEAR	F(270)	0.09	not evaluated - noise	
2.5-4	22.30-22.35	CLEAR	F(305; foF2=3.33-3.25MHz)	0.06	not evaluated - noise	
1-6.5*)	23.20-23.35	CLEAR	F(335-345-325; foF2=3.1-3.2MHz)	0.27	NS;EW (2-4min)	periods 2-4 min: NS=0.53 at t=-130s EW=0.61 at t=-15s B=0.54 at t=-128s
>20	20.00-21.10	CLEAR	F(250-265)	not calc.	NS;EW	not calc.
12-20	21.40-22.15	CLEAR	F(265-305; foF2=3.5-3.33MHz)	0.1	No	NS=0.7 at t=-36s B=0.67 at t=-45s
12-17	23.35-24	CLEAR	F(345-325; foF2=3.16-3.2MHz)	not calc.	No	not calc.

*) The cross correlation between the Doppler signal and geomagnetic records is rather weak in period range 1-6.5 min. According to the wavelet transform, fluctuations of horizontal components of the local geomagnetic field with periods 2-4 min occurred simultaneously with ionospheric waves. The data are correlated in the period range 2-4 min.

Appendix II

Weather situation, geomagnetic conditions, and ionospheric observations are summarized for convective storm events in May – August 2006.

The results of Doppler shift observations are in detail listed in tables which contain

Col.1: period of observed waves

Col.2: time of observation

Col.3: periods of observed waves, whose amplitudes exceed upper quartile of the reference Fourier spectrum.

Col.4: quality of the Doppler trace, other effects observed in the Doppler record

Col.5: Virtual height of reflection of the 3.59 MHz wave

Col.6: Amplitude of waves in observed period range (band pass filter was used). Waves of amplitudes lower than 0.1 Hz were considered as noise.

Col.7: Wavelet analysis of components of the local geomagnetic field, occurrence of geomagnetic fluctuations in the corresponding time and period range (NS: north-south component; WE: west-east component; V: vertical component; B: amplitude of the local geomagnetic field)

Col.8: cross-correlation between the Doppler signal and components of the local geomagnetic field. The maximum (of the absolute value) and time shift of maximum are shown, in case the absolute value is higher than 0.5. Negative time shift means that geomagnetic fluctuations precede the Doppler signal. However, the sign must be interpreted very cautiously, since in most cases it was not possible to determine the exact start of the event in both Doppler shift and geomagnetic records. The symbols are same like in Col.7.

The CD-ROM contains following plots for each event:

1. Detailed Doppler shift spectrogram recorded at the measuring path Panská Ves - Prague.

2. Height of reflection of the 3.59 MHz wave. Blue line: reflection from the Es layer. Red line: reflection from the F layer – ordinary wave. Green line: reflection from the F layer – extraordinary wave.

3. Fourier transform of the signal at Panská Ves path. Red line: amplitude spectrum. Black lines: reference Fourier spectrum (dashed lines: lower quartile and upper quartile; solid line: median).

4. Wavelet transform of the signal at Panská Ves path; periods 1-30 min.

5. Wavelet transform of fluctuations of the north-south and the west-east component of the geomagnetic field at observatory Budkov, periods 1-30min.

6. Wavelet transform of fluctuations of the vertical component of the geomagnetic field at observatory Budkov, periods 1-30min.

9 May 2006 18:00 – 22:00 UT

Weather

Synoptic situation: occluded front and an instability line

Time of passage of convective storms under the measuring path: ~13:00-15:30 UT; in the interval 18:00-22:00 UT abating storms in Southern Bohemia

Hourly average of wind speed at Milešovka observatory: 7.5-8.3 $m \cdot s^{-1}$

Height of clouds: lower than the tropopause

Geomagnetic conditions

Minimum Dst = -12 nT at 02:00 UT

Maximum Kp = 1+

Doppler observations

Waves of periods longer than ~11 min occurred at ~18:00-19:35 UT; spectral peaks of the Fourier amplitude spectrum at ~12-14 min, ~15 min, ~17-25 min exceeded significantly mean values for quiet days. Waves of periods ~13-24 min occurred at ~19:35-20:15 UT; spectral peaks at ~14 min, ~15 min, ~17-24 min exceeded significantly mean values for quiet days. Waves of periods ~14-25 min occurred at ~20:30-21:40 UT; spectral peaks at ~14 min, ~15 min, and ~17-25 min exceeded significantly mean values for quiet days. Geomagnetic oscillations were observed in the corresponding time and period range. Doppler signal and geomagnetic record are correlated.

13 May 2006 18:00 – 23:59 UT

Weather

Synoptic situation: instability line, low horizontal pressure gradient

Time of passage of convective storms under the measuring path:

~14:00-14:30 UT; in the interval 18:00-23:59 UT storms in Moravia and Southern Bohemia

Hourly average of wind speed at Milešovka observatory: 6.1 – 10.5 $m \cdot s^{-1}$

Height of clouds: reaching to the tropopause altitude

Geomagnetic conditions

Minimum Dst = -17 nT at 05:00-06:00 UT

Maximum Kp = 3+

Doppler observations

The Doppler sounding wave reflected mainly from the F layer. Wave activity was observed particularly in the period range of tenths of minutes. Waves of periods longer than ~17 min occurred at ~18:15-19:05 UT, spectral peaks of the Fourier amplitude spectrum at ~20 min and ~24 min exceeded significantly mean values for quiet days. Waves of periods longer than ~18 min occurred at ~19:30-20:10 UT, spectral peaks at ~20 min and ~24 min exceeded significantly mean values for quiet days. Waves of periods longer than ~14 min occurred at ~20:35-21:30 UT, spectral peaks at ~15 min, ~20 min, and ~24 min exceeded significantly mean values for quiet days. Geomagnetic oscillations were observed in the corresponding time and period range. Doppler signal and geomagnetic record are correlated.

Waves of periods longer than ~20 min occurred at ~21:50-22:50 UT, spectral peaks at ~20 min and ~24 min exceeded significantly mean values for quiet days. Wavelet analysis revealed fluctuations of horizontal components of the local geomagnetic field in the same time and period range. Cross-correlations between the Doppler signal and fluctuations of the components of the local geomagnetic field were not computed; the periods of observed waves exceed 30 min and a narrow period range is left after filtering the signal, therefore the results might be distorted. Cautious interpretation of the result is necessary, since the Doppler trace was disturbed by spread and discrete

trace between ~22:00-22:20 UT. The signal was replaced by signal with a constant Doppler shifts in this time interval. It might have caused a “discrete like” Doppler trace at the beginning and at the end of the interval. Subsequently, the wavelet analysis showed a wide spectrum (20 to more than 60 min) in a relatively short time interval.

14 May 2006 18:00 – 20:00 UT

Weather

Synoptic situation: cold front

Time of passage of convective storms under the measuring path: Convective storms did not pass under the measuring path. In the interval 18:00-19:30 UT abating storms in Moravia.

Hourly average of wind speed at Milešovka observatory: 9.4-10.0 $m \cdot s^{-1}$

Height of clouds: reaching to the tropopause region

Geomagnetic conditions

Minimum Dst = -10 nT at 03:00-04:00 UT

Maximum Kp = 3

Doppler observations

Waves of periods ~13-25 min occurred at ~18:55-19:30 UT, spectral peaks at ~13-21 min exceeded significantly mean values for quiet days. Geomagnetic oscillations were observed in the corresponding time and period range. Doppler signal and geomagnetic record are correlated.

16 May 2006 18:00 – 23:59 UT

Weather

Synoptic situation: cold front

Time of passage of convective storms under the measuring path: ~12:30-21:00 UT.

Hourly average of wind speed at Milešovka observatory: 6.1-8.1 $m \cdot s^{-1}$

Height of clouds: lower than the tropopause

Geomagnetic conditions

Minimum Dst = -7 nT at 01:00-02:00 UT

Maximum Kp = 1-

Doppler observations

Very low wave activity was observed on 16 May 2006. Till 22:00 UT, the Es layer was present. Waves of periods longer than 14 min were detected by the wavelet analysis. However, the Doppler record was spread and the signal was weak in the mentioned time interval. Therefore, the results of spectral analysis cannot be considered as reliable.

20 May 2006 18:00 – 23:59 UT

Weather

Synoptic situation: cold front

Time of passage of convective storms under the measuring path: ~19:30-20:00 UT

Hourly average of wind speed at Milešovka observatory: 18.1-18.6 $m \cdot s^{-1}$

Height of clouds: reaching to the tropopause region

Geomagnetic conditions

Minimum Dst = -12 nT at 01:00-02:00 UT

Maximum Kp = 2-

Doppler observations

Very low wave activity was observed on 20 May 2006. A transparent Es layer was present for most of the analysed interval. Waves of periods longer than 18 min occurred at ~19:10-19:30 UT and waves of periods longer than 20 min occurred at ~20:10-20:40 UT; however the amplitudes did not significantly exceed mean values for quiet days.

22 May 2006 18:00 – 23:59 UT

Weather

Synoptic situation: cold front and an instability line

Time of passage of convective storms under the measuring path: ~19:00-20:00 UT

Hourly average of wind speed at Milešovka observatory: 7.5-15.6 $m \cdot s^{-1}$

Height of clouds: reaching to the tropopause region

Geomagnetic conditions

Minimum Dst = -7 nT at 01:00-02:00; 04:00 UT

Maximum Kp = 4-

Doppler observations

The wave activity was rather low on 22 May 2006. Waves of periods longer than 13 min occurred at ~19:20-19:50 UT, spectral peaks in the Fourier amplitude spectrum at ~13 min, ~14 min, ~16.5 min, and ~18 min exceeded significantly mean values for quiet days. Precipitation area with rather weak convective storms was passing under the ionospheric reflection point of the Doppler sounding wave between ~19:30 and 21:00 UT. Geomagnetic oscillations were observed in the corresponding time and period range. Doppler signal and geomagnetic record are correlated.

Waves of periods ~14-21 min occurred at ~22:25-23:10 UT, spectral peaks ~14 min, ~16.5 min, and ~18 min exceeded significantly mean values for quiet days. Geomagnetic oscillations were observed in the corresponding time and period range. Doppler signal and geomagnetic record are correlated.

16 June 2006 18:00 – 23:59 UT

Weather

Synoptic situation: cold front

Time of passage of convective storms under the measuring path: ~16:00-17:30 UT. After ~18:00 UT, convective storms in western and eastern Bohemia and in Germany. After ~21:00 UT extensive precipitation area with convective storms passing from the west, under the Doppler path around midnight.

Hourly average of wind speed at Milešovka observatory: 5.3-8.3 $m \cdot s^{-1}$

Height of clouds: penetrating the tropopause

Geomagnetic conditions

Minimum Dst = -30 nT at 01:00-02:00 UT

Maximum Kp = 3

Doppler observations

The Doppler sounding wave reflected predominantly from the F layer. Waves of periods over 15 min occurred at ~18:45-19:45 UT, spectral peaks at ~15-18 min and ~20-30 min exceeded significantly mean values for quiet days. Waves of periods over 13 min occurred at ~19:35-21:35 UT, spectral peaks at ~13-18 min and ~20-30 min exceeded significantly mean values for quiet days. Waves of periods over ~16 min occurred at ~21:50-22:50 UT, spectral peaks at ~16-18 min and ~20-30 min exceeded significantly mean values for quiet days. Waves of periods over ~9 min occurred at ~22:50-23:45 UT, spectral peaks at ~10-18 min and ~20-30 min exceeded significantly mean values for quiet days. Intense geomagnetic fluctuations of periods over ~5 min were detected during the whole interval of ionospheric Doppler shift observation. Geomagnetic oscillations were observed in the corresponding time and period range. Doppler signal and geomagnetic record are correlated.

17 June 2006 16:00 – 23:59UT

Weather

Synoptic situation: cold front

Time of passage of convective storms under the measuring path:

~00:00-03:00 UT; in the interval ~16:00-23:59 UT convective storms in Moravia and in southern Poland

Hourly average of wind speed at Milešovka observatory: 5.8-8.1 $m \cdot s^{-1}$

Height of clouds: penetrating the tropopause

Geomagnetic conditions

Minimum Dst = -23 nT at 22:00 UT

Maximum Kp = 3+

Doppler observations

Very low wave activity occurred on 17 June 2006. Waves of periods ~19-26 min were observed at ~20:40-20:55 UT, waves of periods ~20-27 min at ~22:15-22:35 UT. However, the amplitudes did not exceed significantly mean values for quiet days.

19 June 2006 18:00 – 23:59 UT

Weather

Synoptic situation: cold front and instability lines

Time of passage of convective storms under the measuring path: ~15:00-15:30 and 18:00-19:00 UT. Later, convective storms in eastern Bohemia and in Moravia.

Hourly average of wind speed at Milešovka observatory: 4.7-11.9 $m \cdot s^{-1}$

Height of clouds: penetrating the tropopause

Geomagnetic conditions

Minimum Dst = -18 nT at 21:00 UT

Maximum Kp = 2

Doppler observations

The Doppler record was disturbed by spread, smear, multiple trace and S-shapes in several time intervals. The strength of signal was unstable after ~20:30 UT.

Waves of periods ~5-30+ min occurred at ~19:10-19:50 UT, spectral peaks at ~ 6-8.5 min, ~10-14.5 min, and ~19-20 min exceeded significantly mean values for quiet day. In corresponding time intervals, oscillations of components of the local geomagnetic field were observed. Geomagnetic oscillations were observed in the corresponding time and period range. Doppler signal and geomagnetic record are correlated.

Waves of periods ~6-30 min at ~20:10-21:05 UT are shown by the wavelet transform; spectral peaks at ~6-8.5 min, ~10-14.5 min, and ~19-20 min exceed significantly mean values for quiet days. However, the reliability of the result is questionable, since in the second half of the interval the Doppler trace was disturbed by spread and the strength of the signal was unstable. Wavelet analysis showed fluctuations of the west-east component of the local geomagnetic field in corresponding time and period range. The Doppler signal is correlated with west-east component; the correlation is not very strong.

Waves of periods ~6-25 min occurred at ~22:05-22:45 UT, spectral peaks at~ 6-8.5 min; ~10-14.5 min; and ~19-20 min exceeded significantly mean values of quiet days. The correlation with geomagnetic fluctuations is rather weak.

Waves of periods ~7-30 min occurred at ~22:45-23:25 UT, spectral peaks at ~7-8.5 min, ~10-14.5 min, and ~19-20 min exceeded significantly mean values for quiet days. The wavelet analysis shows fluctuations of the east-west component of the local geomagnetic field, but the Doppler signal is correlated with the north-south and vertical component and with the fluctuations of the amplitude of the local geomagnetic field.

The fluctuations of local geomagnetic field were rather weak on 19 June 2006, particularly after ~21:00 UT. Waves in the ionosphere were observed after ~19:00 UT; it means after the passage of intense convective storms under the measuring path at ~18:00-19:30 UT and at about the time of passage of a frontal line. To decide about the origin of waves with confidence, more input data are needed. If multipoint measurements were available on 19 June 2006, it would be possible to compute the propagation speed of waves. Then magneto-hydrodynamic waves and acoustic-gravity waves could be distinguished from the different speed of propagation.

21 June 2006 16:00 – 23:59 UT

Weather

Synoptic situation: cold front and an instability line

Convective storm activity in the monitored area: ~8:30-23:59 UT

Time of passage of convective storms under the measuring path: ~15:30-17:30 UT. ~16:30-17:30 UT intense storm with height of clouds over 14 km, reflectivity 60+ dBz. At ~19:30-21:00 UT, a squall line to the south east of the ionospheric reflection point.

Hourly average of wind speed at Milešovka observatory: 4.4-8.1 $m \cdot s^{-1}$

Height of clouds: penetrating the tropopause

Geomagnetic conditions

Minimum Dst = -3 nT at 03:00-06:00 UT

Maximum Kp = 1-

Doppler observations

Waves of periods ~16-22 min occurred at ~18:00-18:30 UT and at ~20:00-20:20 UT, waves of periods ~21-25 min occurred ~21:30-21:50 UT; however the amplitudes did not exceed significantly the mean values for quiet days.

Waves of periods ~10-20 min occurred at ~19:00-19:20 UT, spectral peaks in the Fourier amplitude spectrum at ~10-13 min exceeded significantly mean values for quiet days. Waves of periods ~11-18 min occurred ~21:05-21:25 UT, spectral peaks at ~11-13 min exceeded significantly mean values for quiet days. Geomagnetic oscillations were observed in the corresponding time and period range. Doppler signal and geomagnetic record are correlated.

An intense convective storm developed directly under the Doppler measuring path at ~17:00-17:30 UT. The height of clouds was over 14 km, they penetrated the tropopause. High values of radar reflectivity (60+ dBz) indicate occurrence of hail. Unusual ionospheric effects, which could be potentially ascribed to the convective storm, were not observed. The Doppler sounding wave reflected from the non-transparent Es layer at heights ~105 km.

22 June 2006 16:00 – 23:59 UT

Weather

Synoptic situation: cold fronts

Time of passage of convective storms under the measuring path: Convective storms did not pass under the measuring path. In the interval ~16:00-23:59 UT, convective storms in the northern part of Austria and in the southern part of the Czech Republic.

Hourly average of wind speed at Milešovka observatory: 4.4-9.4 $m \cdot s^{-1}$

Height of clouds: reaching to the tropopause region

Geomagnetic conditions

Minimum Dst = -5 nT at 20:00-21:00 UT

Maximum Kp = 2

Doppler observations

The Doppler record was often disturbed by spread, multiple trace and S-shapes in several time intervals, and it was not possible to perform a reliable spectral analysis.

25 June 2006 16:00 – 23:59 UT

Weather

Synoptic situation: cold front

Time of passage of convective storms under the measuring path: Convective storms did not pass under the measuring path. In the interval ~16:00-23:59 UT convective storms in southern Bohemia (till ~18:30 UT and in south- eastern Germany (~18:30-22:00 UT).

Hourly average of wind speed at Milešovka observatory: 8.1-11.9 $m \cdot s^{-1}$

Height of clouds: penetrating the tropopause

Geomagnetic conditions

Minimum Dst = -8 nT at 05:00 and 23:00-24:00 UT

Maximum Kp = 2

Doppler observations

The Doppler record was often disturbed by spread, smear and multiple trace in several time intervals, and therefore not suitable for a reliable spectral analysis. Discrete Doppler trace is obviously caused by the change of the reflection height of Doppler signal between Es layer and F layer. In the wavelet analysis, this effect is seen as a broad spectrum in a relatively narrow time interval. Waves of periods ~5-12 min occurred at ~16:00-16:20 UT with amplitudes exceeding mean values for quiet days. Waves of periods longer than ~16 min occurred at ~20:35-21:10 UT, spectral peaks in the Fourier amplitude spectrum at ~20 min exceeded significantly mean values for quiet days. Waves of periods ~9-22 min occurred at ~22:00-22:40 UT, spectral peaks at ~11-12 min, ~15 min, ~20 min exceeded the mean values for quiet days. Waves of periods ~7-12 min occurred at ~22:40-23:00 UT, spectral peaks at ~7-12 min exceeded significantly the mean values for quiet days. Geomagnetic oscillations were observed in the corresponding time and period range. Doppler signal and geomagnetic record are correlated.

Waves of periods ~4-10 min occurred at ~17:50-18:10 UT with amplitudes exceeding mean values for quiet days. Doppler signal and geomagnetic record are correlated, but geomagnetic fluctuations in the corresponding time and period range were not

revealed by the wavelet analysis. It would be possible to confirm or to exclude the geomagnetic origin of ionospheric waves from the speed of propagation of waves. However, on 25 June 2006 one point measurements are available for further analysis.

27 June 2006 16:00 – 23:59 UT

Weather

Synoptic situation: cold front

Time of passage of convective storms under the measuring path: ~16:30-17:00 UT. Later, convective storms in Moravia and in Slovakia.

Hourly average of wind speed at Milešovka observatory: 5.6-19.4 $m \cdot s^{-1}$

Height of clouds: penetrating the tropopause

Geomagnetic conditions

Minimum Dst = -1 nT at 01:00 UT

Maximum Kp = 2

Doppler observations

The Doppler record was often disturbed by spread, smear, multiple trace and S-shapes in several time intervals; the strength of signal was unstable till ~17:00 UT. Therefore it was not possible to perform a reliable spectral analysis. Discrete Doppler trace occurred several times. In one case a transparent Es layer was present, in the other cases the Doppler signal reflected from the F layer. Intense fluctuations of local geomagnetic field with periods longer than 5 min were observed in the analysed interval.

Waves of periods ~5-9 min occurred at ~18:55-19:00 UT, spectral peaks of the Fourier amplitude spectrum at ~5-7 min and ~8-9 min exceeded the mean values for quiet days. The length of the time interval in which the waves were observed was shorter than one wave cycle. Waves of periods ~11-16 min occurred at ~19:35-19:55 UT, spectral peaks at ~11-14 min exceeded significantly mean values for quiet days. Waves of periods ~2.5-3.5 min occurred at ~19:40-19:47 UT with amplitudes exceeding mean values for quiet days. Waves of periods ~13-18 min occurred at ~21:35-21:50 UT, spectral peaks at ~13-14 min exceeded mean values for quiet days. Waves of periods longer than ~18 min occurred at ~22:40-23:35 UT, spectral peaks at ~19-30 min exceeded significantly mean values for quiet days. Geomagnetic oscillations were observed in the corresponding time and period range. Doppler signal and geomagnetic record are correlated.

At ~21:10-22:10 UT, waves of periods longer than 18 min occurred, spectral peaks at periods longer than ~19 min exceeded significantly mean values. The waves were observed long time after the passage of the convective storm line under the Doppler measuring path (~16:30-17:30 UT). Wavelet analysis revealed geomagnetic fluctuations in corresponding time and period range. The Doppler signal is correlated with fluctuation of the west-east component of the local geomagnetic field; however there is a relatively large time shift between the two signals (1245 s). There is probably not a direct relationship between ionospheric and geomagnetic oscillations. To decide between the magnetic and non-magnetic origin of the waves, it is necessary to have measurements from 3 or more sounding path. Then, it would be possible to compute horizontal speed of propagation of waves and to conclude about the origin.

6 July 2006 18:00 – 23:59 UT

Weather

Synoptic situation: instability line in a trough of low air pressure

Time of passage of convective storms under the measuring path:

Convective storms did not pass under the measuring path. In the interval ~16:00-23:59 UT, convective storms in western and southern Bohemia (till ~18:00 UT) and in Germany.

Hourly average of wind speed at Milešovka observatory: 5.6-12.5 $m \cdot s^{-1}$

Height of clouds: penetrating the tropopause

Geomagnetic conditions

Minimum Dst = -30 nT at 01:00-02:00 UT

Maximum Kp = 3+

Doppler observations

Low wave activity occurred on 6 July 2006. The Doppler sounding wave reflected from the Es layer. The Doppler record was often disturbed by spread and multiple trace. Therefore it was not possible to perform a reliable spectral analysis. Waves of periods ~5-11 min occurred at ~21:05-21:25 UT. The Doppler signal is correlated with fluctuations of components of the local geomagnetic field.

7 July 2006 16:00 – 22:00 UT

Weather

Synoptic situation: instability lines in a trough of low air pressure

Time of passage of convective storms under the measuring path:

~19:00-22:00 UT

Hourly average of wind speed at Milešovka observatory: 6.1-10.6 $m \cdot s^{-1}$

Height of clouds: reaching to the tropopause region

Geomagnetic conditions

Minimum Dst = -21 nT at 02:00-03:00 UT

Maximum Kp = 2+

Doppler observations

Low wave activity occurred on 7 July 2006. The Doppler sounding wave reflected predominantly from the Es layer. Discrete trace observed at ~18:20 UT is obviously connected with change of the sounding wave reflection height from Es to F. On the other hand between 19:00 and 19:15 UT when the reflection height changed from F to Es layer, a discrete trace did not occur. Waves of periods ~6-17 min occurred at ~17:15-17:35 UT, spectral peaks at ~6.5 min, ~9 min, ~10 min, and ~13 min exceeded significantly mean values for quiet days. Geomagnetic oscillations were observed in the corresponding time and period range. Doppler signal and geomagnetic record are correlated.

8 July 2006 16:00 – 22:00 UT

Weather

Synoptic situation: cold front with an instability line

Time of passage of convective storms under the measuring path:

~13:00-14:30 UT. In the interval ~18:00-22:00 UT convective storms in southern Moravia, in Germany, and in Poland.

Maximum hourly average of wind speed at Milešovka observatory: 3.3-6.1 $m \cdot s^{-1}$

Height of clouds: reaching to the tropopause region

Geomagnetic conditions

Minimum Dst = -21 nT at 01:00 UT

Maximum Kp = 1

Doppler observations

Low wave activity occurred on 8 July 2006. The Doppler sounding wave reflected predominantly from the Es layer. The Doppler trace was disturbed by multiple trace and spread during the analysed interval.

9 July 2006 16:00 – 20:00 UT

Weather

Synoptic situation: weak anticyclone

Time of passage of convective storms under the measuring path:

~16:00-18:00 UT.

Maximum hourly average of wind speed at Milešovka observatory: 3.6-5.6 $m \cdot s^{-1}$

Height of clouds: reaching to the tropopause region

Geomagnetic conditions

Minimum Dst = -11 nT at 02:00 UT

Maximum Kp = 3+

Doppler observations

The Doppler record was most of the time disturbed by spread, smeared traced, and multiple trace. Observed discrete Doppler trace might be connected with changes of the Doppler sounding wave reflection height between Es and F layer.

Waves of periods ~4-8 min occurred at ~17:20-17:25 UT, with amplitudes exceeding mean values for quiet days. Geomagnetic oscillations were observed in the corresponding time and period range. Doppler signal and geomagnetic records are correlated.

12 July 2006 16:00 – 20:00 UT

Weather

Synoptic situation: cold front

Time of passage of convective storms under the measuring path:

~14:00-15:30 UT. In the interval 16:00-20:00 UT, convective storm in southern and western Bohemia (till ~18:30 UT), then convective storms in Germany and in Slovakia.

Hourly average of wind speed at Milešovka observatory: 5.3-6.9 $m \cdot s^{-1}$

Height of clouds: reaching to the tropopause region

Geomagnetic conditions

Minimum Dst = -17 nT at 20:00 and 23:00 UT

Maximum Kp = 4

Doppler observations

Wave activity was very low on 12 July 2006. The Doppler sounding wave reflected practically all the time from the Es layer. The Doppler record was most of the time smeared. Discrete trace occurred at ~18:30 and ~18:40 UT, in this time interval transparent Es layer changed to non transparent Es. The discrete Doppler trace is most probably connected with the change of the reflection height of the sounding wave. S-shape was observed in the Es layer at ~16:30 UT.

13 July 2006 18:00 – 20:00 UT

Weather

Synoptic situation: cold front

Time of passage of convective storms under the measuring path:

~11:00-15:30 UT. In the time interval 18:00-20:00 UT convective storms in Germany along the north-western boarder of the Czech Republic.

Hourly average of wind speed at Milešovka observatory: 5.3-5.8 $m \cdot s^{-1}$

Height of clouds: reaching to the tropopause region

Geomagnetic conditions

Minimum Dst = -17 nT at 17:00 UT

Maximum Kp = 2+

Doppler observations

Low wave activity was observed in the short period range on 13 July 2006. Waves of periods longer than ~25 min occurred at ~18:00-19:40 UT, spectral peaks at ~20 min and ~30 min exceeded significantly mean values for quiet days. Wavelet analysis revealed fluctuations of horizontal components of the local geomagnetic field in the same time and period range. Cross-correlations between the Doppler signal and fluctuations of the components of the local geomagnetic field were not computed; the periods of observed waves exceed 30 min and a narrow period range is left after filtering the signal, therefore the results might be distorted.

23 July 2006 16:00 – 24:00 UT

Weather

Synoptic situation: instability line, low horizontal pressure gradient

Time of passage of convective storms under the measuring path:

~06:30-07:30 UT. In the interval 16:00-24:00 UT convective storms in western and southern Bohemia, in Moravia. Later convective storms in eastern Bohemia.

Hourly average of wind speed at Milešovka observatory: 5.0-8.1 $m \cdot s^{-1}$

Height of clouds: reaching to the tropopause region

Geomagnetic conditions

Minimum Dst = -1 nT at 01:00 UT

Maximum Kp = 1+

Doppler observations

Waves of periods ~4-12 min occurred at ~19:10-19:35 UT, spectral peaks of the Fourier amplitude spectrum exceeded significantly mean values for quiet days at ~4-6.25 min and ~7-12 min. Waves of periods ~5-12 min occurred at ~21:40-22:00 UT, spectral peaks at ~5-6.25 min and ~7-12 min exceeded significantly mean values for quiet days. Waves of periods longer than 13 min occurred at ~20:35-21:10 UT, spectral peaks at ~13-15 min, ~18 min, and ~20-25 min exceeded significantly mean values for quiet days. Waves of periods longer than ~18 min occurred at ~21:25-22:15 UT, spectral peaks at ~18 min and ~20-25 min exceeded significantly mean values for quiet days. Waves of periods ~15-22 min occurred at ~22:00-22:30 UT, spectral peaks at ~15 min, ~18 min, and ~20-25 min exceeded significantly mean values for quiet days. Geomagnetic oscillations were observed in the corresponding time and period range. Doppler signal and geomagnetic record are correlated.

Waves of periods ~5-17 min occurred at ~19:30-20:10 UT, spectral peaks at ~5-6.25 min and ~7-15 min exceeded significantly mean values for quiet days. Waves of periods longer than ~18 min occurred at ~19:35-20:20 UT. Wavelet analysis revealed fluctuations of the north-south component of the local geomagnetic field of periods longer than 10 min at ~18:15-19:35 UT and at ~19:55-22:15 UT. The band-pass filtered Doppler signal and geomagnetic records are not correlated in the period range

5-17 min. In the period range 18-30 min, the Doppler signal is correlated with horizontal components and with the amplitude of the local geomagnetic filed.

Clouds with light showers were observed meteorological radars below the Doppler measuring paths between ~19:30-20:20 UT. The height of clouds was lower than 10 km. Weather fronts were not passing on 23 July 2006; instability lines developed in Central Europe. The 3.59 MHz wave reflected predominantly from the F layer (210-230 km). The Brunt-Väisälä frequency increases rapidly in the lower thermosphere and at heights ~210-230 km is ~13 min (USSA1976). Thus, waves of periods shorter than ~13 min propagating directly from the troposphere (non-linear processes are omitted) are filtered.

The Doppler sounding wave was significantly Doppler shifted to higher frequencies at ~19:35 UT and a discrete trace with significant Doppler shift to lower frequencies occurred at ~19:50 UT. At 19:45- 20:00 UT, a transparent Es layer was present. Thus, a sudden change of the reflection height might be possibly observed in the Doppler record rather than waves.

Waves of periods longer than 24 min occurred at ~22:40-23:10 UT, spectral peaks at ~25 min exceeded significantly mean values for quiet days. Wavelet analysis showed fluctuations of the north-south component of the local geomagnetic field in the same time and period range. Cross-correlations between the Doppler signal and fluctuations of the components of the local geomagnetic field were not computed; the periods of observed waves exceed 30 min and a narrow period range is left after filtering the signal, therefore the results might be distorted.

26 July 2006 16:00 – 20:00 UT

Weather

Synoptic situation: instability line, low horizontal pressure gradient

Time of passage of convective storms under the measuring path:

Convective storms did not pass under the measuring path. In the interval 16:00-20:00 UT convective storms in south-western Bohemia and in south-eastern Germany.

Hourly average of wind speed at Milešovka observatory: 0.8-2.2 $m \cdot s^{-1}$

Height of clouds: reaching to the tropopause region

Geomagnetic conditions

Minimum Dst = -10 nT at 01:00 UT

Maximum Kp = 3-

Doppler observations

The Doppler record was disturbed by double trace, discrete trace, and spread in most of the analysed interval.

31 July 2006 16:00 – 22:00 UT

Weather

Synoptic situation: cold front with an instability line

Time of passage of convective storms under the measuring path:

~11:30-16:30 UT. In the interval 16:00-22:00 UT convective storms in south Bohemia, in Moravia and in Austria.

Hourly average of wind speed at Milešovka observatory: 2.8-8.6 $m \cdot s^{-1}$

Height of clouds: reaching to the tropopause region

Geomagnetic conditions

Minimum Dst = -24 nT at 22:00-23:00 UT

Maximum Kp = 4

Doppler observations

Waves of periods longer than 16 min occurred at ~18:15-19:20 UT, spectral peaks at ~18-19 min and ~25 min exceeded significantly mean values for quiet days. Wavelet analysis showed fluctuations of north-south and west-east component of the local geomagnetic field in corresponding time and period range; the Doppler signal is correlated with the west-east component. According to the visual comparison of the Doppler trace at Panská Ves path and at Průhonice path, waves on both paths occurred simultaneously after 18:40 UT; it indicates rather the geomagnetic origin of the waves. Between ~18:15 and 18:40 UT, the record from Průhonice path is too weak and does not allow the comparison.

Waves of periods ~14-26 min occurred at ~19:40-20:25 UT, spectral peaks at ~15.5 min, ~18-19 min, and ~25 min exceeded significantly mean values for quiet days. Waves of periods ~12-25 min occurred after ~21:40 UT, spectral peaks at ~12-14 min and ~15.5 min exceeded significantly mean values for quiet days. Geomagnetic oscillations were observed in the corresponding time and period range. Doppler signal and geomagnetic record are correlated.

Waves of periods longer than 22 min occurred at ~17:35-18:15 UT and after ~21:00 UT, spectral peak in the Fourier amplitude spectrum at 25 min exceeded significantly mean values for quiet days. Wavelet analysis showed fluctuations of the north-south

component of the local geomagnetic field in the same time and period range. Cross-correlations between the Doppler signal and fluctuations of the components of the local geomagnetic field were not computed; the periods of observed waves exceed 30 min and a narrow period range is left after filtering the signal, therefore the results might be distorted.

1 August 2006 16:00 – 18:00 UT

Weather

Synoptic situation: cold front

Time of passage of convective storms under the measuring path:

~14:30 UT. In the interval 16:00-18:00 UT convective storms in eastern Bohemia and in Moravia.

Hourly average of wind speed at Milešovka observatory: 9.2-9.7 $m \cdot s^{-1}$

Height of clouds: reaching to the tropopause region

Geomagnetic conditions

Minimum Dst = -23 nT at 06:00 UT

Maximum Kp = 3+

Doppler observations

Low wave activity was observed, though the Doppler sounding wave was reflected from the F layer. The Doppler trace was disturbed by the double trace, which disabled to conduct reliable spectral analysis, particularly in the short period range.

9 May 2006

Period [min]	**Time (UT)**	**Fourier [min]**	**Doppler record**	**Reflection height, layer [km]**	**Amplitude [Hz]**	**Wavelets geomag. field**	**Cross-correlation**
>11	18.00-19.35	12-14;15;17-25	CLEAR(double trace)	transp.Es,F(250;125-245;120-250-250-245-240-230-245)	0.4	NS;EW	NS=0.73 at t=601s EW=0.64 at t=1356s V=0.57 at t=1271s B=0.62 at t=637s
13-24	19.35-20.15	14;15;17-24	CLEAR	F(230-245-255-255)	0.17	NS;EW	NS=0.76 at t=38s V=-0.53 at t=50s B=0.7 at t=36s
>26	19.50-21.05	-					
14-25	20.30-21.40	14;15;17-25	CLEAR(after 21.30 sharp shift and smeared)	F,transp.Es,Es(255-265;120-265;105-255;110-270;100-105)	0.19	NS;EW	NS=0.81at t=-327s EW=-0.71 at t=22s V=-0.74 at t=-341s B=0.73 at t=-327s

13 May 2006

Period [min]	Time (UT)	Fourier [min]	Doppler record	Reflection height, layer [km]	Amplitude [Hz]	Wavelets geomag. field	Cross-correlation
>17	18.15-19.05	20;24	CLEAR (till 18.30 discrete triple trace,till 18.45 double trace)	F,transp.Es,F(265-260;115-265-265)	0.16	NS;EW	NS=-0.61 at t=-59s EW=0.86 at t=488s V=-0.57 at t=372s B=-0.61 at t=0s
12-16	19.10-19.20	13;15	CLEAR	F(265-250)	0.07	not evaluated - noise	
>18	19.30-20.10	20;24	CLEAR(at 19.45 discrete trace)	F(250-255)	0.15	NS;EW;V	NS=0.78 at t=71s EW=0.55 at t=468s V=-0.79 at t = 126s B=-0.67 at t=1011s
>14	20.35-21.30	15;20;24	CLEAR	F(260-265)	0.18	NS;EW	NS=-0.83 at t=-149s V=-0.55 at t =912s B=-0.82 at t=156s
8-11	21.15-21.25	9-10	CLEAR	F(265)	0.09	not evaluated - noise	
>20	21.50-22.50	20;24	CLEAR(22.00-22.20 spread, discrete trace)	F,transp Es,F(265-260;105-270;110 -285-290-290)	not calc.	NS;EW	not calc.
13-18	22.15-22.35	13;15	CLEAR(smeared)	transp.Es,F(270;110-285-290)	0.09	not evaluated - noise	
>22	23.25-23.35	24	CLEAR	F(300)	0.06	not evaluated - noise	

14 May 2006

Period [min]	Time (UT)	Fourier [min]	Doppler record	Reflection height, layer [km]	Amplitude [Hz]	Wavelets geomag. field	Cross-correlation
20-26	18.20-18.40	20-21	CLEAR (double trace)	transp.Es,F,transp.Es (250;113--250-250;120)	0.07	not evaluated – noise	
13-25	18.55-19.30	13-21	CLEAR	transp.Es,F(250;120-245-250-240)	0.14	NS;EW	NS=-0.77 at t=40s EW=-0.73 at t=-1331s V=0.68 at t=-1306s B=-0.83 at t=37s

16 May 2006

Period [min]	Time (UT)	Fourier [min]	Doppler record	Reflection height, layer [km]	Amplitude [Hz]	Wavelets geomag. field	Cross-correlation
14-30	22.35-23.25	18	spread,signal strength	F(250-295)			
>26	23.35-24	-	spread,signal strength	F(295-310,approaching fxF2)			

20 May 2006

Period [min]	Time (UT)	Fourier [min]	Doppler record	Reflection height, layer [km]	Amplitude [Hz]	Wavelets geomag. field	Cross-correlation
5-8	23.45-23.50	5.5	CLEAR(double trace)	transp.Es(370;110,approaching fxF2)	0.09	not evaluated -noise	
>18	19.10-19.30	-					
>20	20.10-20.40	-					

22 May 2006

Period [min]	**Time (UT)**	**Fourier [min]**	**Doppler record**	**Reflection height, layer [km]**	**Amplitude [Hz]**	**Wavelets geomag. field**	**Cross-correlation**
>13	19.20-19.50	13;14;16.5;18	CLEAR	Es,F(115-260-270-270)	0.21	NS;EW	NS=0.61at t=-1396s EW=0.77 at t=1609s V=0.7at t=-518s B=0.63at t=-1360s
>21	21.10-22.50	-					
14-21	22.25-23.10	14;16.5;18	CLEAR	F(280-275-290-295-295)	0.12	NS;EW	EW=0.54 at t=-254s V=0.63 at t=237s
10-14	23.10-23.20	10.5-11;12; 13;14	S-shape	F(295)			

16 June 2006

Period [min]	**Time (UT)**	**Fourier [min]**	**Doppler record**	**Reflection height, layer [km]**	**Amplitude [Hz]**	**Wavelets geomag. field**	**Cross-correlation**
2-12	21.35-21.45	2-8;10-12	ripple,signal strength	F,Es(280-105)			
12-20	18.05-18.35	12-18;20	CLEAR(signal strength, multiple	F(280-270)	0.09	not evaluated - noise	
15-30+	18.45-19.45	15-18;20-30	CLEAR(spread)	transp.Es, F(270;100-250-270--280-275)	0.17	NS;EW	NS=0.52 at t=-430s B=-0.55 at t=-1051s
>13	19.35-21.35	13-18;20-30	CLEAR	F(280-265)	0.31	NS;EW;V	NS=0.72 at t=-409s EW=0.58at t=-730s V=-0.61 at t=-523s B=0.71 at t=-388s
12-14	21.10-21.20	12-14	CLEAR	F(265)	0.07	not evaluated - noise	
>16	21.50-22.50	16-18;20-30	CLEAR(signal strength)	Es,F(105-285-285-280-285)	0.23	NS;EW;V	NS=-0.7 at t=-640s EW=0.8at t=-322s B=-0.75 at t=-609s
>9	22.50-23.45	10-18;20-30	CLEAR(23.35 discrete trace)	F,transp.Es(290-285-290-270--280;105)	0.61	NS;EW;V	NS=0.62 at t=-244s EW=0.57 at t=-189s V=0.67 at t=516s B=0.52 at t=-268s

17 June 2006

Period [min]	Time (UT)	Fourier [min]	Doppler record	Reflection height, layer [km]	Amplitude [Hz]	Wavelets geomag. field	Cross-correlation
4-8	22.10-22.20	5;6	CLEAR	transp. Es,Es (300;105-300)	0.08	not evaluated - noise	
6-12	23.20-23.35	6;9.25	double trace, smeared	Es,transp.Es (110-330;105)			
19 -26	20.40-20.55	-					
20-27	22.15-22.35	-					

19 June 2006

Period [min]	Time (UT)	Fourier [min]	Doppler record	Reflection height, layer [km]	Amplitude [Hz]	Wavelets geomag. field	Cross-correlation
4-9	19.05-19.15	4;4.75;6-8.5	spread	Es,transp.Es(100-265;100)			
4.5-6	19.35-19.40	4.75;6	CLEAR (double trace)	F(250)	0.07	not evaluated - noise	
4-5	19.50-19.55	4.75	spread	F,Es(250-105)			
2-3	20.32-20.37	2-3	spread,signal strength	transp.Es(255;100)			
4-6	20.32-20.47	4.75;6	spread,signal strength	transp.Es(255;100)			
7-9	21.05-21.10	7-8.5	spread	transp.Es(250;100)			
3	21.15	3	CLEAR(spread)	transp.Es(250;100)	0.07	not evaluated - noise	
3-5	22.15-22.25	3-4;4.75	spread	transp.Es,Es(250;105-105)			
3-4	22.50-22.55	3-4	signal strength	transp.Es,F(255;110-260)			
6-9	23.30-23.40	6-8.5	spread,signal strength	F(300-310)			
5-30+	19.10-19.50	6-8.5;10-14.5; 19-20	19.20-19.45 CLEAR, before and after spread	transp.Es,F(265;105-255-255)	0.35	NS;EW	NS=0.63 at t=22s EW=-0.58at t=461s V=0.59 at t=444s B=0.61 at t=52s
6-30	20.10-21.05	6-8.5;10-14.5; 19-20	20.10-20.30 CLEAR, then spread,signal strength	Es,transp.Es(100-250;100-260;100 -250;100)	0.45	EW	EW=-0.51 at t=542s
16-22	21.40-21.50	19-20	spread				
6-25	22.05-22.45	6-8.5;10-14.5; 19-20	22.15-22.45 CLEAR before spread	transp.Es,Es,transp.Es(215;110-250;105-105-255;110)	0.28	No	V=-0.57 at t=444s
7-30+	22.45-23.25	7-8.5;10-14.5; 19-20	CLEAR (signal strength)	transp.Es,F(255;110-260-275-295)	0.31	EW	NS=0.61 at t=24s V=0.53 at t=-1124s B=0.59 at t=54s

21 June 2006

Period [min]	Time (UT)	Fourier [min]	Doppler record	Reflection height, layer [km]	Amplitude [Hz]	Wavelets geomag. field	Cross-correlation
6-8	17.35-17.45	6.5-7.25	CLEAR	Es (105)	0.08	not evaluated - noise	
5-6	18.11-18.22	5-6	spread				
4-5	20.10-20.40	4-5	till 20.25 CLEAR, then S-trace and double trace	F (250); 20.30 transp. Es (110)	0.07	not evaluated – noise	
5-6	23.20-23.30	5-6	CLEAR	transp.Es (300; 105-100)	0.06	not evaluated - noise	
10-20	19.00-19.20	10-13	CLEAR (double trace)	transp. Es (245-235; 110)	0.13	EW	EW=-0.66 at t=-464s V=-0.8 at t=-0.5s
16-22	18-18.30	-	till 18.20 spread, then CLEAR				
7-15	19.30-20.20	7-13	CLEAR	F (230-250)	0.25	EW	NS=-0.7 at t=621s EW=-0.63 at t=789s V=0.74 at t=677s B=0.55 at t=242s
16-22	20-20.20	-	CLEAR				
11-18	21.05 – 21.25	11-13	CLEAR	F (250-260)	0.14	EW	NS=-0.7 at t=88s EW=-0.65 at t=-617s V=-0.55 at t=584s B=-0.77 at t=52s
21-25	21.30-21.50	-	CLEAR				
9-14	22.15-22.30	10-13	CLEAR, 22.30 multiple trace	F (270)	0.08	not evaluated - noise	

22 June 2006

Period [min]	Time (UT)	Fourier [min]	Doppler record	Reflection height, layer [km]	Amplitude [Hz]	Wavelets Cross-correlation geomag. field
5-8	16.20-16.35	5.5-7.25	CLEAR	Es (110)	0.08	not evaluated-noise
5-7	17.05-17.10	5.5-7.25	CLEAR (spread)	transp.Es (315; 120)	0.07	not evaluated-noise
6-9	17.15-17.20	6-7.25;8-8.25	spread	Es (110)		
7- 11	18.10-18.20	7-7.25;8-8.25 9-9.5	CLEAR	Es (110)	0.08	not evaluated – noise
3-6	18.25-18.30	3-5;5.5-6	double trace	transp.Es (255; 110)		
7-12	18.30-18.40	7-7.25;8-8.25 9-9.5	triple trace	transp. Es (255;110)		
4- 10	18.48-18.58	4-5;5.5-7.25 8-8.25;9-9.5	triple trace	transp Es (O250;X275;Es105) Es (115)		
3.5-5	20.22-20.29	3.5-5	spread	transp.Es (220;110-240;105)		
8-9	22.32-22.38	8-8.5	spread	transp.Es (340; 100)		
6-10	22.58-23.05	6-7.25;8-8.25; 9-9.5	spread	transp.Es (285;105)		
15-17	17.35-17.45	16	till 17.40 spread,then CLEAR	transp. Es(320;105-O320;X280;Es105)		
13-24	18.45-19.30	13-15;16;22	triple trace, S-shape, double trace	transp.Es (O250;X275;Es105)Es(115) F (245-234)		
11-16	19.40-19.55	13-15;16	S-shape	transp Es(220;120-110)		
12-22	20.15-20.40	13-15;16;22	spread	(220;105-235;110)		
18-26	21.00-21.20	22	till 21.10 CLEAR (spread) then double trace (spread)	transp.Es (265;110)	0.09	not evaluated-noise
14-23	23.35-23.55	14-15;16;22	CLEAR	F (330)	not calc.	
>23	22.30-23.10	-	spread			

25 June 2006

Period [min]	Time (UT)	Fourier [min]	Doppler record	Reflection height, layer [km]	Amplitude [Hz]	Wavelets geomag. field	Cross-correlation
5-12	16.00-16.20	5-12	CLEAR	transp. Es (250-230;120)	0.21	NS	NS=0.79 at t=115s EW=0.64 at t=378s V=-0.54 at t=471s B=0.71at t=116s
4-5	16.30-16.35	4-5	signal strength	Es (110)			
5-8	16.55-17.25	5-8	CLEAR	Es, transp.Es, Es (110-358;110-110)	0.09	not evaluated-noise	
4-10	17.50-18.10	4-10	CLEAR (17.50 discrete trace 18.10 discrete trace)	Es, transp.Es (105-280;105-270;100)	0.28	No	NS=-0.72 at t=-129s EW=0.71 at t=358s V=0.59 at t=550s B=-0.73 at t=-144s
3-5	18.40-18.45	3-5	multiple trace spread	transp.Es (245;100)			
3-5	18.55-19.05	3-5	CLEAR (spread)	transp.Es (230;110)	0.09	not evaluated - noise	
2.5-4	19.25-19.30	2.5-4	spread	transp.Es (230;105)			
6-10	19.30-19.40	6-10	spread	transp Es (230-240;105)			
2-8	19.45-19.55	2-8	spread	transp.Es (240;105)			
4-7	20.05-20.15	4-7	20.05 discrete trace	transp.Es, Es (240;105-110)			
6-13	20.40-21.05	6-12	double trace, spread	Es (105)			
3-4	21.10	3-4	multiple trace,spread	Es,transp.Es (105-240;105)			
2.5-5	21.55-22.00	2.5-5	spread	transp.Es(260,105)			
3-4	22.20	3-4	double trace, spread	F(275-285)			
4-5	22.30	4-5	double trace, spread	F(275-285)			

25 June 2006 (cont.)

Period [min]	Time (UT)	Fourier [min]	Doppler record	Reflection height, layer [km]	Amplitude [Hz]	Wavelets geomag. field	Cross-correlation
13-26	17.45-18.10	15;20	17.50 discrete trace 18.10 discrete trace	Es,transp.Es(105-280;105-270;100)			
>10	18.25-19.05	15;20	18.40 discrete trace, multiple trace,spread	Es,transp.Es(105-245;100-230;110)			
>22	19.10-19.50	-					
>16	20.35-21.10	20	CLEAR (double trace,spread)	Es(105)	0.13	NS;EW	NS=-0.9 at t=3s EW=0.9 at t=437s V=-0.74 at t=-940s B=-0.86 at=38s
11-14	21.20-21.50	11-12	till 21.40 CLEAR (spread), then spread	transp.Es(240;105-240;105-255;110)	0.08	not evaluated – noise	
9-22	22.00-22.40	11-12;15;20	CLEAR (spread)	transp.Es,F,transp.Es(105;260-275-285--290;110)	0.24	NS;EW	EW=0.61 at t=-135s
7-12	22.40-23.00	7-12	CLEAR (smeared)	transp.Es (290;110-300;110)	0.21	NS	NS=-0.78 at t=321s V=0.65 at t=-294s B=-0.76 at t=-330 s
>25	22.20-23.10	-					
>10	23.30-24	15;20	CLEAR (22.45 double trace)	transp.Es(300;110)	not calc.		

27 June 2006

Period [min]	Time (UT)	Fourier [min]	Doppler record	Reflection height, layer [km]	Amplitude [Hz]	Wavelets geomag. field	Cross-correlation
3-4	16.00-16.07	3-4	smeared,signal strength	transp.Es (260;120)			
5-12	16.10-16.20	5-7;8-12	smeared,signal strength	Es (120)			
5-12	16.30-16.45	5-7;8-12	S-shapes,smeared,signal strength	Es+2Es(113/133)			
4.5-7.5	16.53-17.00	4.5-7	S-shape,signal strength	transp.Es (300,140)			
4-9	17.35-18.00	4-7;8-9	17.35 multiple trace, 17.45-17.55 discrete trace	transp.Es,F(295;120-245;125-277)			
7-14	18.00-18.25	7;8-14	till 18.10 CLEAR,then S-shapes, double trace	F(275-295)			
3-4	18.00-18.10	3-4	CLEAR	F(275-295)	0.06	not evaluated - noise	
3-6	18.30-18.35	3-6	S-shape,double trace	F(275)			
2.5-4.5	18.42-18.49	2.5-4.5	18.45 discrete trace,then CLEAR	F(O270;X290)			
9-16	18.40-18.55	9-14	18.45 discrete trace,then CLEAR	F(O270;X290)			
5-9	18.55-19.00	5-7;8-9	CLEAR	F(260)	0.12	NS	NS=0.55 at t=384s EW=0.56 at t=498s B=0.58 at t=371s
6-12	19.10-19.20	6-7;8-12	double trace,19.10 discerete trace	F(O255;X265)			
2.5-3.5	19.40-19.47	2.5-3.5	CLEAR (spread)	F(250)	0.13	EW	NS=-0.61 at t=-119s EW=-0.7at t=32s V=0.66 at t=-96s B=-0.61 at t=-127s
3.5-5.5	19.50-19.55	3.5-5.5	CLEAR	F(240)	0.09	not evaluated - noise	
4-6	20.50-20.57	4-6	spread	F(250-260)			
3.5-6	22.00-22.10	3.5-6	spread	F(250-240)			

27 June 2006 (cont.)

Period [min]	Time (UT)	Fourier [min]	Doppler record	Reflection height, layer [km]	Amplitude [Hz]	Wavelets geomag. field	Cross-correlation
4-6	23.05-23.30	4-6	spread	F(255-275-280)			
7-9	23.30-23.35	7;8-9	double trace spread	F(280)			
12-18	16.35-17.10	12-14	S-shapes,smeared,signal strength	Es+2Es,F(113/133-300;140)			
15-30	17.35-18.20	19-30	double trace,17.45-17.55 discrete trace,18.15 S-shape	transp.Es,F (295;120-245;120--275-295)			
>17	18.40-19.45	19-30	double trace, 18.45 and 19.10 discrete trace	F(270-250)			
11-16	19.35-19.55	11-14	CLEAR	F(250-240)	0.13	EW	EW=0.6 at t=391s
>17	20.10-20.50	19-30	till 20.30 CLEAR,then spread	F(240-260)			
12-22	20.50-21.10	12-14;19-22	spread	F(250-260)			
13-18	21.35-21.50	13-14	CLEAR (spread)	F(260)	0.16	NS	NS=-0.73 at t=793s EW=0.7 at t=-399s V=0.72at t=820s B=0.78 at t=86s
>18	21.10-22.10	19-30	21.20-22.00 CLEAR,before and after spread	F(260-240)	0.21	NS;EW	EW=0.57 at t=1245s
17-26	22.10-22.40	19-26	till 22.20 spread, then CLEAR (spread)	F(250-240-230-250)			
>18	22.40-23.35	19-30	CLEAR (spread)	F(250-280)	0.3	NS;EW;V	NS=0.59 at t=-830s V=0.63 at t=117s B=0.56 at t=-855s

6 July 2006

Period [min]	**Time (UT)**	**Fourier [min]**	**Doppler record**	**Reflection height, layer [km]**	**Amplitude [Hz]**	**Wavelets geomag. field**	**Cross-correlation**
5-10	18.40-18.45	5-6.5;7-9.5	multiple trace, spread	Es(105)			
5-9	19.40-20.05	5-.6.5;7-9	spread	Es(105-110)			
4-6.5	21.05	4-6.5	multiple trace spread	Es(110)			
5-11	21.15-21.25	5-6.5;7-9.5;11	CLEAR(spread)	Es(110)	0.11	No	NS=-0.54 at t=-474s EW=0.61 at t=140s V=0.65 at t=-119s B=-0.6 at t=-470s
18-30	18.35-19.05	-					
>20	20.35-21.15	-					

7 July 2006

Period [min]	**Time (UT)**	**Fourier [min]**	**Doppler record**	**Reflection height, layer [km]**	**Amplitude [Hz]**	**Wavelets geomag. field**	**Cross-correlation**
6.5-9	20.40-20.50	6.5;9	CLEAR	Es(105)	0.05	not evaluated - noise	
6-17	17.15-17.35	6.5;9;10;13	CLEAR	Es(115-110)	0.1	NS;EW	NS=-0.9 at t=554s EW=0.7at t=351s V=0.8 at t=629s B=-0.88 at t=541s
13-26	18.15-18.40	13	till118.20 CLEAR,then discrete trace,double trace	Es,F(105-265-250)			
7-13	19.00-19.20	9;10;13	CLEAR	F,Es (240-105)	0.09	not evaluated - noise	

8 July 2006

Period [min]	Time (UT)	Fourier [min]	Doppler record	Reflection height, layer [km]	Amplitude [Hz]	Wavelets geomag. field	Cross-correlation
5-9	17.40-18.00	5-7	CLEAR	Es(105)	0.08	not evaluated - noise	
4-7.5	18.40-18.50	4-7	multiple trace	Es(105)			
3-6	19.00-19.05	3-6	multiple trace	Es(105)			
2-3	19.10	2-3	multiple trace	Es(105)			
3-3.5	19.20	3-3.5	multiple trace,spread	Es(105)			
3.5-5	19.35	3.5-5	spread	Es(105)			
6-11	19.10-19.40	6-7;9.5	multiple trace, spread	Es,transp.Es(105-105-245;105)			
6.5-8.5	19.40-19.55	6.5-7	CLEAR(spread)	transp. Es, Es(245;105-105)	0.05	not evaluated - noise	
>20	16.40-17.00	-					
>18	21.10-21.35	-					

9 July 2006

Period [min]	**Time (UT)**	**Fourier [min]**	**Doppler record**	**Reflection height, layer [km]**	**Amplitude [Hz]**	**Wavelets geomag. field**	**Cross-correlation**
4-8	17.20-17.25	4-8	CLEAR	Es(115)	0.11	No	NS=0.57 at t=286s EW=-0.64 at t=282s B=-0.64 at t=-60s
5-10	17.35-17.55	5-10	multiple trace,ripples	Es,transp.Es,Es(115-280;120-115)			
4.5-7.5	18.20-18.35	4.5-7.5	CLEAR	Es(110)	0.08	not evaluated - noise	
2-3	18.50	2-3	discrete trace,smeared	transp.Es(255;110)			
4-7	18.50-18.55	4-7	discrete trace, smeared	transp.Es(255;110)			
4-8	19.00-19.10	4-8	multiple trace,spread	transp.Es(250;110)			
4-8.5	19.20-19.35	4-8.5	spread	transp.Es(250;110-255;110)			
12-22	17.20-17.45	12;14;17.5; 21.5	till 17.25 CLEAR,then ripples, double trace	Es,transp.Es(120-115-280;120)			
9-17	18.45-19.05	9-10;12;14 17.5;21.5	double trace,discrete trace	transp.Es(250;110)			
>17	19.15-19.50	17.5;21.5	spread	transp.Es(250;110-255;105)			

12 July 2006

Period [min]	**Time (UT)**	**Fourier [min]**	**Doppler record**	**Reflection height, layer [km]**	**Amplitude [Hz]**	**Wavelets geomag. field**	**Cross-correlation**
4-6	16.25-16.35	4-6	S-shape	Es(115)			
4.5-7	18.00	4.5-6.25;7	smeared,double trace	Es(110)			
3.5-7	18.25-18.30	3.5-6.25;7	double trace,smeared	transp.Es(255;110)			
7-16	18.30-18.45	7-10;13	at 18.30 and 18.40 discrete trace, smeared	transp.Es,Es(255;110-110)			
5-7.5	18.55-19.20	5-.6.25;7-7.5	till 19.00 CLEAR then smeared	Es(110)			
16-27	19.15-19.45	-					

13 July 2006

Period [min]	**Time (UT)**	**Fourier [min]**	**Doppler record**	**Reflection height, layer [km]**	**Amplitude [Hz]**	**Wavelets geomag. field**	**Cross-correlation**
4-6	18.30-18.40	4-6	CLEAR(discrete double trace)	transp.Es,F(270;115-265)	0.09	not evaluated - noise	
4.5-7.5	19.30-19.35	4.5-7.5	CLEAR(19.35 discrete trace)	F(260),19.45 transp.Es(260;110)	0.07	not evaluated - noise	
14-25	18.00-18.25	19;24-25	till 18.20 spread	transp.Es(280;125-265;120-270;115)			
>25	18.00-19.40	25;30	CLEAR(spread,double trace)	transp.Es,F,transp.Es(280;125-265;120--270;115-265-260-260-260-260;110)	not calc.	NS;EW	not calc.

23 July 2006

Period [min]	Time (UT)	Fourier [min]	Doppler record	Reflection height, layer [km]	Amplitude [Hz]	Wavelets geomag. field	Cross-correlation
5-7.5	17.20-17.25	5-6.25;7-7.5	S-shape,signal strength	Es,F(120-320)			
4-6.5	17.30-17.40	4-6.25	signal strength	F,transp.Es(320-265;110)			
6.5-13	18.20-18.30	7-13	double trace	F(250)			
4-12	19.10-19.35	4-6.25;7-12	CLEAR	F(240)	0.31	EW	NS=-0.6 at t=-410s EW=-0.56 at t=-349s V=0.61 at t=-349s B=-0.62 at t=-429s
5-12	21.40-22.00	5-6.25;7-12	CLEAR	F(240-245)	0.2	No	NS=0.64 at t=-454s EW=-0.73 at t=143s V=0.67 at t=50s B=0.68 at t=-477s
11-17	17.10-17.40	12-15	double trace,S-shape,signal strength	F,Es,F,transp.Es(300-120-310--265;110)			
>15	17.20-19.20	18;20-25	(till 18.30 signal strength,spread, double trace)	Es,F,transp.Es,F(120-310--265;110-260-255-250--240-240-240)			
5-17	19.30-20.10	5-6.25;7-15	CLEAR (19.50 discrete trace)	F,transp.Es,F(245-255;110--245-250)	0.55	NS	No
>18	19.35-20.20	18;20-25	CLEAR (19.50 discrete trace)	F,transp.Es,F,transp.Es(245-255; 110-245-250-260;110)	0.18	NS	NS=0.68 at t=1575s EW=-0.58 at t=1621s B=0.7 at t=1567s

23 July 2006 (cont.)

Period [min]	Time (UT)	Fourier [min]	Doppler record	Reflection height, layer [km]	Amplitude [Hz]	Wavelets geomag. field	Cross-correlation
>13	20.35-21.10	13-15;18;20-25	CLEAR(spread)	transp.Es,F(260;110-260;110-250-240)	0.18	NS;EW	NS=0.56 at t=384s EW=0.64 at t=-768s V=-0.58 at t=397s B=0.55 at t=381s
>18	21.25-22.15	18;20-25	CLEAR(spread)	F(240)	0.22	NS;EW;V	NS=-0.88 at t=-1263s EW=0.9 at t=-784s V=-0.79 at t=1366s B=-0.89 at t=-1242s
15-22	22.00-22.30	15;18;20-25	CLEAR	F(240-250)	0.14	NS;EW	NS=0.84 at t=-365s EW=-0.6 at t=61s V=-0.53 at 478s B=0.78 at t=-343s
>24	22.40-23.10	25	CLEAR	F(265-260)	not calc.	NS	not calc.
>15	23.00-24	15;18;20-25	CLEAR	F(260-270)	not calc.		

26 July 2006

Period [min]	Time (UT)	Fourier [min]	Doppler record	Reflection height, layer [km]	Amplitude [Hz]	Wavelets geomag. field	Cross-correlation
6-9.5	17.10-17.20	6-9.5	CLEAR(spread)	Es(115)	0.09	not evaluated - noise	
5.5-9.5	17.35-17.40	5.5-9.5	CLEAR(spread)	Es(115)	0.06	not evaluated - noise	
3.5-9	17.50-18.00	3.5-9	17.50,17.55 discrete trace	Es,F(115-300)			
3.5-11	18.20-18.55	3.5-9.5	18.30,18.50,19.10 discrete trace; double trace	F,transp.Es(270-270;115-275;115--270;110)			
3.5-4	19.20	3.5-4	spread	transp.Es(270;110)			
>12	17.40-19.45	13;15;18; 23-30	17.50-19.15 discrete trace, double trace,before and after CLEAR	Es,F,transp.Es(115-300-270-270;115--275;115-270;110-270;110-270;110)			

31 July 2006

Period [min]	Time (UT)	Fourier [min]	Doppler record	Reflection height, layer [km]	Amplitude [Hz]	Wavelets geomag. field	Cross-correlation
5.5-7.5	17.50-18.00	5.5-7.5	17.50 discrete trace; double trace	transp.Es,F(265;115-260)			
>22	17.35-18.15	25	CLEAR(17.50 discrete trace; double trace)	Es,transp.Es,F(105-265;115-260-260)	not calc.	NS;EW	not calc.
>16	18.15-19.20	18-19;25	CLEAR(double trace,smeared)	F,transp.Es,F(260-260-260;115-250-250)	0.16	NS;EW	EW=-0.55 at t=0
14-26	19.40-20.25	15.5;18-19;25	CLEAR	F(245-240-245-250-250)	0.14	NS;EW	EW=-0.64 at t=58s B=-0.53 at t=319s
14-20	20.40-21.00	15.5;18-19	20.40-20.50 double trace,spread	F(245-240)			
>22	21.00-22	25	CLEAR (21.45-22.00 double trace, spread)	F(240-235-245-245-280)	not calc.	NS;EW	not calc.
12-25	21.40-22	12-14;15.5; 18-19;25	CLEAR(21.45-22.00 double trace,spread)	F(240-280)	0.15	NS;EW	NS=0.6 at t=189s EW=0.54 at t=-1058s B=0.6 at t=200s

1 August 2006

Period [min]	Time (UT)	Fourier [min]	Doppler record	Reflection height, layer [km]	Amplitude [Hz]	Wavelets geomag. field	Cross-correlation
3-4	17.25	3-4.5	double trace,signal strength	F(265-280)			
12-19	17.05-17.20	13-13;15-17	till 17.10 double trace, then CLEAR	F(250-280)			
12-15	17.35-17.55	12-13	CLEAR(till 17.45 double trace)	F(280-260)	0.06Hz	not evaluated - noise	